Grid Integrated Type 3 Wind Systems - Modeling, and Line Protection Performance Analysis using the RTDS

A Thesis

Presented in Partial Fulfillment of the Requirements for the

Degree of Master of Science

with a

Major in Electrical Engineering

in the

College of Graduate Studies

University of Idaho

by

Rishabh Jain

July 2014

Major Professor: Herbert L. Hess, Ph.D.

Authorization to Submit Thesis

This thesis of Rishabh Jain, submitted for the degree of Master of Science with a major in Electrical Engineering and titled "Grid Integrated Type 3 Wind Systems - Modeling, and Line Protection Performance Analysis using the RTDS," has been reviewed in final form. Permission, as indicated by the signatures and dates given below, is now granted to submit final copies to the College of Graduate Studies for approval.

Major Professor _____Date_____
Herbert L. Hess, Ph.D.

Committee Members _____Date_____
Brian K. Johnson, Ph.D.

_____Date_____
Daniel Cordon, Ph.D.

Department Administrator _____Date_____
Fred Barlow, III , Ph.D.

Discipline's College Dean _____Date_____
Larry Stauffer, Ph.D.

Final Approval and Acceptance by the College of Graduate Studies

Dean of the College of Graduate Studies _____Date_____
Jie Chen, Ph.D.

Abstract

In this thesis, the line protection elements and their supervisory elements are analyzed in context of Type 3 (Doubly Fed Induction Generator based) grid integrated wind turbine systems. The underlying converter and controller design algorithms and topologies are discussed. A detailed controller for the Type 3 wind turbine system is designed and integrated to the grid using the Real Time Digital Simulator (RTDS). An alternative to the conventional Phase Locked Loop (PLL) for tracking of rotor frequency is designed and implemented. A comparative analysis of the performance of an averaged model and the corresponding switching model is presented. After completing the Wind Turbine (WT) model design, the averaged model is used to model an aggregate 10-generator equivalent model tied to a 230kV grid via a 22kV collector. This model is a great asset to understand dynamics, and the unfaulted and faulted behavior of aggregated and single-turbine Type 3 WT systems. The model is then utilized to analyze the response of conventional protection schemes (Line current Differential and Mho Distance elements) and their respective supervisory elements of modern commercial protection relays in real time by hardware-in-the-loop simulation using the RTDS. Differences in the behavior of these elements compared to conventional power systems is noted. Fault are analyzed from the relay's perspective and the reasons for the observed behavior are presented. Challenges associated with sequence components and relay sensitivity are discussed and alternate practices to circumvent these issues are recommended.

Acknowledgments

I want to thank *Dr. Herbert L. Hess*, who has been a pillar for me throughout the journey. He is my advisor, guardian, and a great friend. It is because of him, that I have come so far. Also, he happens to be my Major Professor.

I need to express heartfelt gratitude to *Dr. Brian K. Johnson* for his most interesting courses, and very insightful ideas and support throughout. Before attending his courses, I could never have imagined a research career in Power Systems. Discussing ideas with him only makes things better.

My supervisors and mentors, *Mr. M. Venkat Mynam* and *Mr. Armando Guzmán*, from Schweitzer Engineering Laboratories Inc., deserve special mention for their guidance and support throughout. The scope of this thesis may not have been in its present form without their help.

This is also the perfect opportunity to thank *Mr. John Jacksha (JJ)*, *Arleen*, and *the staff of our department of ECE*, for their support throughout with logistics, troubleshooting and advice.

Last but not the least, I would like to acknowledge the support of *my family and well wishers*. It is their unprecedented support, patience and belief, which has made everything possible, in my best and worst times.

Table of Contents

Authorization to Submit Thesis . . . . . **ii**

Abstract . . . . . **iii**

Acknowledgments . . . . . **iv**

Table of Contents . . . . . **v**

List of Tables . . . . . **ix**

Glossary . . . . . **x**

Acronyms . . . . . **xii**

List of Figures . . . . . **xv**

1 Introduction **1**

1.1 Why Wind 2

1.1.1 Growth and Future Prospects 3

1.2 Wind as an energy resource 4

1.2.1 Wind energy content 4

1.2.2 How turbines work 5

1.3 Types of Wind Turbines 6

1.3.1 Contribution of different types in Energy generation 8

1.4 Changing Grid Code 9

1.5 Type 3 Wind Turbine Systems 10

1.5.1 Basic Operation 10

1.5.2 Fault Behavior 11

1.6 What lies ahead? 12
1.7 Scope of this Thesis 12

2 Operation - Doubly Fed Induction Generator (DFIG) 13
2.1 Operation 13

3 Averaged Converter Model - Basics 16
3.1 Introduction 16
3.1.1 Switching Model 16
3.1.2 Averaged Model 17
3.1.3 Differences from a Switching Model 18
3.2 Derivation of the Averaged Model 18
3.3 Summary 22

4 Type 3 Controller - Components 23
4.1 Grid Side Controller 23
4.1.1 Overview - Why and What? 23
4.1.2 Controller Design Assumptions 23
4.1.3 Controller Design 23
4.2 DC Power Port Voltage Regulator 29
4.2.1 Controller Design 30
4.3 Rotor Side Controller 31
4.3.1 Overview - Why and What? 31
4.3.2 Controller Design 31
4.4 PLL Implementation 35
4.4.1 Grid Side Frequency Tracking 35
4.4.2 Rotor Side Frequency Tracking 36
4.5 Summary 37

5 The Test Network 39

5.1 Setup 39

5.1.1 A 10-Machine Aggregated Type 3 Model 39

5.1.2 Transformers 39

5.1.3 The Transmission Lines 40

5.1.4 The Real Time Digital Simulator 42

5.2 Test Network 45

5.3 Summary 45

6 Validation and Operation 47

6.1 Averaged Single Turbine Model 47

6.1.1 Validation 47

6.1.2 Comparing the Switching and Averaged Models 51

6.2 Average Aggregated (Ten Turbines) Model 52

6.2.1 Process of Aggregation 53

6.2.2 Validation 55

6.2.3 Normal Operation 55

6.3 Summary 58

7 Results and Analysis 60

7.1 Supervisory Elements 60

7.1.1 Directional Supervision 61

7.1.2 Fault Selection 62

7.1.3 Loss of Potential 63

7.2 Protection Elements 63

7.2.1 Mho Element - Distance Protection 64

7.2.2 Differential Protection 64

7.3 Permissive Overreaching Transfer Trip (POTT) Scheme 67

7.4 Fault Simulation and Analysis 68
7.4.1 Event 1(a) - Single Line to Ground fault - Phase A (AG) Fault (87COMM active) 69
7.4.2 Event 1(b) - Double Line to Ground fault - Phases A,B (ABG) Fault (87COMM active) 72
7.4.3 Event 1(c) - Line - Line Fault (Phase A - Phase B) (AB) Fault (87COMM active) 75
7.4.4 Event 1(d) - Three phase fault (ABCG) Fault (87COMM active) 84
7.4.5 Event 2(a) - AG Fault (87COMM failed) 86
7.4.6 Event 2(b) - ABG Fault (87COMM failed) 88
7.4.7 Event 2(c) - AB Fault (87COMM failed) 95
7.4.8 Event 2(d) - ABCG Fault (87COMM failed) 96
7.5 Analysis of Results 99
7.6 Summary 104

8 Summary, Conclusions and Future Work 105
8.1 Summary 105
8.2 Conclusions 106
8.3 Suggested Measures - Future Work 107

References 110

List of Tables

1.1 Installed Wind Capacity around the world during 1995-2009 [1] . . . 9

5.1 Parameters for the Doubly Fed Induction Generator for Type 3 System 40

5.2 Parameters for the 3-winding transformer used in the Test Network . 40

5.3 Parameters for the Main transformer used in the Test Network 41

8.1 Summary - Fault Wise Response of the Protection Element Bits . . . 105

8.2 Summary - Fault Wise Response of the Supervisory Element Bits . . 106

Glossary

d Direct axis component of any entity. This will be used as a suffix to represent the direct axis component..

f_s Inductance of the machine's rotor.

$i_n(t)$ Current flowing through the negative voltage rail of the half bridge converter.

$i_p(t)$ Current flowing through the positive voltage rail of the half bridge converter.

L_s Inductance of the Link between Grid and the Half Bridge (HB) converter.

m Modulation Ratio.

N_r Speed of the Rotor.

N_s Synchronous Speed.

P_{betz} Maximum Power that can be extracted according to the Betz Limit.

P_{DC} Power stored in the DC link.

$P_t(t)$ Power transferred at the Phase Terminal of the HB converter to the grid.

P_{wind} Power stored in the wind.

q Quadrature axis component of any entity. This will be used as a suffix to represent the quadrature axis component..

R Radius of the Wind Turbine blade.

R_r Resistance of the machine's rotor.

R_s Resistance of the Link between Grid and the HB converter.

s slip of the Induction machine.

$s_1(t)$ Switching function of the switch number '1' in the half bridge converter.

$s_4(t)$ Switching function of the switch number '4' in the half bridge converter.

v velocity of the wind in meters per second.

V_{DC} Voltage of the DC Link.

V_n Voltage at the negative voltage rail of the half bridge converter.

V_p Voltage at the positive voltage rail of the half bridge converter.

V_s Voltage of the Grid.

$V_t(t)$ Voltage at the terminals of the half bridge converter.

Acronyms

AB Line - Line Fault (Phase A - Phase B).

ABCG Three phase fault.

ABG Double Line to Ground fault - Phases A,B.

AG Single Line to Ground fault - Phase A.

ATP Alternate Transients Program.

BC Line - Line Fault (Phases B, C).

BCG Double Line to Ground fault - Phases B,C.

CB Circuit Breaker.

CG Single Line to Ground fault - Phase C.

CT Current Transformer.

DFIG Doubly Fed Induction Generator.

EMF Electro Motive Force.

FRT Fault Ride Through.

FSA Relay Bit - Fault in Sector A.

FSB Relay Bit - Fault in Sector B.

FSC Relay Bit - Fault in Sector C.

FSFC Full Scale Frequency Converter.

FTS Fault Type Selection.

GB Gear Box.

GEN Generator.

GOOSE Generic Object Oriented Substation Events - A control model defined as per IEC 61850..

GW Gigawatts.

GWEC Global Wind Energy Council.

HB Half Bridge.

IEA International Energy Agency.

KVL Kirchoff's Voltage Law.

LVRT Low Voltage Ride Through.

NA Not Applicable.

PI Proportional - Integral.

PLL Phase Locked Loop.

POTT Permissive Overreaching Transfer Trip.

PSRC Power System Relaying Committee.

PV Photovoltaics.

PWM Pulse Width Modulation.

RTDS Real Time Digital Simulator.

SCIG Squirrel Cage Induction Generator.

SG Synchronous Generator.

TRIP Relay Bit - Trip Asserted.

TRPPRM Relay Bit - Permission to Trip asserted.

VSC Voltage Source Converter.

WRIG Wound Rotor Induction Generator.

WT Wind Turbine.

List of Figures

1.1 Global Wind Speed map at 80 meters above the surface [2] 2

1.2 World Share in Wind Energy Generation [3] 3

1.3 Growth Forecast for Wind Energy sector from 2014-2019 [3] 4

1.4 Basic Principle of Wind Turbine Operation 5

1.5 Type 1 Wind turbine System - Schematic 6

1.6 Type 2 Wind turbine System - Schematic 7

1.7 Type 3 Wind turbine System - Schematic 8

1.8 Type 4 Wind turbine System - Schematic 8

1.9 Schematic : Basic Type 3 Wind Generation System 11

2.1 Coil - Magnet Setup to demonstrate Faraday's law 13

3.1 Switching Model for Half-bridge Converter 16

3.2 Equivalent Averaged Model for Half-bridge Converter 18

3.3 Alternate Transients Program (ATP) Plot Showing the Difference Between Outputs From the Switching and Equivalent Averaged Model . 19

3.4 Switching States of the Two Switches in HB Arm 19

3.5 Plot for a Simple DC-triangle Pulse Width Modulation 21

3.6 Equivalent averaged Model with derived parameters 22

4.1 AC Side of Averaged Model Equivalent System for Grid Side Power Regulator Design 26

4.2 Block Diagram: Grid Side Current Regulator 28

4.3 Grid Side Controller implementation in RSCAD 29

4.4 Block Diagram: DC Link Voltage Regulator 30

4.5 DC Link Voltage Regulator implementation in RSCAD 31

4.6 Block Diagram: Rotor Side Current Regulator 35
4.7 Rotor Side Controller implementation in RSCAD 36
4.8 Block Diagram for 'atan2' Based Phase Locked Loop [4] - Grid side PLL 37
4.9 Implementation of PLL for Rotor Side Controller in RSCAD 37

5.1 Tower Configuration for the 22kV Collector Line 41
5.2 Impedance and Conductor details for the 22kV Collector Line 42
5.3 Tower Configuration for the 230kV Collector Line 43
5.4 Impedance and Conductor details for the 230kV Collector Line 44
5.5 Schematic - Type 3 Wind Farm Test Network 45

6.1 Torque v/s Speed Characteristics for a Doubly Fed Generator 48
6.2 Power Output (Stator and Rotor) v/s Rotor Speed for the 10-turbine aggregated DFIG model 49
6.3 V, I Plots on Collector Bus for a B-C Fault on the 22kV Collector for a single generator 50
6.4 V, I Plots for B-C Fault on the 230kV Line for the Wind Farm from [5] 51
6.5 Stator and Rotor Currents from the Switching Model of a Type 3 Machine During Supersynchronous Operation 52
6.6 Plot - B-C Fault on 230kV Line for the 10-Generator Aggregated DFIG 54
6.7 Speed and Torque for a Type 3 Machine in Supersynchronous Operation 55
6.8 DC Voltage Regulator (reference and actual) During a Temporary Fault on the Collector for the Aggregated Model 56
6.9 Grid and Rotor Side current tracking for a Type 3 machine in super-synchronous operation 57
6.10 Power Output (Stator and Rotor) v/s Rotor Speed for the 10-generator Aggregated DFIG 58

6.11 Stator and Rotor Current Outputs for a Type 3 Aggregated Model During Supersynchronous Operation 59

7.1 Generic Schematic - Distance Element 61
7.2 Generic Schematic - Loss of Potential 63
7.3 Mho Distance Element 65
7.4 Differential Characteristics - Alpha Plane 66
7.5 Event Report for Event 1(a) - Type 3 side Relay 70
7.6 Event Report for Event 1(a) - Grid side Relay 71
7.7 Sequence Current and Voltage Calculations using MATLAB® for Event 1(a) 72
7.8 Directional Element Calculations using MATLAB® for Event 1(a) . . 73
7.9 M Equation Calculations using MATLAB® for Event 1(a) 73
7.10 Differential Characteristic Plots using MATLAB® for Event 1(a) . . . 74
7.11 Event Report for Event 1(b) - Type 3 side Relay 75
7.12 Event Report for Event 1(b) - Grid side Relay 76
7.13 Sequence Current and Voltage Calculations using MATLAB® for Event 1(b) 77
7.14 Directional Element Calculations using MATLAB® for Event 1(b) . . 77
7.15 M Equation Calculations using MATLAB® for Event 1(b) 78
7.16 Differential Characteristic Plots using MATLAB® for Event 1(b) . . 79
7.17 Event Report for Event 1(c) - Type 3 side Relay 80
7.18 Event Report for Event 1(c) - Grid side Relay 80
7.19 Sequence Current and Voltage Calculations using MATLAB® for Event 1(c) 81
7.20 Directional Element Calculations using MATLAB® for Event 1(c) . . 81
7.21 M Equation Calculations using MATLAB® for Event 1(c) 82
7.22 Differential Characteristic Plots using MATLAB® for Event 1(c) . . . 83

7.23 Event Report for Event 1(d) - Type 3 side Relay 84
7.24 Event Report for Event 1(d) - Grid side Relay 85
7.25 Sequence Current and Voltage Calculations using MATLAB® for Event 1(d) 86
7.26 Directional Element Calculations using MATLAB® for Event 1(d) . . 87
7.27 M Equation Calculations using MATLAB® for Event 1(d) 87
7.28 Differential Characteristic Plots using MATLAB® for Event 1(d) . . 88
7.29 Event Report for Event 2(a) - Type 3 side Relay 89
7.30 Event Report for Event 2(a) - Grid side Relay 90
7.31 Sequence Current and Voltage Calculations using MATLAB® for Event 2(a) 90
7.32 Directional Element Calculations using MATLAB® for Event 2(a) . . 91
7.33 M Equation Calculations using MATLAB® for Event 2(a) 91
7.34 Event Report for Event 2(b) - Type 3 side Relay 92
7.35 Event Report for Event 2(b) - Grid side Relay 92
7.36 Sequence Current and Voltage Calculations using MATLAB® for Event 2(b) 93
7.37 Directional Element Calculations using MATLAB® for Event 2(b) . . 93
7.38 M Equation Calculations using MATLAB® for Event 2(b) 94
7.39 Event Report for Event 2(c) - Type 3 side Relay 95
7.40 Event Report for Event 2(c) - Grid side Relay 96
7.41 Sequence Current and Voltage Calculations using MATLAB® for Event 2(c) 97
7.42 Directional Element Calculations using MATLAB® for Event 2(c) . . 98
7.43 M Equation Calculations using MATLAB® for Event 2(c) 98
7.44 Event Report for Event 2(d) - Type 3 side Relay 99
7.45 Event Report for Event 2(d) - Grid side Relay 100

7.46 Sequence Current and Voltage Calculations using MATLAB® for Event 2(d) 101

7.47 Directional Element Calculations using MATLAB® for Event 2(d) . . 102

7.48 M Equation Calculations using MATLAB® for Event 2(d) 102

Chapter 1: Introduction

The demand for energy is increasing worldwide. With the development of technology, and its increasing involvement in our daily life, this demand will only increase in future. For meeting these needs we depend primarily on conventional sources of energy, which are accompanied by greenhouse emissions and increasing pollution. Global warming is a big concern today. With increasing awareness among the population, the interest in less (or 'Zero') emission sources is increasing. The Energy sector is emerging as a big market. It has the potential to support many jobs varying from manufacturing to installation, power system protection to asset management and other service sectors. Energy prices (especially coal and petroleum) have significantly increased in the last two decades. This has made investment in renewable systems more practical.

These developments have captured a lot of political attention. Meeting future energy needs is among the major agendas in political manifestos around the world. As a result, the investments for research in alternative and hybrid sources of energy have increased exponentially.

Also, in past three decades, the applications of power electronics and computational systems is developing exponentially. This is encouraging the interconnectivity of systems across the word. Control systems have become more sophisticated and accurate, as they can deal with more number of variables parallely. Communication based protection schemes (like Transfer Trip and Line current differential schemes) are becoming more popular. They also perform better. Therefore, it is easier for distributed generators to connect to the grid.

Of the various available renewable energy resources, solar, wind and hydro are the most sought after. These resources have a significant potential to meet most of the world's energy needs. Hydro technology is currently the most developed of all

renewable technologies. However, its basic requirements rely heavily on geography and often encompass numerous relocation and environmental concerns.

Photovoltaics (PV) and wind energy are two of the fastest growing energy resources in terms of technology. These resources are still impacted financially, due to high initial cost and long payback. But, with rising prices of energy and better technology, wind and solar energy is getting more accessible.

1.1 Why Wind

According to a report from the International Energy Agency (IEA), wind will be the second largest renewable energy source after hydro, by 2035. Availability is not a major barrier. Modern turbines are known to generate power from winds as low as 3.5 m/s, which is abundant across the world.

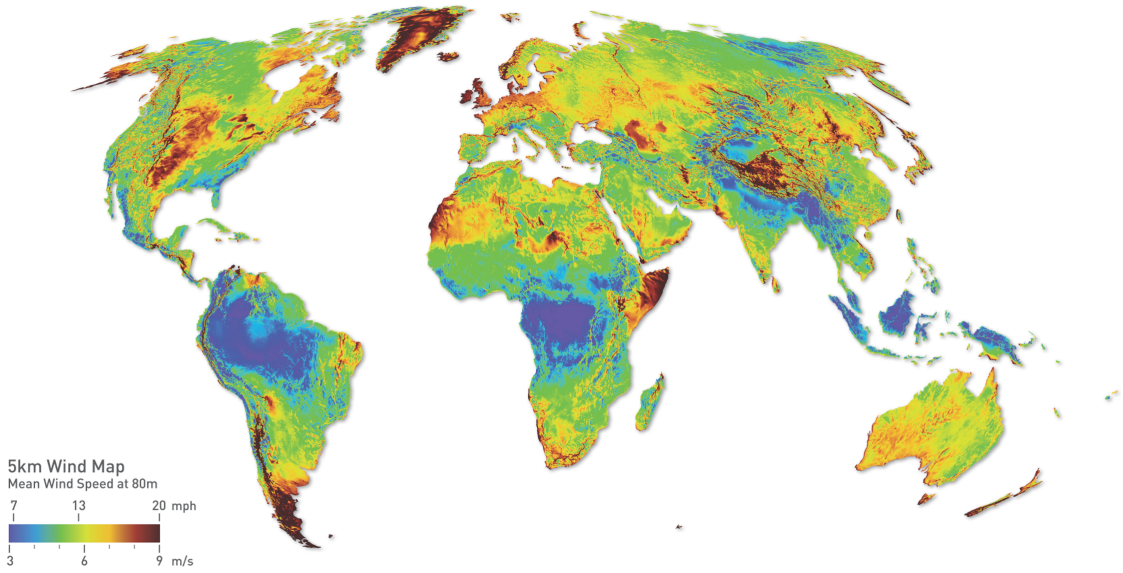

Figure 1.1: Global Wind Speed map at 80 meters above the surface [2]

Figure 1.1 shows the Global Wind Speed Map at 80 meters above the surface. As it can be clearly deduced, most areas around the world have some potential for power generation using Wind.

1.1.1 Growth and Future Prospects

According to the Global Wind Energy Council [3], Wind energy has an installed capacity of more than 318 Gigawatts (GW) around the world. Figure 1.2 shows the cumulative installed capacities of wind energy around the world. This figure also presents the same statistics for new installations during the year 2013.

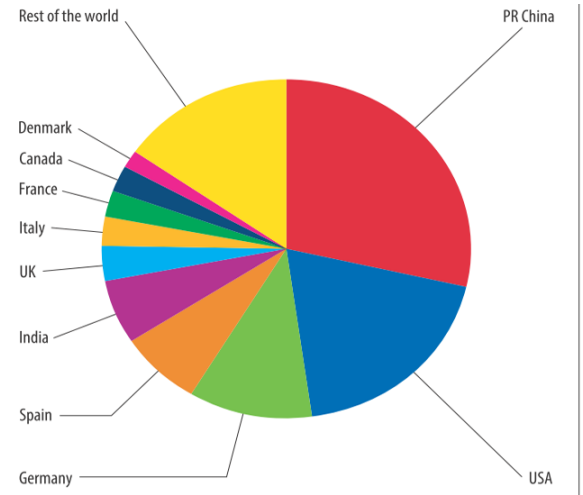

Country	MW	% SHARE
PR China	91,412	28.7
USA	61,091	19.2
Germany	34,250	10.8
Spain	22,959	7.2
India	20,150	6.3
UK	10,531	3.3
Italy	8,552	2.7
France	8,254	2.6
Canada	7,803	2.5
Denmark	4,772	1.5
Rest of the world	48,332	15.2
Total TOP 10	**269,773**	**84.8**
World Total	**318,105**	**100.0**

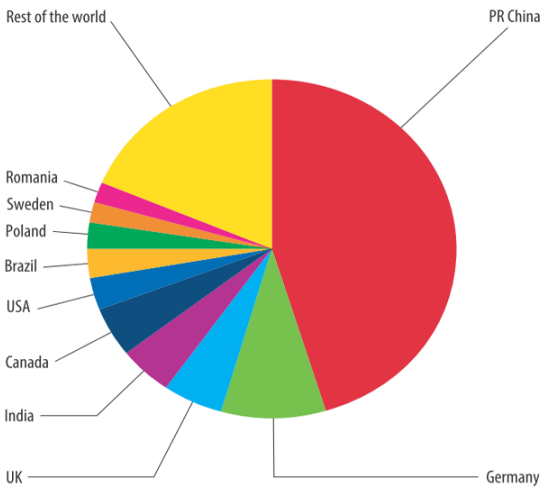

Country	MW	% SHARE
PR China	16,088	45.6
Germany	3,238	9.2
UK	1,883	5.3
India	1,729	4.9
Canada	1,599	4.5
USA	1,084	3.1
Brazil	953	2.7
Poland	894	2.5
Sweden	724	2.1
Romania	695	2.0
Rest of the world	6,402	18.1
Total TOP 10	**28,887**	**82**
World Total	**35,289**	**100.0**

Figure 1.2: World Share in Wind Energy Generation [3]

Based on the forecast by Global Wind Energy Council (GWEC) [3], the net installed capacity will almost double in the next five years (Figure 1.3).

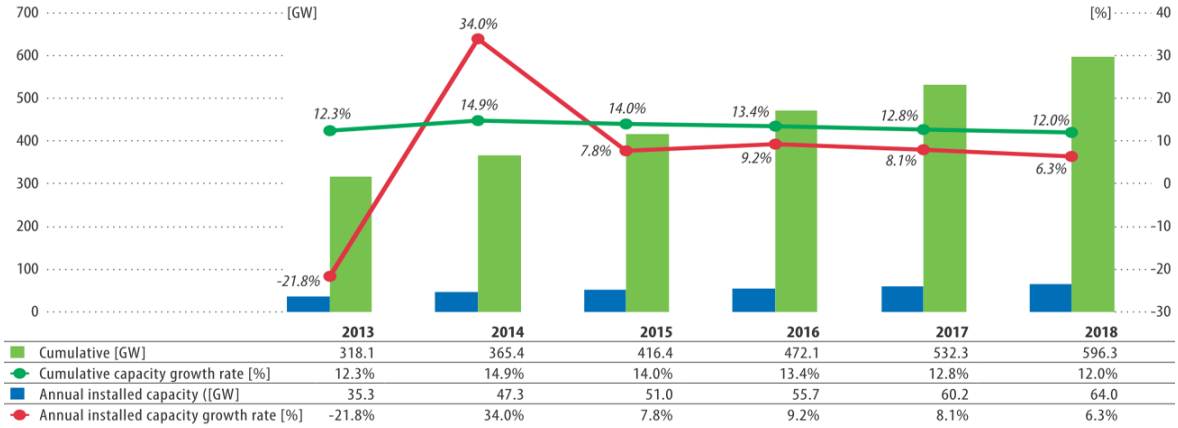

Figure 1.3: Growth Forecast for Wind Energy sector from 2014-2019 [3]

1.2 Wind as an energy resource

1.2.1 Wind energy content

The Power stored in wind blowing at a speed of 'v' m/s is given by (1.1) [1]:

$$P_{wind} = \frac{1}{2}.\rho.\pi.R^2.v^3 P_{wind} = \frac{1}{2}.\rho.\pi.R^2.v^3 \tag{1.1}$$

Here, ρ is the air density in $kg.m^{-3}$ and 'R' is the radius (in meters) of the area swept by the wind turbine. Air density is a function of air temperature, atmospheric pressure, humidity and altitude for any given place at any given time.

The power, P_{wind}, is the total energy available per unit time. However, according to Betz theorem [1], the theoretical maximum power that can be extracted from the wind is given by (1.2):

$$P_{betz} = 0.59.P_{wind} = (0.59).\frac{1}{2}.\rho.\pi.R^2.v^3 \tag{1.2}$$

This is also known as the *Betz Limit*. Hence, even with a lossless method to extract energy from the wind, a maximum of 59% can be extracted.

1.2.2 How turbines work

The principle of harnessing energy from wind is simple. Wind blowing at a velocity 'v', hits the turbine blade and transfers some of its momentum on to it. This, in turn, causes the turbine to rotate. The hub of the turbine is connected to the generator's prime mover using a gearbox (Gear Box (GB)). Older turbines were dependent on the area of the blade. However, modern wind turbines have improvised aerodynamic designs, which are dependent on the pressure difference. As the blades cut through the moving wind, it exerts a lift force on the blades (Figure 1.4 [6]).

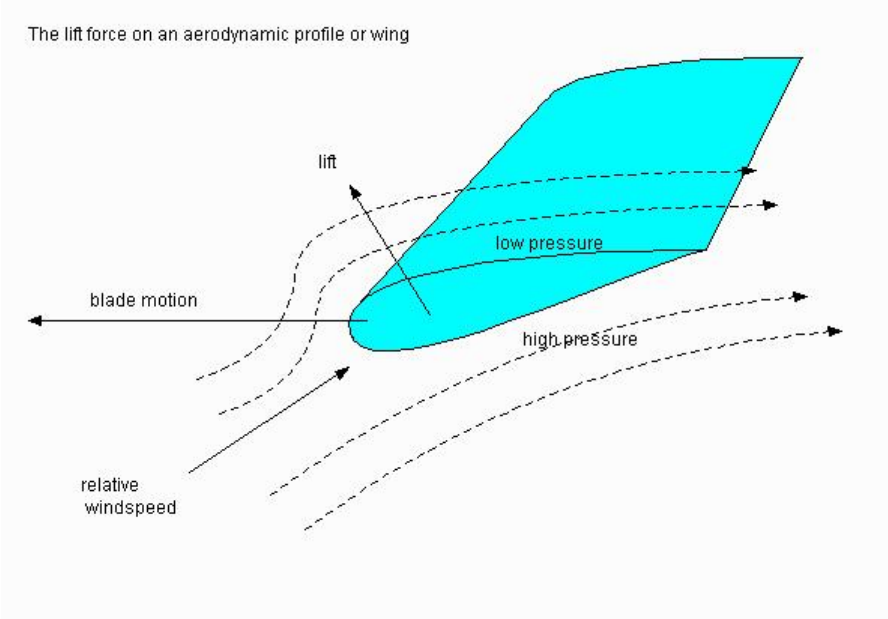

Figure 1.4: Basic Principle of Wind Turbine Operation

The tangential component of this lift force causes the blades to rotate. Therefore, more energy is harnessed as the angle between the lift force and its tangential decreases. Similarly, to stall the turbines, the tangential force needs to be '0'. In other words, the angle of the lift force should be perpendicular to its tangent. The turbine controller regulates this angle by controlling the blade pitch angle of the turbine.

1.3 Types of Wind Turbines

Wind turbines can be broadly classified based on their ability to generate for changing wind speeds.

1. ***Constant Speed Wind Energy Systems:***

   These systems can generate power only when for wind speeds greater than rated. Rated wind speed is defined as the speed at the generator will generate its rated power. The rotor has to spin at supersynchronous speed to generate power. Since there is no controller to regulate the rotor flux for subsynchronous speeds, the turbine can't generate power for low wind speeds. Type 1 wind turbines fall in this category.

2. ***Variable Speed Wind energy systems***

   As the name suggests, these systems have control over the range of wind speeds for which they can generate power to different degrees, based on the design. Type 2, 3, and 4 turbine systems fall under this category.

All four types of Wind Generation systems are discussed in the same order [7]:

1. ***Type 1 Wind Generators:*** A type 1 system (Figure 1.5) consists of a Squirrel Cage Induction Generator (SCIG) directly connected to the grid via the transformer. As the SCIGs always draw reactive power from the grid, a capacitor bank is installed for reactive power compensation.

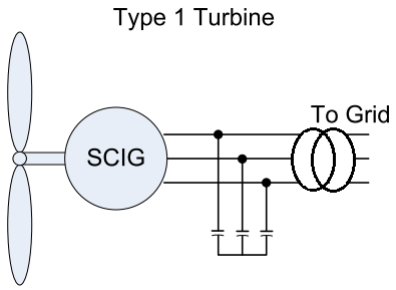

Figure 1.5: Type 1 Wind turbine System - Schematic

As the wind hits the blade, its energy is transferred to the turbine. The rotor is coupled to the turbine via a GB to step up its speed of rotation. Since there are no controllers, fluctuation in the wind speed is directly reflected in the power output from the generator.

2. ***Type 2 Wind Generators:*** A type 2 system (Figure 1.6) consists of a Wound Rotor Induction Generator (WRIG) with a variable rotor resistance controller. This generator is connected to the grid via the transformer. Similar to Type I systems, these also draw reactive power from the grid. Hence, a capacitor bank is installed for reactive power compensation.

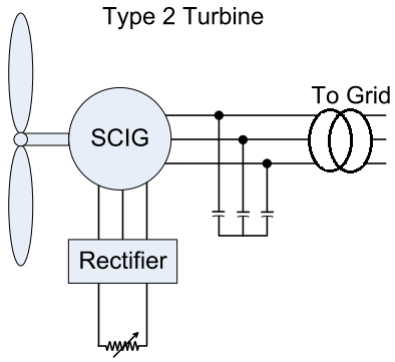

Figure 1.6: Type 2 Wind turbine System - Schematic

Due to the presence of rotor resistance control, there is some control on the rotor current (and, hence, rotor flux).

3. ***Type 3 Wind turbines:*** A Type 3 system (Figure 1.7) consists of a Doubly Fed Induction Generator (DFIG) connected to the grid via the transformer. Its rotor is connected to the grid via a back-to-back Voltage Source Converter (VSC). The VSC is regulated to give up to a +/- 30% control on the rotor's slip. This allows a broader wind speed range for generation. These VSCs handle only a fraction of the net generation, and therefore are rated for about 30% of the generator's capacity. Type 3 WT systems are therefore cheaper. Also, in supersynchronous modes, power can be extracted from rotor in addition to

stator. Therefore, a Type 3 unit can generate up to 130% of its rated capacity.

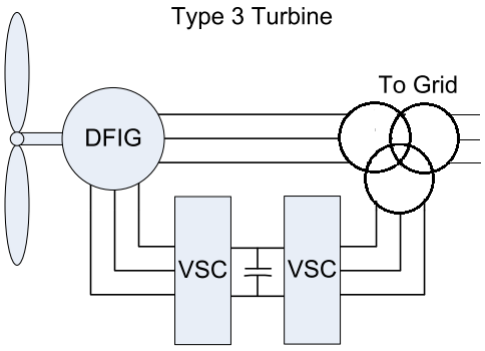

Figure 1.7: Type 3 Wind turbine System - Schematic

4. ***Type 4 Wind turbines:*** A type 4 system (Figure 1.8) consists of a Synchronous Generator (SG) connected to the grid via a back-to-back VSC and a transformer. The VSC is rated for full rating of the generator for this system. This system has an much better control on the useful wind speed range for power generation compared to its predecessors.

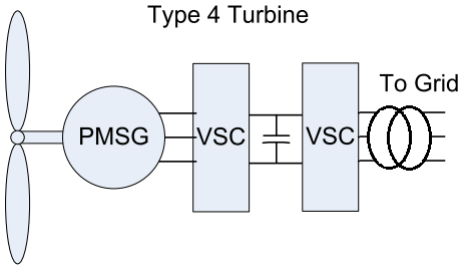

Figure 1.8: Type 4 Wind turbine System - Schematic

1.3.1 Contribution of different types in Energy generation

Table 1.1 shows the new installed capacity for the years 1995 to 2009. As can be noted, cumulatively, Type 3 turbines account for more than 50% (or 80 GW) of the net installation in these 15 years. Therefore, the study of its behavior will be very applicable to a large section of wind industry.

Year	Type1(%)	Type2(%)	Type3(%)	Type4(%)	Installed Cap(MW)
1995	70.10	15.90	0.00	14.00	1161
1996	62.60	23.50	0.10	13.80	1093
1997	54.30	27.40	3.30	15.00	1489
1998	39.50	17.80	26.50	16.10	2345
1999	40.80	17.10	28.10	14.00	3788
2000	39.00	17.20	28.20	15.60	4381
2001	32.40	15.20	37.30	15.10	7175
2002	27.20	5.20	46.70	20.90	7242
2003	20.00	3.10	59.10	17.80	8090
2004	22.90	2.20	55.10	19.90	8247
2005	16.10	0.90	63.60	19.10	11345
2006	12.90	2.10	63.50	20.80	15910
2007	7.80	7.10	64.50	20.60	22062
2008	6.40	7.30	68.30	16.20	30612
2009	4.90	5.90	63.30	22.20	36682
Total	**14.63%**	**6.79%**	**58.18%**	**19.14%**	**161622 MW**

Table 1.1: Installed Wind Capacity around the world during 1995-2009 [1]

1.4 Changing Grid Code

The operating experience from fixed speed (or limited speed variability) wind generators showed that they can aggravate sags by absorbing large amounts of reactive power during disturbances. This leads to longer recovery times during faults. With this in mind, until about a decade back, *wind turbines needed to be disconnected from the grid during disturbances*. This reduced the influence of wind turbine's dynamics on the grid, prevented feeding the fault and eliminated the risk of islanding. This also removed generation, which helped the system to recover faster. However, with the improvement in wind generation technologies (Type 3,4), the situation has changed. *DFIG and Full Scale Frequency Converter (FSFC) systems have inherent Low Voltage Ride Through (LVRT) capabilities due to faster power electronic control [8].*

Therefore, the new grid codes in most countries include LVRT requirements for wind based generation. This means that, during faults, wind turbines should remain connected for a certain period to support the voltage. Therefore, understanding the

behavior of wind turbines during fault has become very significant.

1.5 Type 3 Wind Turbine Systems

1.5.1 Basic Operation

As described in Section 1.3, Type 3 systems are based on Doubly Fed Induction Generators (DFIGs). Doubly Fed machines give a unique ability to control the rotor flux, and, hence, the effective slip of the machine. Details have been described in Chapter 2.

Subsynchronous conditions are those when the rotor speed (by the virtue of wind speed) is less than synchronous. Supersynchronous conditions will imply that rotor is rotating at a speed greater than synchronous. In subsynchronous mode, DFIG's rotor is artificially excited by importing some reactive power from the grid. This helps in maintaining the flux linkage and allows generation of commonly used power more than what is imported from the grid.

The controllers for the Type 3 machine are current regulated. The grid side controller regulates the power being imported or exported from the rotor side circuit. The frequency of this power is matched to the grid's system frequency. DC Regulator maintains a constant DC link voltage by regulating the output power reference of the grid side controller. The rotor side controller tracks the maximum power point based on the wind speed, and corresponding flux requirements. It is responsible for regulating rotor excitation to get the desired power output from the DFIG. Type 3 turbine controllers are rated for about 30% of machine's rating, and therefore, they are less expensive than the back-to-back VSCs for Type 4 systems. During supersynchronous conditions, the rotor is spinning at a speed more than synchronous. In other words, its slip is negative. Again, the rotor control optimizes the flux for maximum output power. Now, the DFIG can produce power from both Stator and

Rotor. Therefore, Type 3 turbines can produce more than rated power of the machine. Figure 1.9 shows a basic schematic of Type 3 system.

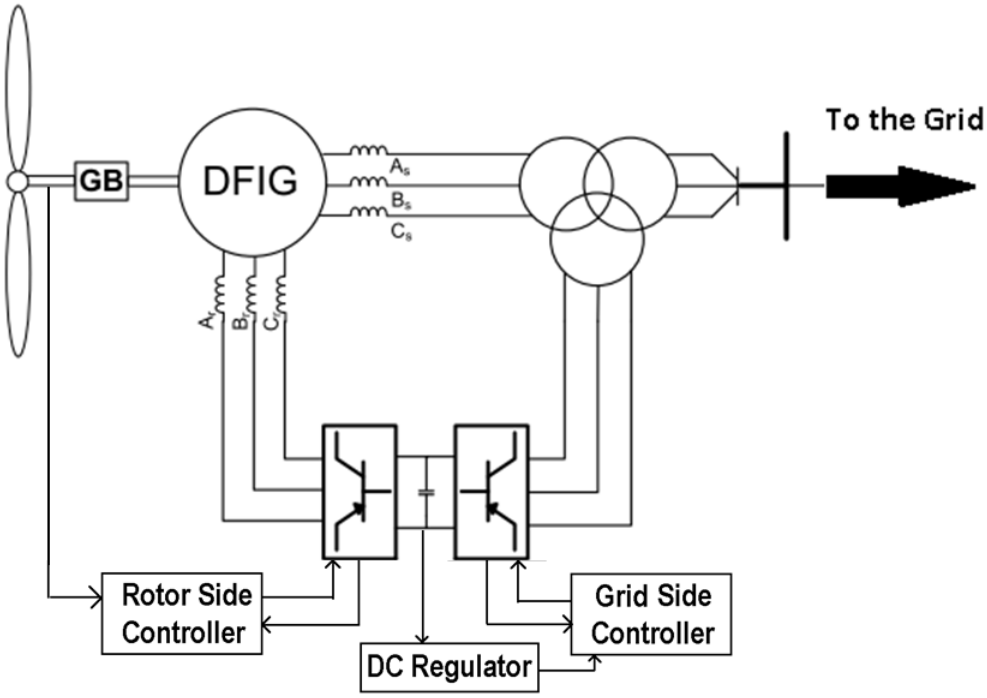

Figure 1.9: Schematic : Basic Type 3 Wind Generation System

1.5.2 Fault Behavior

Severe faults can impose excessive voltages on the WRIG's rotor. However, in order to survive most severe faults, generators will need to be over designed. Instead, a crowbar protection/chopper circuit is added in the control to regulate the maximum fault current. Depending on the manufacturers, different schemes may be utilized.

Crowbar protection essentially shorts the rotor terminals during faults. Therefore, the DFIG becomes a regular SCIG with characteristics similar to a Type 1 or Type 2 wind turbine. Therefore, shorting the rotor during faults will induce a current in the stator windings, depending on its frequency. Given the severity of fault, and slip during fault, the fault current contribution due to these currents can be high.

When the crowbar is not engaged, machine operates as per the control design.

Therefore, the fault behavior without engaged crowbar will vary from one manufacturer to another. In all cases, the fault current will be regulated to the set limits. Chopper circuits are engaged to limit the fault current contribution in the VSCs as per design.

1.6 What lies ahead?

Since the wind turbines are now expected to remain connected to the grid, it is worthwhile to investigate the following:-

1. The behavior of different wind turbine systems for all types of faults.
2. Performance of the ubiquitous protection schemes.
3. Effect of the wind turbine systems on the Sequence components.
4. Performance of the traditional protection elements.
5. Performance of the supervisory elements associated with the corresponding protection elements.

1.7 Scope of this Thesis

Observing these needs, this thesis will work on the following in the same sequence:-

1. Model and validate a Type 3 WT system and its controllers in the RTDS.
2. Development of an aggregated model to be connected to the grid.
3. Analyze the performance of Mho Distance and Line current differential elements.
4. Study of the performance of associated supervisory elements.
5. Study the performance of Permissive Overreaching Transfer Trip scheme.
6. Utility of the Weak In-feed Logic for systems involving Type 3 wind farms.
7. Proposing recommendations based on the challenges as seen by the above elements/relays.

Chapter 2: Operation - DFIG

2.1 Operation

Faraday's law of electromagnetic induction states that any change of flux in a moving coil will 'induce' a voltage in the coil. This voltage is proportional to the rate of change of flux and the number of turns in the coil. Mathematically,

$$\boxed{\varepsilon = -N_t \frac{\mathrm{d}\Phi_\mathrm{B}}{\mathrm{dt}}} \tag{2.1}$$

where, ε :- Electro Motive Force (EMF) induced

N_t :- Number of turns in the coil

Φ_B :- Flux

Therefore, if a coil with N_t number of turns is rotated in a magnetic field, as shown in the Figure 2.1, a voltage will be induced. Therefore, this machine can act as a generator. By the same principle, if current is applied in a region with variable magnetic field, force is induced. Therefore, the same machine can act as a motor. Induction machines are most widely used as motors. *Due to their robust performance,*

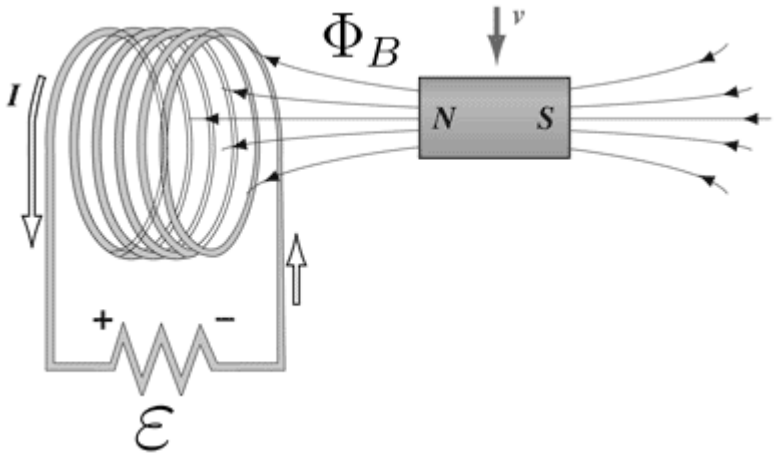

Figure 2.1: Coil - Magnet Setup to demonstrate Faraday's law

they have nearly replaced DC drives, except for areas with critical speed/torque control requirements.

The electrical equivalent circuits for different designs of induction machines are the same. The circuit consists of a three phase stationary winding (*stator*) and a cage/slip ring winding set, which is free to rotate within the stator (*rotor*). When the stator is fed by the power supply, it produces a sinusoidal magnetic field in all three phases. The resultant is a magnetic field rotating at system frequency which induces emf in the rotor.

Operation as a Motor: When the machine starts, the rotor is at rest. Hence, the rate of change of flux is maximum. Currents induced in the rotor are of the same frequency as the the stator. These rotor currents are induced such that their magnetic field offsets the magnetic field of the stator. The interaction of these two fluxes induces a torque on the rotor. If the rotor is free to rotate, it will rotate in the direction of the stator flux vector to reduce the relative flux linkage. As the relative speed of stator field with respect to the rotor decreases, the flux linkage also decreases. Therefore, rotor current and its frequency falls.

If the machine is not loaded, the speed of the rotor will approach synchronous speed (speed of the stator flux vector). As the load increases, the rotor will decelerate, leading to increased flux linkage. This will lead to more emf on the rotor, and hence more current. This current will offset the stator field again, and the machine will gain torque and speed. After a few seconds, the speed will settle to a steady state subsynchronous speed. The ratio of this difference between stator and rotor speed to the stator speed is called Slip.

$$\boxed{s = \frac{N_s - N_r}{N_s}} \tag{2.2}$$

where, s : Slip of the machine

N_s : Synchronous Speed (Speed of the stator)

N_r : Speed of the rotor

This implies that as the load of a machine increases, slip will increase. Therefore, the machine will draw in more current.

Now, if the rotor is driven by an external force such that, the rotor is driven to rotate faster than the synchronous speed, the rotor field will continue trying to minimize flux linkage. However, it will now act in the same direction as stator flux vector since $N_r > N_s$. In other words, *the rotor currents will reverse, and the machine will start acting as a generator.*

The key idea behind generated torque or current, therefore, is the flux linkage and its direction. So, to maintain generation, prime mover must ensure that rotor speed is near optimum.

This is why, wind turbine based generators are challenging. Wind speed changes frequently. The turbines are usually designed for an optimum speed (usually around 12-13 m/s). For wind speed below 9-10 m/s, they can't generate useful power. This is why variable speed turbines (Type 2, 3, 4) have been developed. The control has two aspects: mechanical and electrical. The mechanical aspect of the turbine is optimized by its internal controllers. These adjust turbine's aerodynamics to capture maximum energy from wind at each operating speed. The controllers can also stall the turbines, as a protection measure, for wind speeds significantly above rated.

Optimization of electrical aspect is available with Type 3 and Type 4 Generator controllers. If the rotor current can be regulated at the appropriate frequency, even for low speeds, the coupled generator can produce significantly more power. In these conditions, a small percentage is consumed by the rotor.

Tracking the flux and frequency accurately is very important for the controllers to perform accurately. This is one of the key challenges in designing a robust controller. Details will be discussed in Chapter 4.

Chapter 3: Averaged Converter Model - Basics

3.1 Introduction

3.1.1 Switching Model

A switching model of any power electronic circuit represents a simplified equivalent or the actual topology itself. The components (switches, resistors, inductors and others) can be modeled as ideal components for a simpler representation of the output. More detailed (and, hence, complex) models will model these components closer to their real life counter parts. Phenomena like switching transients, switching losses, non-linearity of the load, and other similar effects will then be observed. At the same time, detailed models will be computationally more intensive and may not be very suitable of use during intial design.

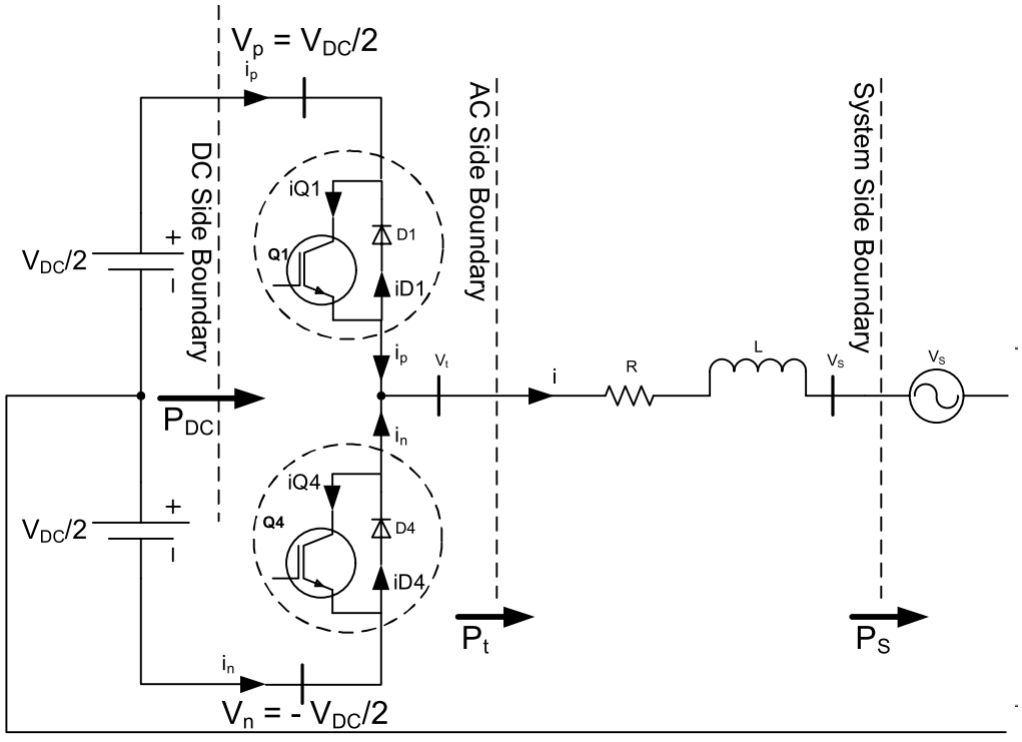

Figure 3.1: Switching Model for Half-bridge Converter

Figure 3.1 represents the basic diagram of a half bridge converter. The transistors are acting as switches. The anti-parallel diodes are connected to:

1. represent the actual behavior of IGBTs.

2. allow the converter to supply loads with lagging power factor.

These are reverse biased when their corresponding switch is conducting. However, when the switch is turned off, the current through it doesn't immediately decreases to '0'. During this period, the diodes provide the alternate path to cycle the current still flowing through the switch.

This level of detail is useful for modeling the behavior of the converter. The output also gives a fair idea about the harmonics of the switching frequency introduced and any other discrepancies.

However, this is not the best model to start with, when testing controls and slower dynamics. These transient behaviors can significantly distort the performance of the controller in its initial design phase.

Therefore, a much simpler model, but with comparable steady state behavior is used initially. This model is also referred to as the 'Averaged Model' of the converter.

3.1.2 Averaged Model

The averaged model replaces the switches and associated phenomenon by equivalent current and voltage sources. Switching model can represent the transient behavior of the converter properly. However, its averaged nature is not immediately evident, especially at low switching frequencies. With an averaged model, the relationship between the modulation function and the system voltage/current is easily represented. The input and output can be modeled in terms of modulating functions and sources.

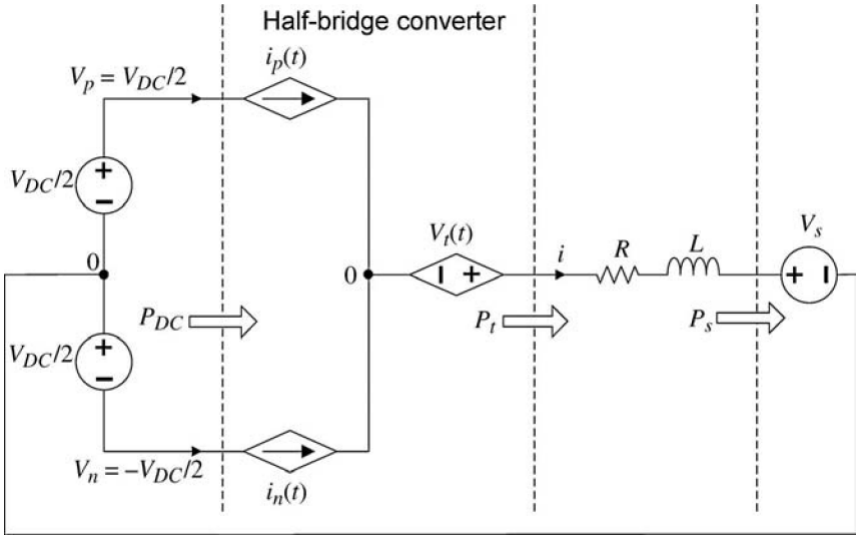

Figure 3.2: Equivalent Averaged Model for Half-bridge Converter

Figure 3.2 shows the averaged equivalent of the converter presented in Figure 3.1. In the following subsection, the differences between switching and averaged model will be contrasted. After that, the averaged model will be derived for a half-bridge converter.

3.1.3 Differences from a Switching Model

The differences between the two models is evident in the current output plot from ATP in Figure 3.3. The 'green' plot shows the actual output (switched behavior) from the switching model. The'red' plot is the output of its averaged equivalent. As the switching frequency is increased, the two become similar to each other.

3.2 Derivation of the Averaged Model

Figure 3.4 presents the relationship between the duty cycle of the two switches shown in Figure 3.1. With reference to Figure 3.4,

$$s_1(t) + s_4(t) \equiv 1 \tag{3.1}$$

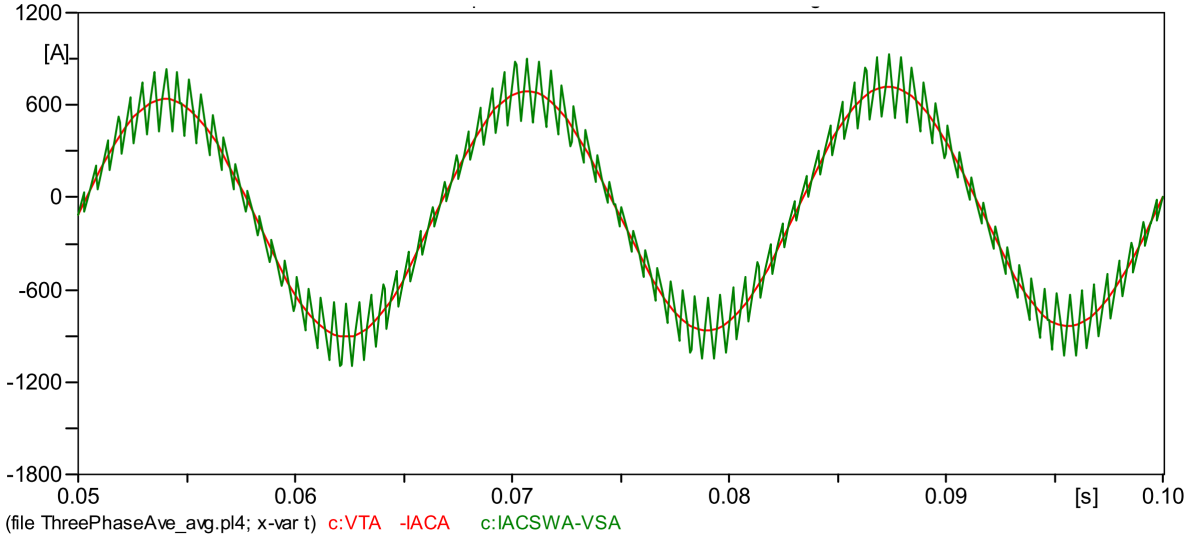

Figure 3.3: ATP Plot Showing the Difference Between Outputs From the Switching and Equivalent Averaged Model

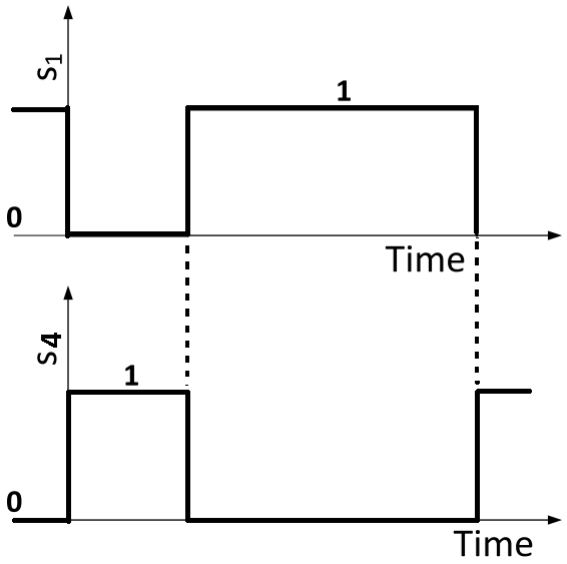

Figure 3.4: Switching States of the Two Switches in HB Arm

Here, $s_1(t)$ and $s_4(t)$ are the switching states of the switches Q_1 and Q_4 in Figure 3.1.

$$V_t(t) = \frac{V_{DC}}{2} s_1(t) - \frac{V_{DC}}{2} s_4(t) \tag{3.2}$$

$$i_p(t) = i s_1(t) \tag{3.3}$$

$$i_n(t) = is_4(t) \tag{3.4}$$

$$P_{DC}(t) = V_p i_p + V_n i_n = \frac{V_{DC}}{2}[s_1(t) - s_4(t)]i \tag{3.5}$$

We know that, the power transfer from the DC source, $P_{DC}(t)$, will be equal to the sum of power transferred across the terminals, $P_t(t)$ and the losses within the converter, $P_{loss}(t)$. Neglecting the switching losses and conductor losses,

$$P_{DC}(t) = P_t(t) \tag{3.6}$$

Therefore, from the circuit in Figure 3.2 and using (3.6), the AC power, $P_t(t)$ is given by,

$$P_t(t) = V_t(t)i = \frac{V_{DC}}{2}[s_1(t) - s_4(t)]i \tag{3.7}$$

Now, equating (3.6) and (3.7)

$$\boxed{V_t(t) = \frac{V_{DC}}{2}[s_1(t) - s_4(t)]} \tag{3.8}$$

$$\bar{s}_1(t) = d \tag{3.9}$$

$$\bar{s}_4(t) = 1 - d \tag{3.10}$$

Equations (3.8), (3.9), and (3.10) imply,

$$\boxed{V_t(t) = \frac{V_{DC}}{2}[2d - 1]} \tag{3.11}$$

Figure 3.5 shows the pulse width modulation for a simple DC-triangle Pulse Width Modulation (PWM). Analytically, as 'm' varies between limits -1 to +1, duty ratio, 'd', varies between limits 0 to 1.

$$d = \frac{1 + m}{2} \tag{3.12}$$

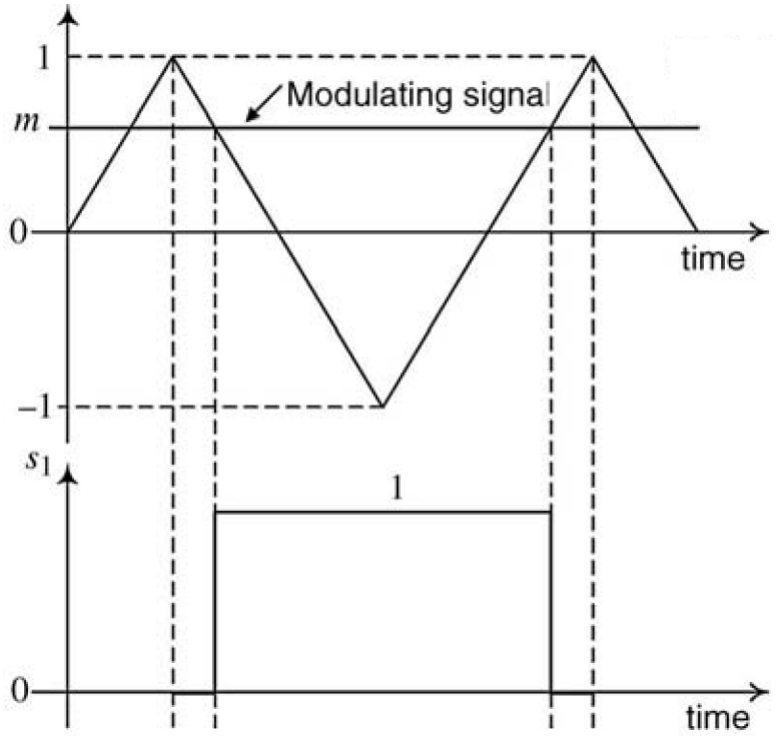

Figure 3.5: Plot for a Simple DC-triangle Pulse Width Modulation

Also, the same result can be derived using simple geometry.

Equations (3.3), (3.4), (3.11) and (3.12) imply that,

$$\boxed{V_t(t) = m\frac{V_{DC}}{2}} \tag{3.13}$$

$$\boxed{i_p(t) = i\frac{1+m}{2}} \tag{3.14}$$

$$\boxed{i_n(t) = i\frac{1-m}{2}} \tag{3.15}$$

Using the averaged converter model, it is possible to represent the terminal voltage, V_t as a controlled voltage source, in terms of the modulation function and the DC Bus voltage. These expressions will later be utilized in the grid side and rotor side controller blocks to obtain modulation functions from the regulated V_t required. Figure 3.6 presents a averaged model for the HB converter with parameters derived in this

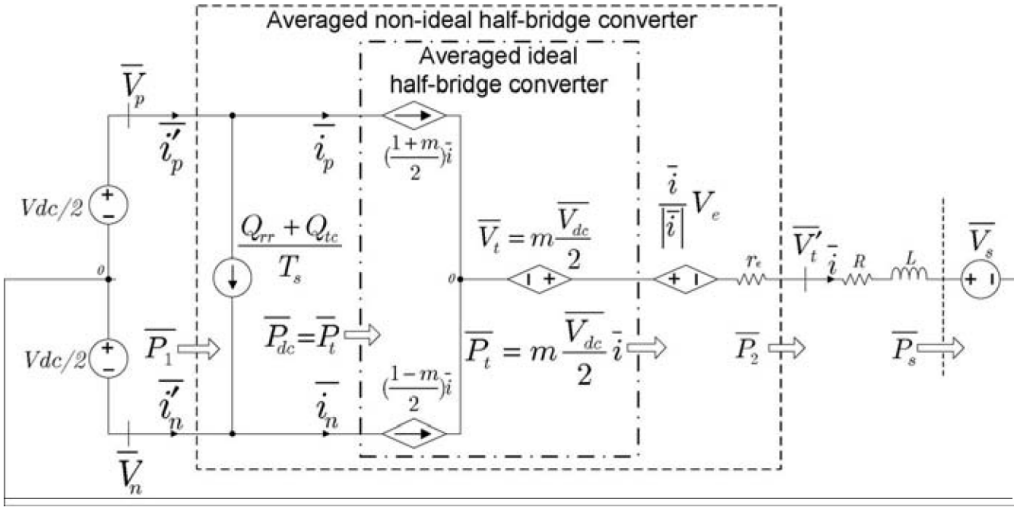

Figure 3.6: Equivalent averaged Model with derived parameters

chapter.

3.3 Summary

In this chapter, switching and averaged models of a half bridge rectifier were discussed. The differences between the two were contrasted. It is shown that averaged model is better for initial controller design. Later, switching model should be used to tune the controllers. Finally, the basic modulation equations to relate Pulse width modulation to terminal voltage are established. In the next chapter, the controller designs are discussed. *Note that, synchronous d-q reference frames will be used throughout. The details of the reference frames are described in Chapter 3 of [9].*

Note that, all the controller designs use synchronous reference frame. The reference frame being used has been described in [9]. The work has also been presented in [10].

Chapter 4: Type 3 Controller - Components

4.1 Grid Side Controller

4.1.1 Overview - Why and What?

The Grid Side Controller regulates the magnitude and direction of the power flow between VSC and the grid. Under rated conditions, *real power (close to generator rotor rating) will flow from the VSC to the grid.* The reactive power is usually regulated to zero. *Usually, the power output from the back-to-back VSCs is up to 30%* of the generator rating.

During *operation at speed less than rated, the amount of power flowing from the VSC into the grid will reduce.* The grid side controller may even import some power from the grid during periods of low wind speeds to continue generation from the stator.

4.1.2 Controller Design Assumptions

Consider an infinite DC source, with a fixed voltage across the terminals. This means that the source can supply any amount of current at the given voltage. With this said, *the inherent assumption behind all VSCs is that the DC Source voltage is constant.*

4.1.3 Controller Design

Reference commands on power set points, $P_{sref}(t)$ and $Q_{sref}(t)$, are derived using the real and reactive power set points respectively. To do so, corresponding d and q frame reference currents will be calculated in subsection 4.1.3.1. Note that, synchronous dq reference frame used here assumes that 'q' leads 'd' by $frac\pi 2$ radians. The reference current thus obtained, will be tracked by controlling the switching of the converter

phases. The regulator to accomplish this will be presented in 4.1.3.3.

4.1.3.1 Current Reference Generators

We know that, three phase power in a system is given by,

$$S(t) = \frac{3}{2}\vec{v(t)}\vec{i^*(t)} \tag{4.1}$$

Therefore, real power,

$$P(t) = Re\left\{\frac{3}{2}\vec{v(t)}\vec{i^*(t)}\right\} \tag{4.2}$$

and reactive power,

$$Q(t) = Im\left\{\frac{3}{2}\vec{v(t)}\vec{i^*(t)}\right\} \tag{4.3}$$

In the synchronous dq reference frame considering that 'q' leads 'd' by 90°,

$$\vec{f(t)} = (f_d + jf_q)e^{j\rho(t)} \tag{4.4}$$

So,

$$\vec{v(t)} = (v_d + jv_q)e^{j\rho(t)} \tag{4.5}$$

and

$$\vec{i^*(t)} = (i_d - ji_q)e^{j\rho(t)} \tag{4.6}$$

Substituting these values in equation (4.2), we get,

$$P(t) = \frac{3}{2}\left[v_d(t)i_d(t) + v_q(t)i_q(t)\right] \tag{4.7}$$

and,

$$Q(t) = \frac{3}{2}\left[-v_d(t)i_q(t) + v_q(t)i_d(t)\right] \tag{4.8}$$

4.1.3.2 Grid Side Power Flow - Current Mode control

Based on the above equations, the AC system side power flow can be calculated as:

$$P_s(t) = \frac{3}{2}\left[V_{sd}(t)I_{sd}(t) + V_{sq}(t)I_{sq}(t)\right] \tag{4.9}$$

and,

$$Q(t) = \frac{3}{2}\left[-V_{sd}(t)I_{sq}(t) + V_{sq}(t)I_{sd}(t)\right] \tag{4.10}$$

A PLL (Section 4.4) is being used to track the frequency. When the PLL is tracking the frequency properly,

$$V_{sq} = 0; \tag{4.11}$$

In this case, equations (4.9) and (4.10) simplify to,

$$P_{sPLL}(t) = \frac{3}{2}\left[V_{sd}(t)I_{sd}(t)\right] \tag{4.12}$$

and,

$$Q_{sPLL}(t) = \frac{3}{2}\left[-V_{sd}(t)I_{sq}(t)\right] \tag{4.13}$$

Therefore, the reference currents i_{dref} and i_{qref} can be calculated as:

$$i_{dref}(t) = \frac{1}{V_{sd}}\frac{2}{3}P_{sPLL}(t)) \tag{4.14}$$

and,

$$i_{qref}(t) = \frac{-1}{V_{sd}}\frac{2}{3}Q_{sPLL}(t) \tag{4.15}$$

$P_{sref}(t)$ and $Q_{sref}(t)$ are the reference power-set points which can be defined by the user or regulated by an outer control loop. For the grid side power controller, ideally, reactive power flow, $Q_{sref}(t)$, will be set to '0'. $P_{sref}(t)$ will be regulated by a DC power port Voltage regulator, which is described in detail in Section 4.2.

4.1.3.3 Inner Current Regulator

For the system shown in the Figure 4.1, let V_t and V_s be the phase voltages at the two ends of the line. I_s is the current flowing from the converter through the R-L network.

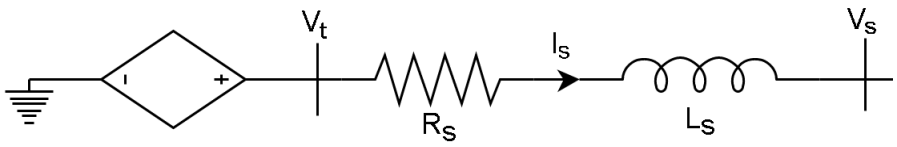

Figure 4.1: AC Side of Averaged Model Equivalent System for Grid Side Power Regulator Design

By Kirchoff's Voltage Law (KVL) on Figure 4.1,

$$V_{tabc} = V_{sabc} + R_s I_{sabc} + L_s \frac{\mathrm{dI_{sabc}}}{\mathrm{dt}} \tag{4.16}$$

The notation is explained in chapter 2 of [9]. Multiplying $Ae^{-j\Theta(t)}$ to both sides, where $A = \frac{2}{3}\begin{bmatrix} 1 & a & a^2 \end{bmatrix}$, we get,

$$Ae^{-j\Theta(t)}V_{tabc} = Ae^{-j\Theta(t)}V_{sabc} + R_s Ae^{-j\Theta(t)}I_{sabc} + L_s Ae^{-j\Theta(t)}\frac{\mathrm{dI_{sabc}}}{\mathrm{dt}}$$

Converting to dq frame,

$$\bar{V}_{tdq} = \bar{V}_{sdq} + R_s \bar{I}_{sdq} + L_s Ae^{-j\Theta(t)}\frac{\mathrm{dI_{sabc}}}{\mathrm{dt}} \tag{4.17}$$

By product rule,

$$d(xy) = ydx + xdy$$

or,

$$xdy = d(xy) - ydx$$

Therefore,

$$Ae^{-j\Theta(t)}\frac{\mathrm{dI_{sabc}}}{\mathrm{dt}} = \frac{\mathrm{d}\left(\mathrm{Ae^{-j\Theta(t)}I_{sabc}}\right)}{\mathrm{dt}} - I_{sabc}Ae^{-j\Theta(t)} - j\frac{\mathrm{d\Theta(t)}}{\mathrm{dt}} = \frac{\mathrm{d\bar{I}_{sdq}}}{\mathrm{dt}} + j\bar{I}_{sdq}\frac{\mathrm{d\Theta(t)}}{\mathrm{dt}}$$

(4.17) transforms to,

$$\bar{V}_{tdq} = \bar{V}_{sdq} + R_s\bar{I}_{sdq} + L_s\frac{\mathrm{d\bar{I}_{sdq}}}{\mathrm{dt}} + jL_s\bar{I}_{sdq}\frac{\mathrm{d\Theta(t)}}{\mathrm{dt}} \tag{4.18}$$

Using the synchronous dq reference frame as defined previously,

$$(V_{td} + jV_{tq}) = V_{sd} + jV_{sq} + R_s\left(I_{sd} + jI_{sq}\right) + L_s\frac{\mathrm{d\left(I_{sd} + jI_{sq}\right)}}{\mathrm{dt}} + jL_s\left(I_{sd} + jI_{sq}\right)\omega(t)$$

Separating the real and imaginary parts from the equation, we get,

$$V_{td} = V_{sd} + R_sI_{sd} + L_s\frac{\mathrm{d\left(I_{sd}\right)}}{\mathrm{dt}} - L_sI_{sq}\omega \tag{4.19}$$

and,

$$V_{tq} = V_{sq} + R_sI_{sq} + L_s\frac{\mathrm{dI_{sq}}}{\mathrm{dt}} + L_sI_{sd}\omega \tag{4.20}$$

Equations (4.19) and (4.20) give the basic structure of the dq current controllers. For Equation, (4.19), taking the Laplace transform,

$$V_{td}(s) = V_{sd}(s) + \left(R_s + sL_s\right)I_{sd} - L_sI_{sq}(s)\omega \tag{4.21}$$

Here, circuit's 'R' and 'L' result in $(R_s + sL_s)$ which behaves as a Proportional - Integral (PI) Controller. The resulting feedback control block will be replaced with 'u_d'. The control equation is therefore,

$$V_{td}(s) = V_{sd}(s) + u_d - L_sI_{sq}\omega \tag{4.22}$$

Using (3.13), we get,

$$m_d = \frac{2}{V_{DC}} \left(V_{sd} + u_d - L_s I_{sq} \omega \right) \tag{4.23}$$

Similarly, from (3.13) and (4.20), we can obtain,

$$m_q = \frac{2}{V_{DC}} \left(V_{sq} + u_q + L_s I_{sd} \omega \right) \tag{4.24}$$

It may be noted that, the dynamics of the 'd' and 'q' frames are cross-coupled. Therefore, the dynamics of any of the references will effect the other frame as well.

Figure 4.2 shows the resulting inner current controller for grid side converter.

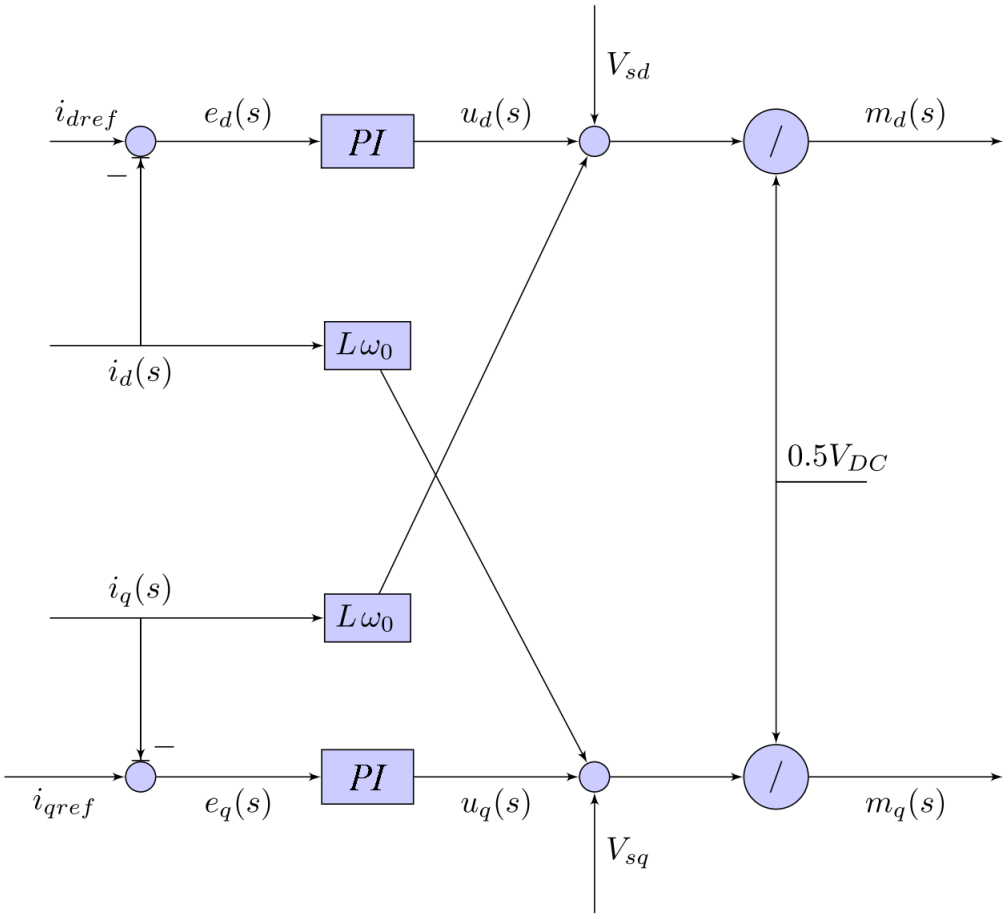

Figure 4.2: Block Diagram: Grid Side Current Regulator

The grid side controller has been successfully implemented in RSCAD as shown in Figure 4.3.

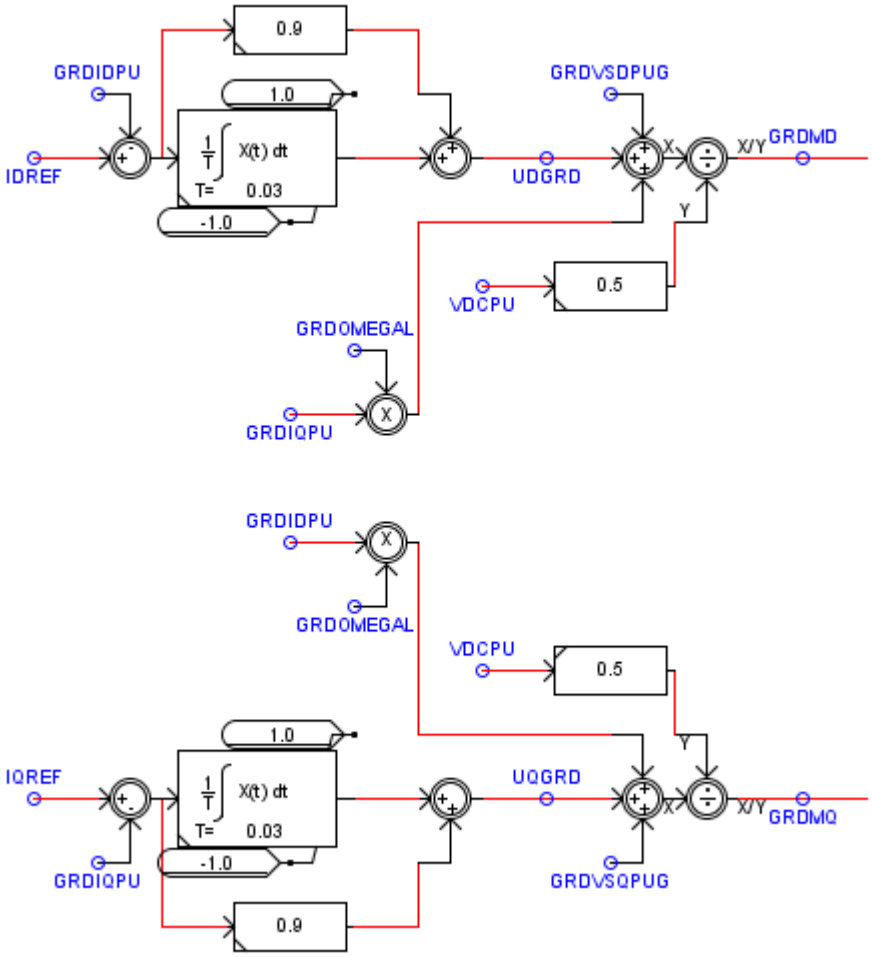

Figure 4.3: Grid Side Controller implementation in RSCAD

4.2 DC Power Port Voltage Regulator

A DC power port voltage regulator (hereafter referred as 'DC regulator') is essential for the back-to-back VSC scheme. Section 4.1.2 states that the controller assumes an ideal DC Source. But, ideal sources with fixed voltage do not exist. If, however, the DC link voltage can be regulated, the grid side controller designed previously can still be used. The DC regulator accomplishes this.

During subsynchronous operation, power will flow to the Rotor via the DC link to the grid side. Here, the grid becomes the source, and rotor becomes the load. At any point of time, the net power input to the DC Link must be equal to the power

out, irrespective of the direction of power flow. If "$P_{in} > P_{out}$", the DC Link voltage will rise. If "$P_{in} < P_{out}$", the DC Link voltage will fall.

If the reference power for grid side, P_{sref}, is regulated to keed V_{DC} fixed, this can be accomplished.

4.2.1 Controller Design

For a capacitor 'C_{dc}', the energy stored, E_{dclink}, is given by,

$$E_{dclink} = \frac{1}{2} C_{dc} V_{dc}^2 \tag{4.25}$$

There is a quadratic relation between V_{dc} and E_{dclink}. Therefore, the controls will be more complicated. But, if the relation between the input and output can be linearized, the design will be simplified. To accomplish this, V_{dc}^2 is treated as the control variable instead of V_{dc}. The scheme is implemented using a compensation scheme as shown in Figure 4.4.

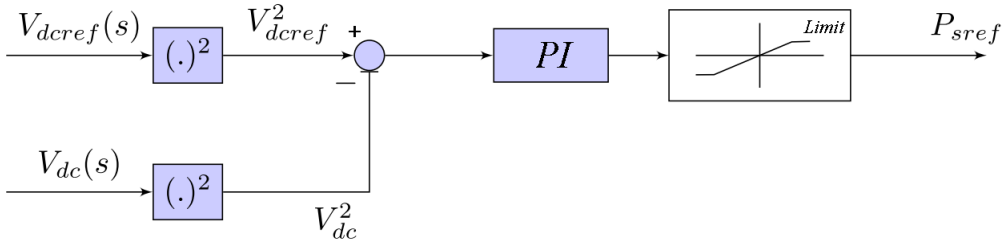

Figure 4.4: Block Diagram: DC Link Voltage Regulator

The controller has been successfully implemented in RSCAD as shown in Figure 4.5.

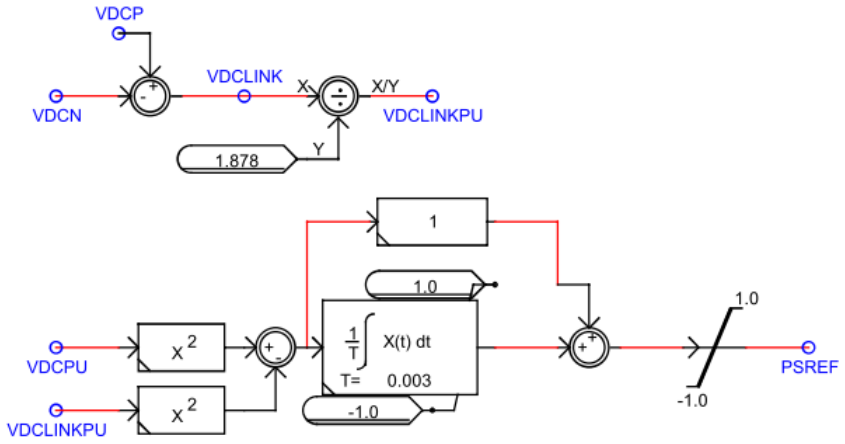

Figure 4.5: DC Link Voltage Regulator implementation in RSCAD

4.3 Rotor Side Controller

4.3.1 Overview - Why and What?

The Rotor Side Controller regulates the flux in the DFIG. *For supersynchronous speeds, it extracts the power from the rotor and supplies it to the grid via the DC link and the grid side controller. During subsynchronous operation, it imports power from the grid to excite the rotor. This regulates the optimum flux to produce maximum torque for any given frequency.*

Since, the rotor current changes its magnitude and frequency with the slip, this controller needs to accurately track the frequency over a wide range to ensure proper operation using Phase Locked Loops (Section 4.4).

4.3.2 Controller Design

Reference flux and corresponding 'd' and 'q' rotor currents are calculated based on the precalculated optimum torque for the given wind speed. The controller implements the machine model including a PI controller to track the currents. The design to accomplish this has been presented in 4.3.2. In the following description, the variables have their usual meaning, with reference to an Induction machine.

In a space phasor representation, the flux,

$$\vec{\lambda_s} = \widehat{\lambda}_s e^{j\theta(t)} \tag{4.26}$$

where θ is the angle of the space vector as a function of time. The angle θ can be defined as:

$$\theta(t) = \rho(t) + \theta_r(t) \tag{4.27}$$

Using (4.27), (4.26) can be re-written as:

$$\vec{\lambda_s} = \widehat{\lambda}_s e^{j(\rho+\theta_r)} \tag{4.28}$$

From the mathematical model of a three phase induction machine [9], we know that,

$$v_{ds} = r_s i_{ds} + \frac{\mathrm{d}\lambda_{\mathrm{ds}}}{\mathrm{dt}} - \omega\lambda_{qs} \tag{4.29}$$

$$v_{qs} = r_s i_{qs} + \frac{\mathrm{d}\lambda_{\mathrm{qs}}}{\mathrm{dt}} + \omega\lambda_{ds} \tag{4.30}$$

$$v_{0s} = r_s i_{0s} + \frac{\mathrm{d}\lambda_{\mathrm{0s}}}{\mathrm{dt}} \tag{4.31}$$

where,

$$\lambda_{ds} = L_{ls} i_{ds} + L_m(i_{ds} + i'_{dr}) \tag{4.32}$$

$$\lambda_{qs} = L_{ls} i_{qs} + L_m(i_{qs} + i'_{qr}) \tag{4.33}$$

$$\lambda_{0s} = L_{ls} i_{0s} \tag{4.34}$$

For the rotor,

$$v'_{dr} = r'_r i'_{dr} + \frac{\mathrm{d}\lambda_{\mathrm{dr}}}{\mathrm{dt}} - (\omega - \omega_r)\lambda_{qr} \tag{4.35}$$

$$v'_{qr} = r'_r i'_{qr} + \frac{\mathrm{d}\lambda_{\mathrm{qr}}}{\mathrm{dt}} + (\omega - \omega_r)\lambda_{dr} \tag{4.36}$$

$$v'_{0r} = r'_r i'_{0r} + \frac{\mathrm{d}\lambda_{\mathrm{0r}}}{\mathrm{dt}} \tag{4.37}$$

where,

$$\lambda'_{dr} = L'_{lr} i'_{dr} + L_m(i_{ds} + i'_{dr}) \tag{4.38}$$

$$\lambda'_{qr} = L'_{lr} i'_{qr} + L_m(i_{qs} + i'_{qr}) \tag{4.39}$$

$$\lambda'_{0r} = L'_{lr} i'_{0r} \tag{4.40}$$

The Machine's stator and rotor leakage factors are given by σ_s and σ_r, defined as:

$$\sigma_s = \frac{L_s}{L_m} - 1 \tag{4.41}$$

and,

$$\sigma_r = \frac{L'_r}{L_m} - 1 \tag{4.42}$$

The Machine's total leakage factor, σ is defined as:

$$\sigma = 1 - \frac{1}{(1 + \sigma_r)(1 + \sigma_s)} \tag{4.43}$$

In Synchronous frame, $\omega = \omega_s$, and $\omega_r = \frac{\mathrm{d}\theta_{\mathrm{r}}}{\mathrm{dt}}$

Therefore, in space vector notation, equations (4.29) - (4.43) can be re-written as:

$$\frac{\mathrm{d}\vec{\lambda_s}}{\mathrm{dt}} = \vec{V_s} - R_s \vec{i_s} \tag{4.44}$$

$$\frac{\mathrm{d}\vec{\lambda_r}}{\mathrm{dt}} = \vec{V_r} - R_r \vec{i_r} \tag{4.45}$$

$$\vec{\lambda_s} = L_m \left[(1 + \sigma_s)\vec{i_s} + e^{j\theta_r} \vec{i_r} \right] \tag{4.46}$$

$$\vec{\lambda_r} = L_m \left[(1+\sigma_r)\vec{i_r} + e^{-j\theta_r}\vec{i_s} \right] \tag{4.47}$$

Using (4.28) and (4.46), we get,

$$\vec{i_s} = \frac{\widehat{\lambda} e^{j\rho} - L_m \vec{i_r}}{(1+\sigma_s)L_m} e^{j\theta_r} \tag{4.48}$$

Now, equations (4.47) and (4.48) imply

$$\vec{\lambda_r} = \sigma(1+\sigma_r)L_m \vec{i_r} + \frac{1}{1+\sigma_s}\widehat{\lambda_s} e^{j\rho} \tag{4.49}$$

Using equations (4.41), (4.42), (4.43) and (4.51), we get,

$$\left(\sigma\tau_r \frac{\mathrm{di_{rd}}}{\mathrm{dt}} + i_{rd} \right) = \sigma\tau_r \omega i_{rq} - \frac{(1-\sigma)\tau_r}{L_m} \frac{\mathrm{d}\widehat{\lambda_s}}{\mathrm{dt}} + \frac{V_{rd}}{R_r} \tag{4.50}$$

$$\left(\sigma\tau_r \frac{\mathrm{di_{rq}}}{\mathrm{dt}} + i_{rq} \right) = -\sigma\tau_r \omega i_{rd} - \frac{(1-\sigma)\tau_r}{L_m} \omega\widehat{\lambda_s} + \frac{V_{rq}}{R_r} \tag{4.51}$$

Using $u_d = \sigma\tau_r \frac{\mathrm{di_{rd}}}{\mathrm{dt}} + i_{rd}$ and $u_q = \sigma\tau_r \frac{\mathrm{di_{rq}}}{\mathrm{dt}} + i_{rq}$, the controller equations can be presented as equations (4.52) and (4.53).

$$\boxed{V_{rd} = R_r \left[u_d - \sigma\tau_r \omega i_{rq} + \frac{(1-\sigma)\tau_r}{L_m} \frac{\mathrm{d}\widehat{\lambda_s}}{\mathrm{d}t} \right]} \tag{4.52}$$

$$\boxed{V_{rq} = R_r \left[u_q + \sigma\tau_r \omega i_{rd} + \frac{(1-\sigma)\tau_r}{L_m} \omega\widehat{\lambda_s} \right]} \tag{4.53}$$

It may be noted that, similar to the grid side controller, the dynamics of 'd' and 'q' frames are cross-coupled for the rotor side too. In addition, regulating the flux of the machine, regulates the current.

Figure 4.6 shows the resulting controller for Rotor Side.

The rotor side controller has been successfully implemented in RSCAD as shown in Figure 4.7.

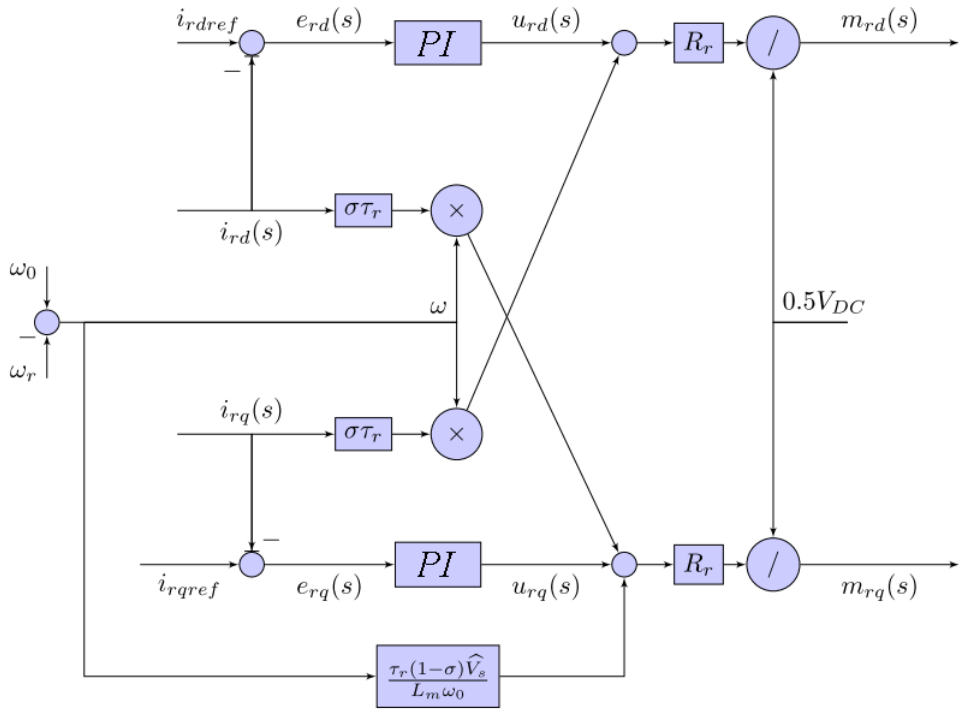

Figure 4.6: Block Diagram: Rotor Side Current Regulator

4.4 PLL Implementation

A PLL is necessary for maintaining the synchronous DQ reference frame. They track the frequency and angle of the output voltages and currents in the given system.

4.4.1 Grid Side Frequency Tracking

For the grid side, an atan2 type PLL block is used to implement the frequency tracking for the grid side. The principle utilizes an ABC to α-β conversion to extract the real and imaginary parts of the 3-phase quantity being tracked. This information is passed through a feed-forward block with PI controller among others [4]. Base frequency is 60Hz. The block diagram for the *atan2 controller* is presented in Figure 4.8.

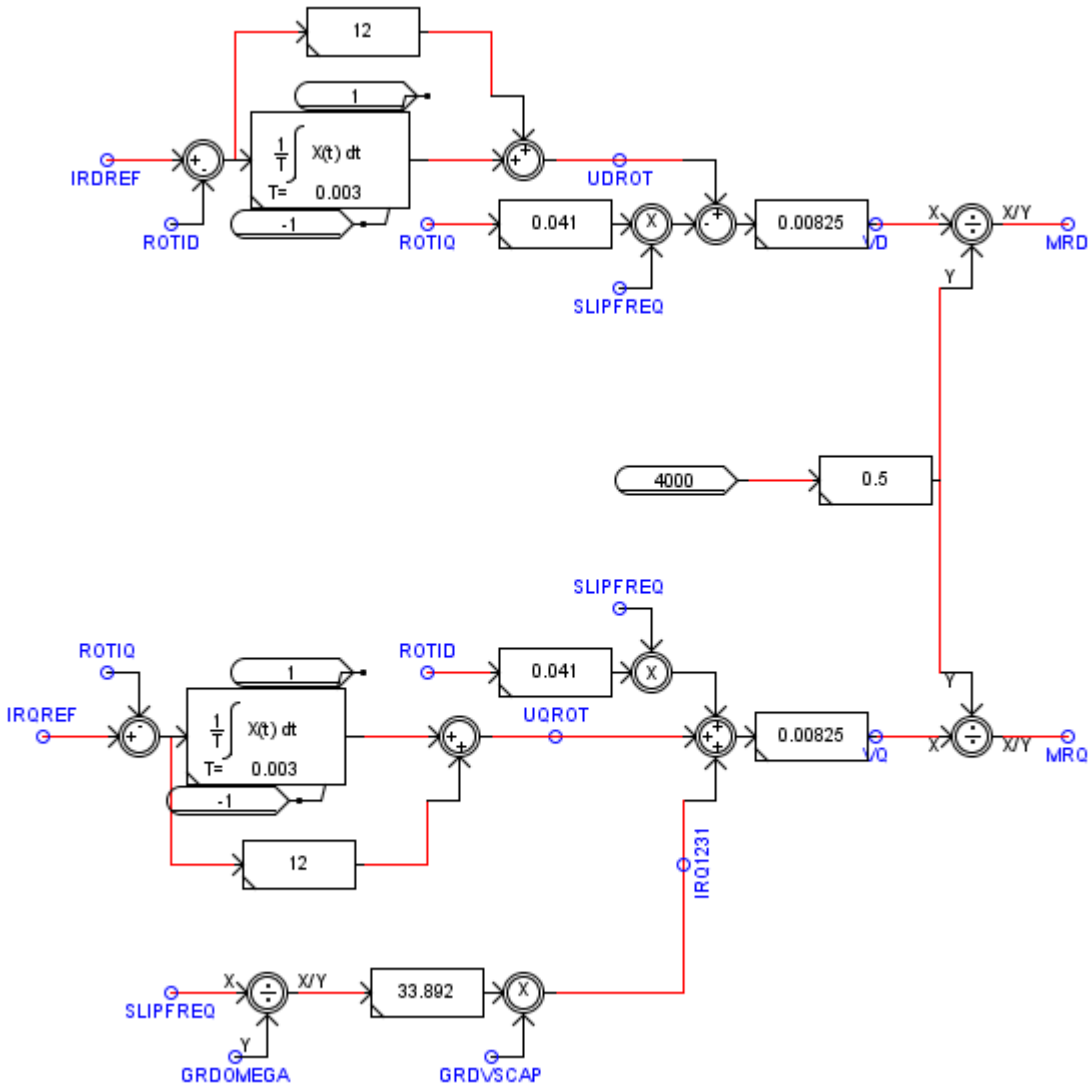

Figure 4.7: Rotor Side Controller implementation in RSCAD

4.4.2 Rotor Side Frequency Tracking

The Rotor side frequency has a broad window. It is difficult to set a base frequency for the rotor current, and then implement a PI-based PLL.

Therefore, an alternate method to track the frequency of the rotor current was used. The Machine's Slip depends on the rotor speed. This slip is directly proportional to the frequency of the current induced in the rotor. Therefore, by tracking the rotor speed, frequency of the rotor current can be accurately tracked. For the

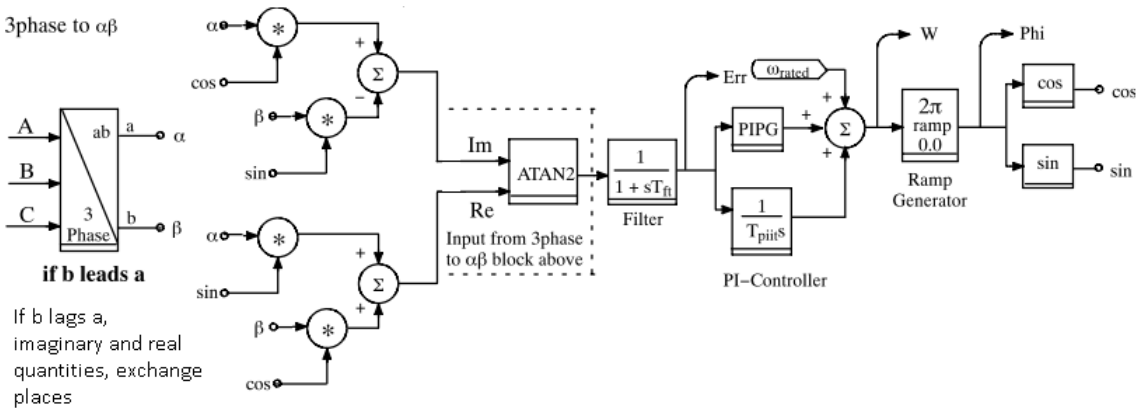

Figure 4.8: Block Diagram for 'atan2' Based Phase Locked Loop [4] - Grid side PLL

implementation in the model, the rotor angle is measured from the machine and then used to track slip frequency of the machine, instead of a conventional PLL.

PLL for the rotor side controller has been successfully implemented in RSCAD as shown in Figure 4.9.

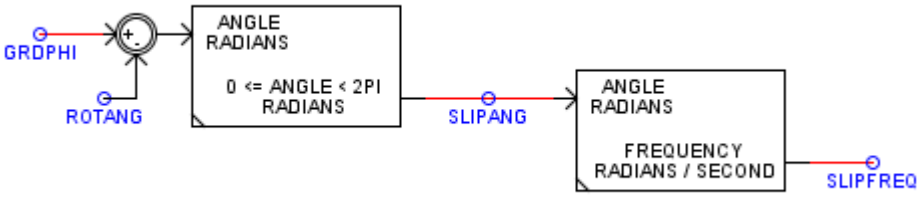

Figure 4.9: Implementation of PLL for Rotor Side Controller in RSCAD

4.5 Summary

In this chapter, the design of the type 3 controllers and underlying principles were visited. The requirement and implementation of a DC Voltage regulator is discussed. It is observed that the tracking of frequency is necessary for both grid and rotor side controllers. Therefore, phase locked loops (PLLs) are implemented. Grid and rotor side controllers implement different methods to track the frequency of their corresponding sides.

In the next chapter, the test network is discussed and the modeling parameters are presented.

Chapter 5: The Test Network

5.1 Setup

The basic DFIG design parameters used in this work were adopted from [11]. A 'one' wind turbine system is modeled using the averaged model of a VSC. After designing stable controllers for the type-3 system using the averaged model [11], the controllers were implemented for its switching model, building on the work from earlier chapters. The averaged model helped with initial converter design by eliminating the effect of switching transients and harmonics on the behavior. *The digital filters in protective relays will remove this behavior, so the averaged model is useful for protection studies. It still captures the dynamics that do impact relay response. The converter is then efficiently fine-tuned using a switching model.* Comparing the averaged model with its switching counterpart serves as a check on the modeling process.

Next, the different components of the test network are discussed.

5.1.1 A 10-Machine Aggregated Type 3 Model

The model developed in chapter 4 is being used as the Type 3 source. It may be noted, that wind farms are usually rated for 100MW or more. This aggregated setup is rated for 18MW and represents the condition when the wind speed is not uniform across the farm, and the generation of the farm is below par.

Parameters for the doubly fed induction generator are given in the table 5.1 as under:

5.1.2 Transformers

Two transformers are used in this test network.

Quantity	*Value (units)*	*Value(p.u.)*	*Notes*
Base Power	1.678MW	1.0	Rated Power for one unit
Base Voltage	1878V	1.0	L-N Peak Voltage
Base Current	596A	1.0	Peak Value
Base Frequency	377rad/s	1.0	ω_0, ω_{base}
Base Torque	4451 Nm	1.0	Electrical Torque
n_{rotor}/n_{stator}	1.0		Rotor to Stator Turns ratio
Rs	29mΩ	0.00920	
Rr	26mΩ	0.00825	Includes R_{ON} of the Switches
Lm	34.52mH	4.130	
Ls	34.12mH	4.202	
Lr	34.12mH	4.202	

Table 5.1: Parameters for the Doubly Fed Induction Generator for Type 3 System

a. A three winding transformer is located inside the turbine. It is used to step up the power produced at 2.3kV L-L to 22kV L-L. Its parameters are given in table 5.2:

Parameter	Value
Rated MVA	100 MVA
Rated Voltage (Winding 1)	22kV - Delta connected
Rated Voltage (Winding 2)	2.3kV - Wye connected
Rated Voltage (Winding 3)	2.3kV - Wye connected
Positive Sequence Leakage reactance	0.01 pu
Leakage Current	1%
No load losses	0.01pu

Table 5.2: Parameters for the 3-winding transformer used in the Test Network

b. TRF2: This transformer steps up the power generated in the farm from 22kV to 230kV for transmission using the Main line to rest of the Grid. Its parameters are given in the table 5.3 as under:

5.1.3 The Transmission Lines

Two transmission line design are used in this model, namely:

Parameter	Value
Rated MVA	100 MVA
Rated Voltage (Winding 1)	22kV - Delta connected
Rated Voltage (Winding 2)	230kV - Wye connected
Positive Sequence Leakage reactance	0.1 pu
Leakage Current	1%
No load losses	0.01pu

Table 5.3: Parameters for the Main transformer used in the Test Network

5.1.3.1 The 22kV Collector

As the name suggests, a collector 'collects' the generated power within the Wind farm, and carries it to the main transmission line. It is rated for 22kV. The tower configuration and line details [12] are given in Figures 5.1 and 5.2.

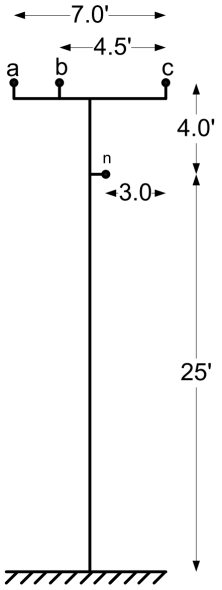

Figure 5.1: Tower Configuration for the 22kV Collector Line

5.1.3.2 The 230kV Transmission Line

Main transmission line collects the power from the Wind farm and supplies it to the grid. It is usually longer than the collector and is rated for 230kV. The tower configuration and line details [**?**] are given in Figures 5.3 and 5.4.

```
UNITS ( Metric or Imperial ):   Metric
# of Bundles:                   3
# of Ground Wires:              1

-------------------------------- MAIN DATA --------------------------
Ground Resistivity (ohm-m):     100.0
Line Length(km):                10.0

------------------------------ CONDUCTOR DATA ------------------------
Conductor # ---->                 1            2            3
Conductor Name:                  336400 ACSR 336400 ACSR 336400 ACSR
Conductor Type(AC/DC):          AC           AC           AC
V(kV)(AC:L-L,rms/DC:L-G,pk):             22.0         22.0         22.0
V Phase(Deg.):                            0.0       -120.0        120.0
Line I (kA)(AC:rms/DC:pk):               100.0        100.0        100.0
Line I Phase(Deg.):                       20.0       -100.0        140.0
# of Sub-Conductors:                        2            2            2
Sub-Cond Radius(cm):                     0.864        0.864        0.864
Sub-Cond Spacing(cm):                    15.72        15.72        15.72
Horiz. Dist. X(m):                        0.0        0.762        1.372
Height at Tower Y(m):                    8.839        8.839        8.839
Sag at Midspan(m):                        0.8          0.8          0.8
DC Resistance(ohms/km):                  0.19         0.19         0.19

---------------------------- GROUND WIRE DATA ------------------------
Ground Wire # ---->                1
Conductor Name:                   4/0 6/1 ACSR
Cond Radius(cm):                         0.715
Horiz. Dist. X(m):                       1.219
Height at Tower Y(m):                     7.62
Sag at Midspan(m):                         0.8
DC Resistance(ohms/km):                  0.368
```

Figure 5.2: Impedance and Conductor details for the 22kV Collector Line

5.1.4 The Real Time Digital Simulator

The RTDS is a power system simulator based on hardware-in-the-loop technique. The system consists of a dedicated set of processors, optional cards for additional input/output, networking, and synchronization capabilities. For this study, the RTDS will directly feed the line voltage and current signals to the protection relays using the low l. So, the protection schemes can be tested in real time. In addition, it offers

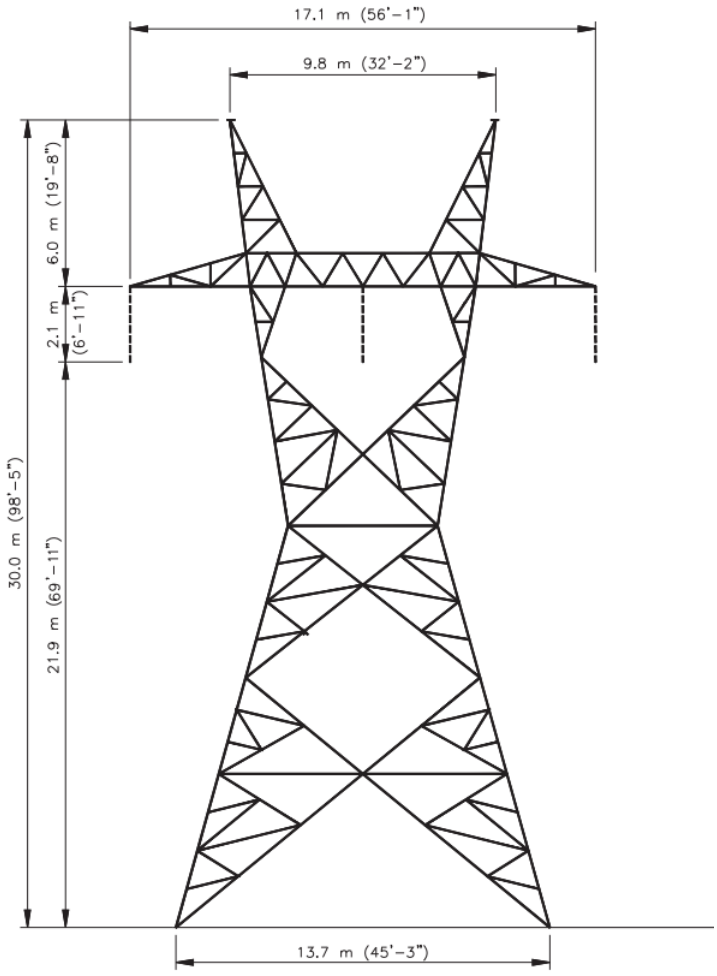

Figure 5.3: Tower Configuration for the 230kV Collector Line

a ''Runtime" which can be used to interact with the model, as it would be, for an actual system. Therefore, development pace improves significantly.

Need for the RTDS:

The Electromechanical relays needed a significant primary current (couple of amperes) to operate. However, digital relays work with with low-level signals. CTs and PTs within the relay, scale down the secondary input V/I values to the mV range. A/D block will then convert these signals for the relay's low-level interface into digital bits for further processing. The output from the analog output cards of the RTDS is directly fed into the low level interface using a GTAO card. An additional scaling factor is included in the model to match the outputs of the RTDS to the acceptable

```
UNITS ( Metric or Imperial ):   Metric
# of Bundles:                  3
# of Ground Wires:             2

--------------------------------- MAIN DATA ----------------------------
Ground Resistivity (ohm-m):     100.0
Line Length(km):                30.0

------------------------------- CONDUCTOR DATA -------------------------
Conductor # ---->                 1            2            3
Conductor Name:                      Mallard      Mallard      Mallard
Conductor Type(AC/DC):          AC           AC           AC
V(kV)(AC:L-L,rms/DC:L-G,pk):           230.0        230.0        230.0
V Phase(Deg.):                           0.0       -120.0        120.0
Line I (kA)(AC:rms/DC:pk):               5.0          5.0          5.0
Line I Phase(Deg.):                     20.0       -100.0        140.0
# of Sub-Conductors:                      2            2            2
Sub-Cond Radius(cm):                  1.405        1.405        1.405
Sub-Cond Spacing(cm):                 45.72        45.72        45.72
Horiz. Dist. X(m):                    -8.55          0.0         8.55
Height at Tower Y(m):                  21.9         21.9         21.9
Sag at Midspan(m):                   5.4864       5.4864       5.4864
DC Resistance(ohms/km):             0.03206      0.03206      0.03206

----------------------------- GROUND WIRE DATA -------------------------
Ground Wire # ---->               1            2
Conductor Name:                   7/16 Steel   7/16 Steel
Cond Radius(cm):                        0.45         0.45
Horiz. Dist. X(m):                      -4.8          4.8
Height at Tower Y(m):                   30.0         30.0
Sag at Midspan(m):                    6.096        6.096
DC Resistance(ohms/km):              2.8645       2.8645
```

Figure 5.4: Impedance and Conductor details for the 230kV Collector Line

limits for the relay. These scaling factors are design specific. For the relays in use,

$$66.6\text{mV at nominal current (1A or 5A)} \tag{5.1}$$

$$446\text{mV at nominal voltage (67V L-N)} \tag{5.2}$$

The scaling factors are therefore given as equations (5.3) and (5.4):

$$scal_I = 5A.\frac{5V}{66.6mV} = 375.375A \tag{5.3}$$

$$scal_V = 5V.\frac{5V}{446mV} = 751.121V \tag{5.4}$$

The output currents and voltages from the RTDS will be scaled by these factors respectively.

5.2 Test Network

The components of the test network discussed previously in this chapter are used to form a test power system setup. The one line diagram of the test network along with the schematic of Type 3 system is presented in Figure 5.5.

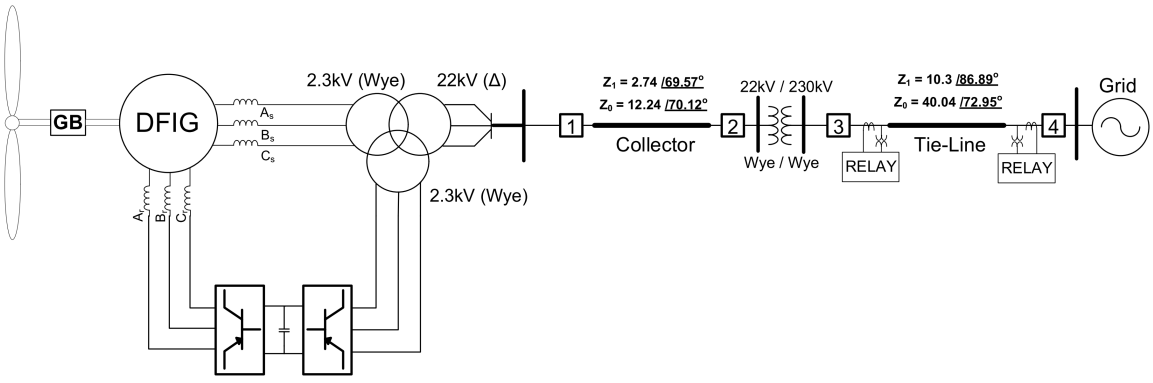

Figure 5.5: Schematic - Type 3 Wind Farm Test Network

This setup will be used to simulate a variety of faults on the main transmission line. Both ends of the line will be monitored by one line protection relay each. The relays are set to provide line current differential and distance element protection.

5.3 Summary

In this chapter, design parameters for the DFIG, and associated collector and main transmission lines along with their transformers are presented. At the end, one line

diagram of the test network diagram is presented.

In the next chapter, operation of the developed model will be discussed. It will be validated against standard published results of normal and fault response.

Chapter 6: Validation and Operation

After finishing the initial design, the accuracy of the model needs to be established. This is done by benchmarking the system for different criteria of steady-state operation and fault response. Reference behavior data are obtained from other published sources, and field event data from physical systems in operation.

6.1 Averaged Single Turbine Model

The machine model is validated using the machine's torque speed characteristics. The system integrated with the test grid is validated for its controller performance by observing the power output for normal operation. Then, the fault response is compared to an event from [5].

6.1.1 Validation

6.1.1.1 Torque - Speed Characteristics

A DFIG Model block is available from standard libraries for the RTDS. Its rotor ends are shorted to have it behave like a WRIG. Therefore, during the test, the rotor side controllers will have no influence on the behavior of the machine. This model and the machine parameters are validated by plotting its torque speed characteristics. For the given test, speed is ramped up from 0 to 2 p.u. in 2 seconds. Also, supply voltage is constant and equal to the rated voltage of the machine model (2.2kV L-L at 60Hz in this case). Also, the rotor terminals are shorted to eliminate the influence of the Type 3 controllers on the machine characteristics. Torque speed characteristics for the modeled machine are plotted as shown in Figure 6.1.

The characteristics are similar to those presented in [13]. This verifies behavior of the machine model. The initial oscillation in plot is due to the start-up transient of

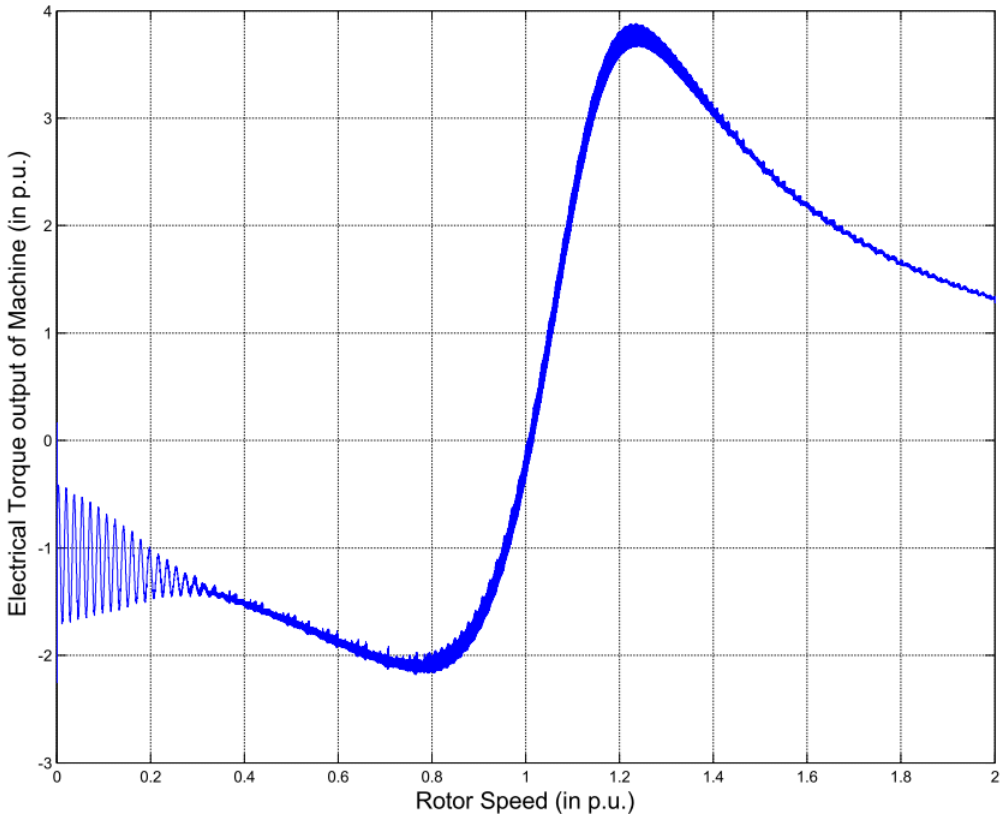

Figure 6.1: Torque v/s Speed Characteristics for a Doubly Fed Generator

the machine.

6.1.1.2 Normal Operation

The validated DFIG model is connected with a back-to-back VSC. The setup is used to implement a Type 3 wind generation system. Figure 6.2 shows the output stator and rotor power with respect to rotor speed.

Around synchronous speed, power output from the rotor changes direction acoording to the slip but power output from the stator remains relatively constant. For wind speeds below the rated, the rotor would rotate at a subsynchronous speed. Therefore, some power needs to flow from the grid to the rotor to artificially excite the rotor at an appropriate frequency. The stator can still produce near rated power for speeds marginally below the synchronous speed. As the rotor speed nears the synchronous

speed, power consumption of the rotor decreases to almost zero. Stator output power is close to rated. In other words, for better wind speed, the machine consumes less reactive power, and the rotor consumes less real power. When speed is greater than synchronous speed, the rotor spins at a supersynchronous speed and, now, generates real power in addition to the stator. This describes the principle of Type 3 wind turbine operation and thus, validates the operation of a Type 3 machine.

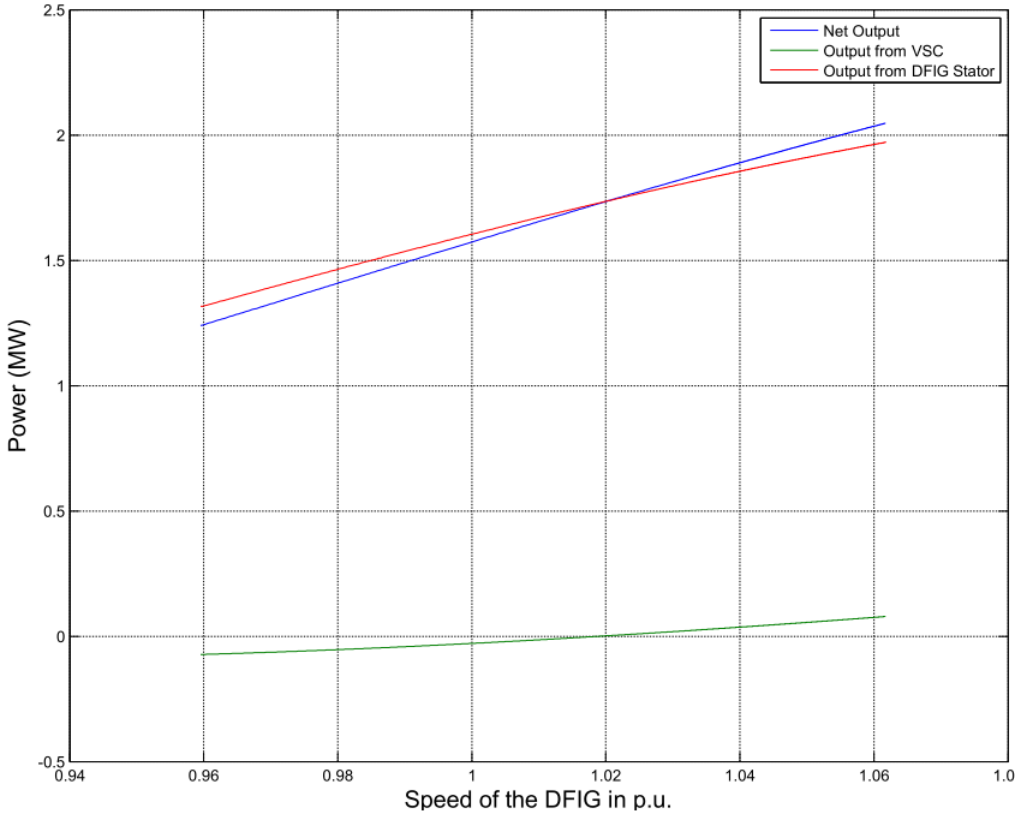

Figure 6.2: Power Output (Stator and Rotor) v/s Rotor Speed for the 10-turbine aggregated DFIG model

6.1.1.3 Comparison with Field Event

In this test, a Line-Line (Line - Line Fault (Phases B, C) (BC)) fault is simulated on the 230kV transmission line with reference to the system in Figure 5.5. The voltage and current from the collector are compared with the plots available from the Power System Relaying Committee (PSRC) report for Type 3 WT response to a similar

fault on a 230kV transmission line [5]. It is important to understand that the model represents a single generator. This would be the case, for example, for days with insufficient wind, when most of the wind turbines in the farm are not generating.

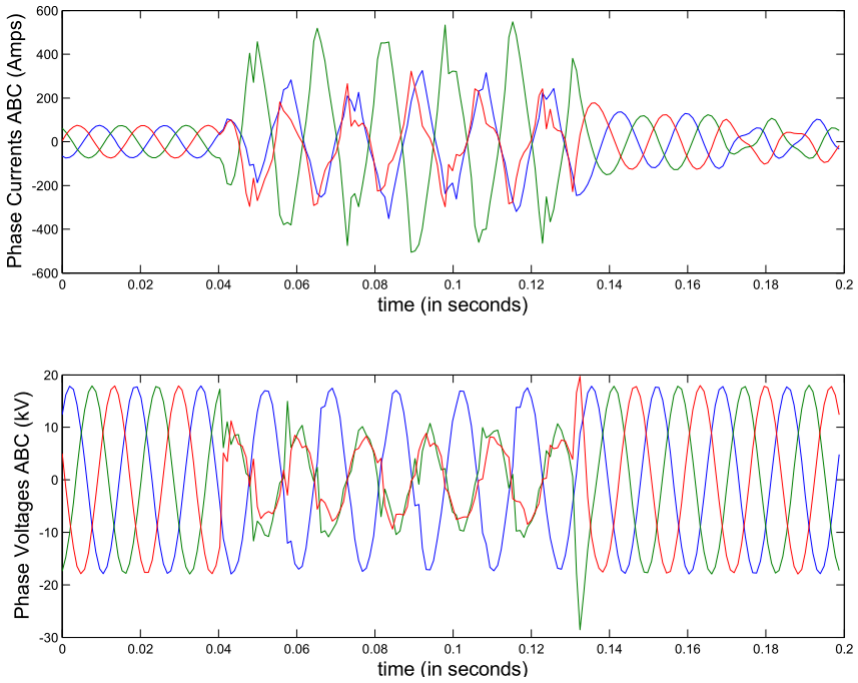

Figure 6.3: V, I Plots on Collector Bus for a B-C Fault on the 22kV Collector for a single generator

Figures 6.3 and 6.4 show the response of Type 3 systems for L-L BC fault on 230kV Line (Actual) and 22kV Collector (Model), respectively. The behavior of the line currents and voltages in the two cases is similar.

A single generator is not a very strong source to feed the fault currents. Since, the model is only one generator rated at 1.678MW, its contribution to the fault current is not significant, especially for transmission level faults. More resemblance is observed at the collector bus (22kV), which is closer (Figure 6.3). The response at the 230kV transformer terminals for a 10-machine aggregated model (Figure 6.6) resembles very closely to the field event response (Figure 6.66.4). Hence, the model is considered valid.

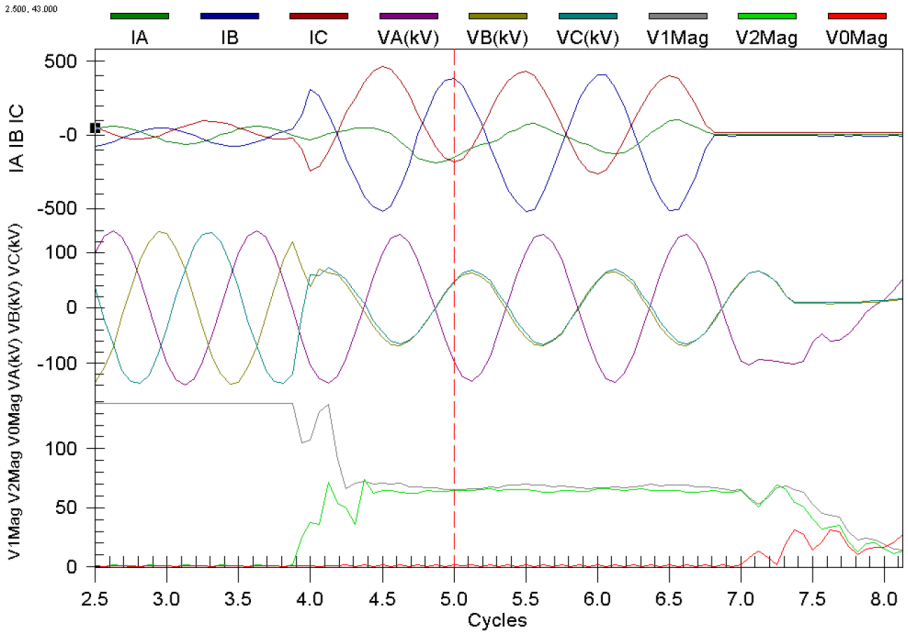

Figure 6.4: V, I Plots for B-C Fault on the 230kV Line for the Wind Farm from [5]

6.1.2 Comparing the Switching and Averaged Models

An averaged model represents the slower non-switching behavior of the converter. When the same controller was implemented with a switching model of the VSC, the output behavior (voltage and current) was similar to the averaged model. However, since the switching model will introduce switching harmonics at the switching frequency, additional L-C filters were added (10% of VSC rating) at the grid side VSC output. The output currents have the same nature as the output currents from the one-machine model. Comparing the output currents from Figure 6.5 with Figure 6.11, the only difference is that the harmonics of the switching frequency are also included in Figure 6.5. The close-in fault behavior could be different for switching model, especially in case of unbalanced faults, if the switching frequency is not too high. The current model switches at 4kHz, which is sufficient. Modern day converters can operate above audible frequencies, which is even higher, compared to power frequency. This validates that the aggregated and switching model behave similarly. The aggregated model will be validated in Section 6.2.

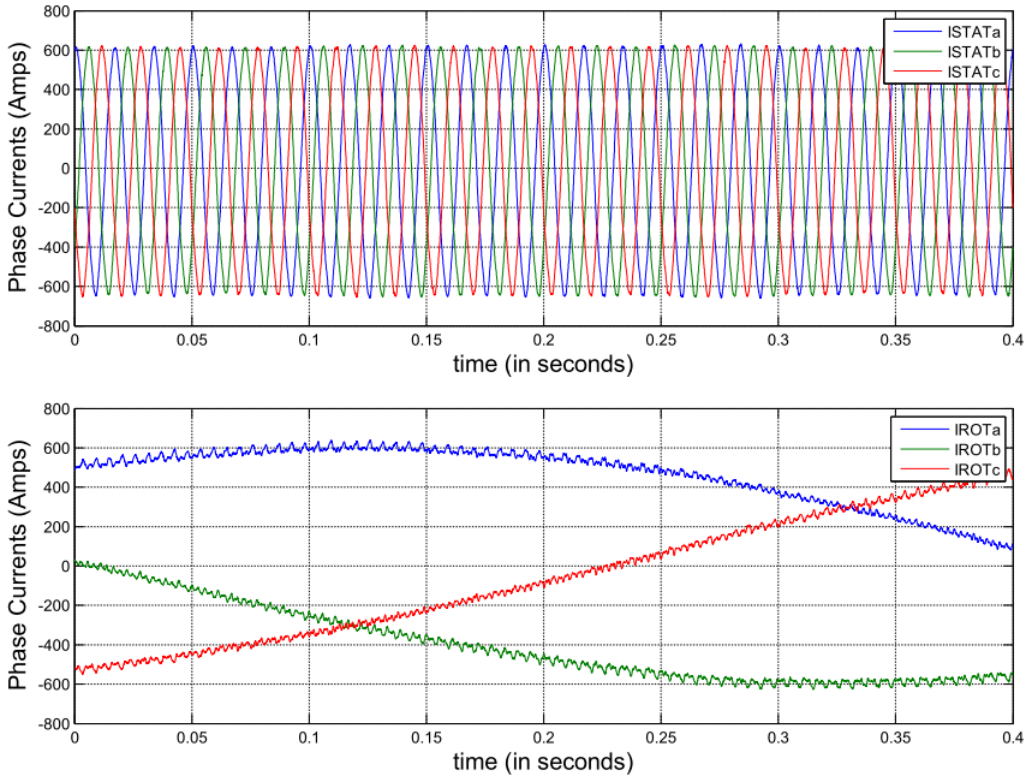

Figure 6.5: Stator and Rotor Currents from the Switching Model of a Type 3 Machine During Supersynchronous Operation

6.2 Average Aggregated (Ten Turbines) Model

A single turbine model is more useful for studying its transient response for nearby internal faults, e.g. the collector bus. However, from a grid protection point of view, response of a wind farm is more useful. In a wind farm, all the wind turbines are geographically located differently. Due to variability of wind across the farm, and the shadowing effects of turbines, different turbines can produce different output power, at any given time. However, depending on the number of turbines connected in a wind farm, the total output of the wind farm will be less dependent on the variability of the wind [1].

However, within the farm's internal cable network, the voltage may vary slightly. There are two aspects for discussion from the protection point of view:

1. Behavior of WTs for faults within the wind farm network

2. Behavior for the faults on the grid (outside the wind farm)

At any point of time, all the wind turbines will be in slightly different states. For the analysis of faults within the network, this information is vital. Simulating all the turbines separately requires significant computation power, especially in real time. With RTDS, this translates into significant hardware (hence cost and space) requirements. In addition, increasing the number of individual wind turbine unit models leads to a higher order model, inappropriate for online system security analysis and stability margin computation [14]. As viewed from the grid, the power from all the systems is combined. Therefore, instead of 'n' inividual models in parallel, the model was aggregated to an 'n' machine model. For this case, 'n' is 10. The usefulness and necessity of aggregation is also advocated in [15] and [16].

For the faults outside the wind farm, an aggregate model for the entire farm can be satisfactorily used. For faults within the wind farm, wind turbines can still be aggregated, but as a collector [16].

The level of complexity for aggregation varies based on the wind turbine types [14]. Type 1, 2 can be modeled as conventional sources with an equivalent impedance in front of them. Type 4 wind turbines can be modeled as current sources, because the behavior of the current output from the turbine is fully controlled by the VSC. However, for Type 3 wind turbines, the DFIG machines need to be modeled [5]. The injected rotor voltage (and current) depends on the slip of the machine. For supersynchronous operations, the Type 3 WT converters are feeding the power back into the grid. However, for subsynchronous operation, the converter is consuming power from the grid to feed the rotor current.

6.2.1 Process of Aggregation

Output from a ten generator equivalent model can be seen as net generation from a collector bus. Accordingly, to aggregate the model to an 'n' machine model, the

output power and current ratings are scaled up by the factor 'n'. The line-to-line voltage remains the same. For the converters, their base current rating increases by the same scale, 'n'. The impedances of the Induction machine need not be changed. All the parameters of the machine are defined in per unit. Therefore, on scaling power rating of the machine, the base impedance will decrease as the effective S_{base} increases.

$$Z_{base_n} = \frac{V_{LL}^2}{n.S_{base}} \tag{6.1}$$

Here, Z_{base_n} represents the equivalent machine impedance for an 'n' machine aggregate model. V_{LL} and S_{base} are the corresponding base Voltage and MVA values for a 'one' machine model. (6.1) states that the per unit impedance for the aggregated machine model will be same. However, the impedance in ohms is scaled down by the same factor, 'n', since there are 'n' machines in parallel.

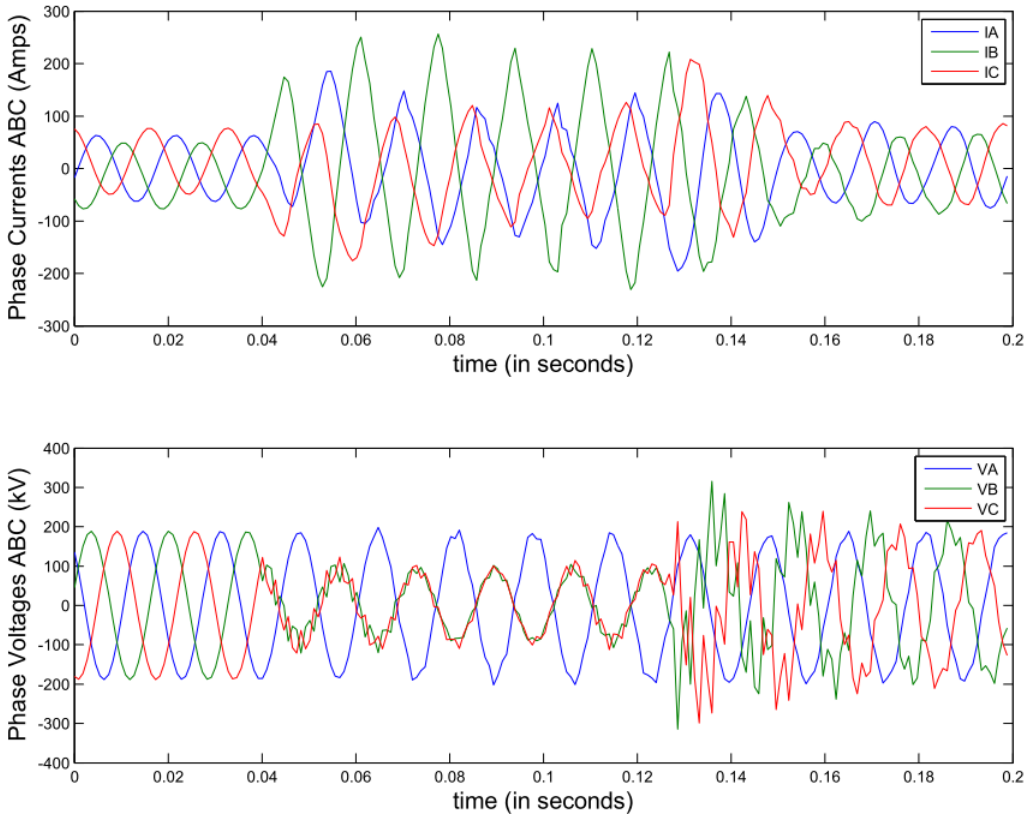

Figure 6.6: Plot - B-C Fault on 230kV Line for the 10-Generator Aggregated DFIG

6.2.2 Validation

Comparing Figures 6.4 and 6.6 allows the evaluation of the output response of the 10-machine model and the field event in [5]. The variation of system voltages and currents for both cases during the L-L faults, experience similar unbalances. The model is considered sufficiently valid. The system associated with the field event is a Type 3 WT farm. However, since the system configuration and connected loads are not known, the unfaulted current magnitudes for the two cases are different.

6.2.3 Normal Operation

Here, the plots for machine torque, rotor speed, DC bus voltage and reference tracking during steady state operation for grid side and rotor side are presented. Power output and its variation with speed has already been presented in Section 6.1.1.2.

6.2.3.1 Torque and Speed

The speed in Figure 6.7 is more than 1p.u. which represents supersynchronous operation. The output electrical torque is calculated after frictional losses and is almost 1pu. This is normal machine behavior and expected.

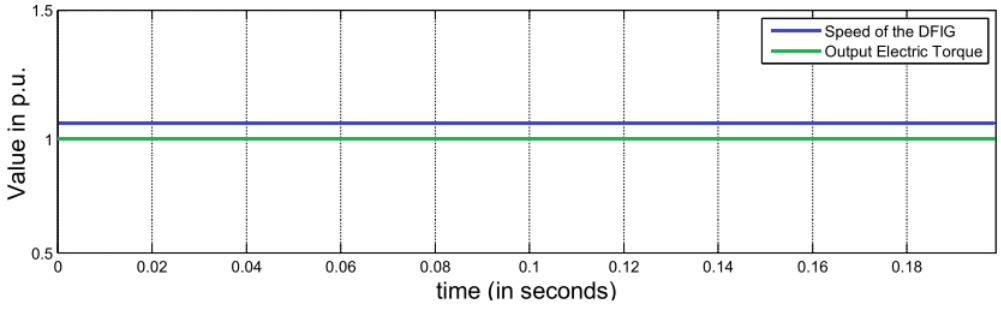

Figure 6.7: Speed and Torque for a Type 3 Machine in Supersynchronous Operation

6.2.3.2 DC Bus Voltage - Regulated

A single line to ground fault is simulated on the main line at t = 4ms, for the developed aggregated model with chopper/crowbar operation (Section 1.5.2) disabled. Crowbar has been disabled for this case to show the unbiased response of the DC Port Regulator. Figure 6.8 shows that the DC voltage regulator is causing the DC bus to track the reference voltages properly during steady state. The fault leads to a sudden change in current and causes the DC voltage to vary abruptly.

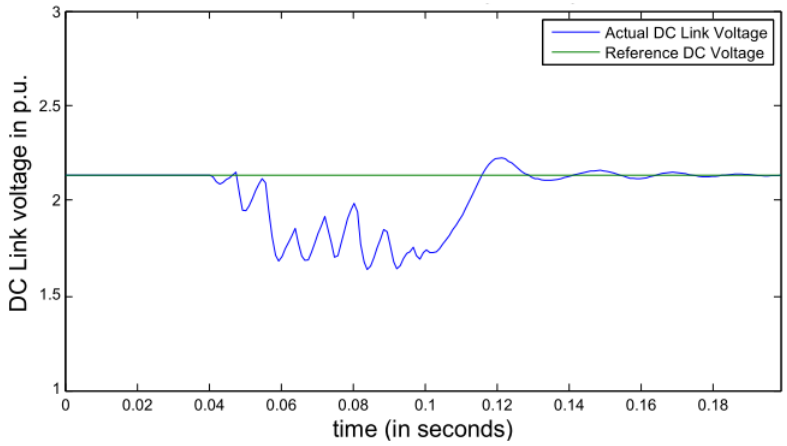

Figure 6.8: DC Voltage Regulator (reference and actual) During a Temporary Fault on the Collector for the Aggregated Model

6.2.3.3 Reference quantities being tracked

As shown in Figure 6.9, the grid and rotor side current controllers are tracking the optimal values closely. The plots are presented for a period during normal operation of the machine. There are no oscillations in the reference quantities for the grid or rotor side controllers for 'd' axis currents and actual system currents. Similar behavior is observed for 'q' axis currents as well. The performance of the controllers was consistent over a range of cases. Therefore, both the methods of frequency tracking (PLL for the grid side and rotor angle for rotor side) are successfully implemented.

The phase sequence of the stator currents is 'ABC'. The phase sequence of the

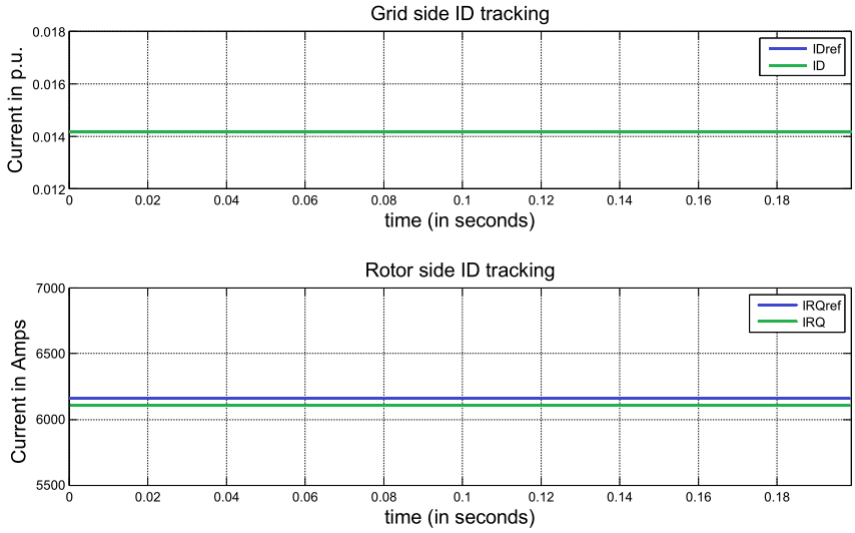

Figure 6.9: Grid and Rotor Side current tracking for a Type 3 machine in supersynchronous operation

rotor currents is 'ACB' and not 'ABC' because rotor is generating current in supersynchronous mode. Hence, its current direction is reversed. Overall, the Type 3 system behaves consistently and the controllers track the reference quantities quickly. Note that, the currents are shown for the aggregated model.

6.2.3.4 Supersynchronous and Subsynchronous Operation

Figure 6.10 shows the variation of power output of stator and rotor with variation in rotor speed above and below synchronous speed for the aggregated 10-turbine equivalent. Note that, as the speed of the DFIG falls, the power output from the rotor decreases proportionally. However, the output from the stator remains relatively constant. For rotor speed low enough, the rotor starts consuming power from the grid to support generation from the stator. This verifies the operation principle of the DFIG.

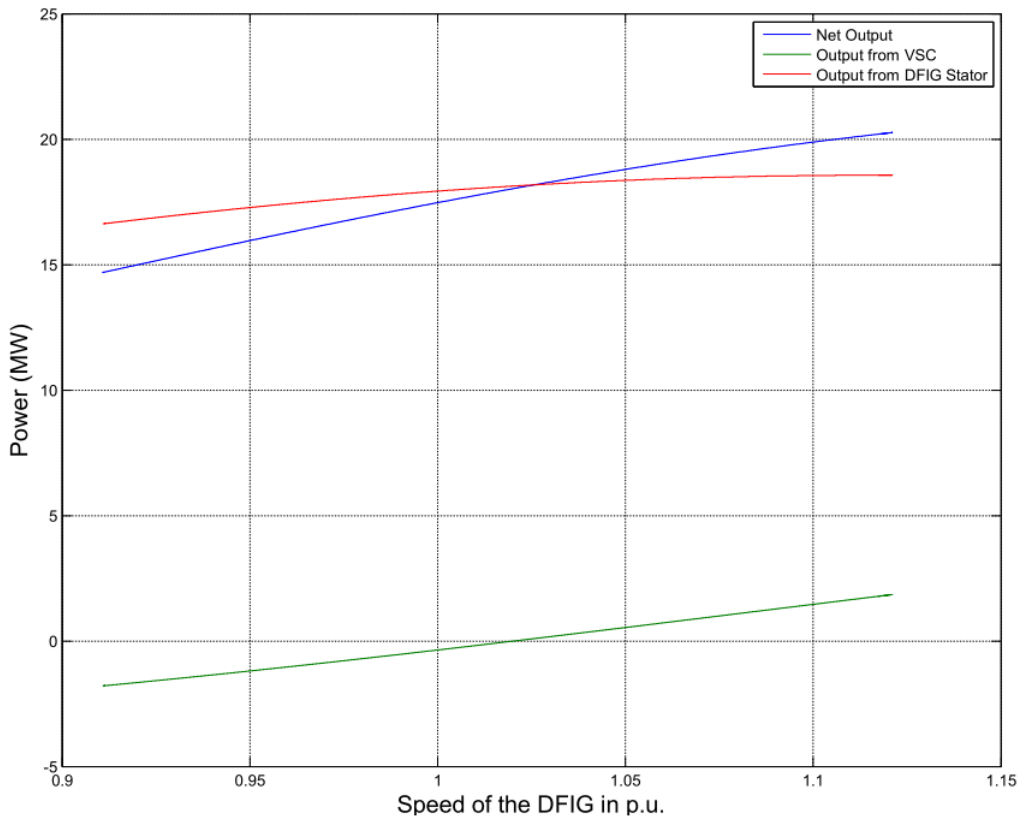

Figure 6.10: Power Output (Stator and Rotor) v/s Rotor Speed for the 10-generator Aggregated DFIG

6.2.3.5 Output Stator and Rotor Currents

Figure 6.11 presents the stator and rotor currents in steady state conditions. The frequency difference between the two may be noted.

6.3 Summary

In this chapter, the single turbine and 10-generator aggregated models for the Type 3 turbine were validated. In addition, the performance of the grid and rotor side controllers is discussed with the plots during normal operation. DC Regulator is shown to track the DC voltage satisfactorily during normal and faulted operation. Finally, plots for the stator and rotor currents during normal operation are presented. The opposite phase sequence of rotor currents during supersynchronous operation and

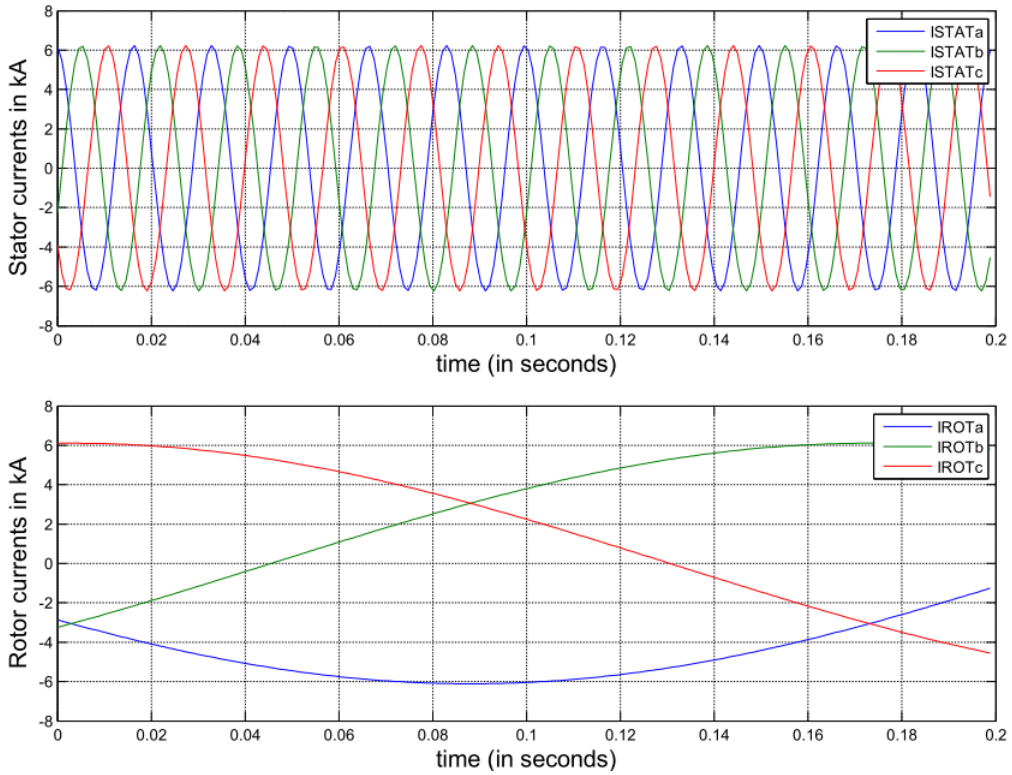

Figure 6.11: Stator and Rotor Current Outputs for a Type 3 Aggregated Model During Supersynchronous Operation

difference in frequency compared to stator currents is notable.

In the next chapter, the underlying principle for the supervisory elements and protection elements of interest (elements of interest) for this work are discussed. This will be followed by the simulation results for different faults on the Type 3 aggregated WT model. The event reports as seen by the relays will be presented, and the response of the elements of interest are discussed.

Chapter 7: Results and Analysis

7.1 Supervisory Elements

The basic operating criteria for any protection element is simple. *If the calculated quantity exceeds a threshold, it will assert.* However, just because the element asserted, doesn't necessarily mean that system had a fault. Faults are not the only conditions, which cause variations in voltage and current. A startup transient, change in loading conditions, or a power swing may also lead to such variations. Often, the fault may not be in the relay's zone, in which case, tripping the breaker may further destabilize the system. The basic operating criteria for any protection element is simple. *If the calculated quantity exceeds a threshold, it will assert.* However, just because the element asserted, doesn't necessarily mean that system had a fault. Faults are not the only conditions, which cause variations in voltage and current. A startup transient, change in loading conditions, or a power swing may also lead to such variations. Often, the fault may not be in the relay's zone, in which case, tripping the breaker may further destabilize the system.

Therefore, it is important to analyze the system conditions before asserting a trip. For example, consider a system, where the relay is not supposed to trip for reverse faults. If there is a fault at 20% of a line behind the relay, the distance element will assert, and ask the relay to trip. However, the relay should be able to see that the fault is not in front of it. In other words, relay should have a direction sensing ability. Therefore, we need a directional element.

There are many such elements in the relay, which are not responsible for asserting a fault condition. Rather, they analyze the situation to get more information about the fault's direction, faulted phases, power swing conditions, fault resistance, and more. These elements are called the "Supervisory Elements."

Supervisory elements improve the performance of operating elements. Most common checks are for fault's direction, fault type (internal or external), faulted phases, breaker open check, power swings and communication failure, among many others. Figure 7.1 shows a sample logic for a protection element with supervisory elements. This case is a general schematic for distance element.

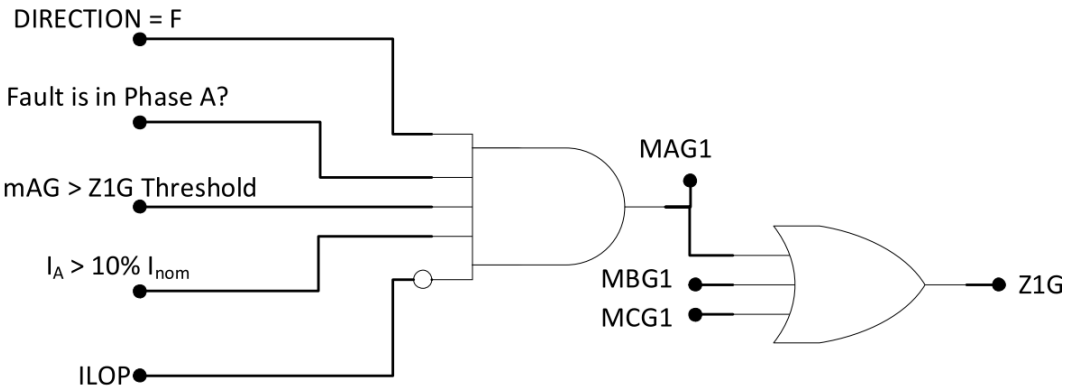

Figure 7.1: Generic Schematic - Distance Element

The following section discusses the primary supervisory elements for distance and differential protection.

7.1.1 Directional Supervision

Directionality is one of the most important supervisors for protection elements like distance and overcurrent.

The basic principle for directionality is to track the angle between voltage and current. For forward faults, the relay should see an effective impedance angle close to the source impedance. Current usually lags the voltage for these faults by close to $\frac{\pi}{2}$ radians.

However, for reverse faults, the angle of the current will change drastically. The angle between the voltage and current usually sees a big jump. Similar behavior is observed for forward faults with unity or leading power factor loads. Fault resistance may affect this, though. However, the influence primarily affects the phase currents.

Sequence currents Therefore, directional elements based on sequence currents are preferred.

The negative or zero sequence impedance seen by the relay is usually higher for reverse faults. It corresponds to the net impedance of the line in front of the relay and the corresponding remote equivalent source.

The relay uses this information to assess the direction of the fault. One of the implementation of the directional element using effective negative sequence impedance is presented in (7.1) below:

$$Z_2 = \frac{Re\left[V_2.(I_2.1\angle\theta_{Z1})^*\right]}{|I_2|^2} \tag{7.1}$$

Details on the idea and implementation of directional element is also discussed in Section 3.5 of [17].

7.1.2 Fault Selection

Motivation to select faulted phases comes from different sources for different relay manufacturers. One of the manufacturers utilize fault selection to improve security of the distance elements during faults with fault resistance. The idea is to disable the elements corresponding to unfaulted phases. This is also used for selection of phases for single pole tripping. Therefore, the fault type selection(Fault Type Selection (FTS)) is useful.

It can be done by monitoring the overcurrent element, distance element torque analysis or comparing the angles between I_0 and I_2. Most manufacturers use some combination of the above to identify the fault types. Angle comparison between I_0 and I_2 is used for all faults involving ground.

General idea of the fault selection logic is also discussed in Section 4.12.1 of [17].

7.1.3 Loss of Potential

The secondary windings of the potential transformers often have fuses for self protection. However, when one or more PTs lose their fuses, it appears as a sudden drop in the corresponding phase voltages on the relay's end. To prevent misoperation during these conditions, loss of potential logic is implemented to supervise many elements including distance elements.

The basic principle is to monitor if the change in voltage is also accompanied by a change in current. In these cases, the relay considers it as normal operation. Thresholds for degrees of change (angle and magnitude) and implementation of the above loss of potential principle varies between different manufacturers.

A basic logic overview for loss of potential is given in the Figure 7.2:

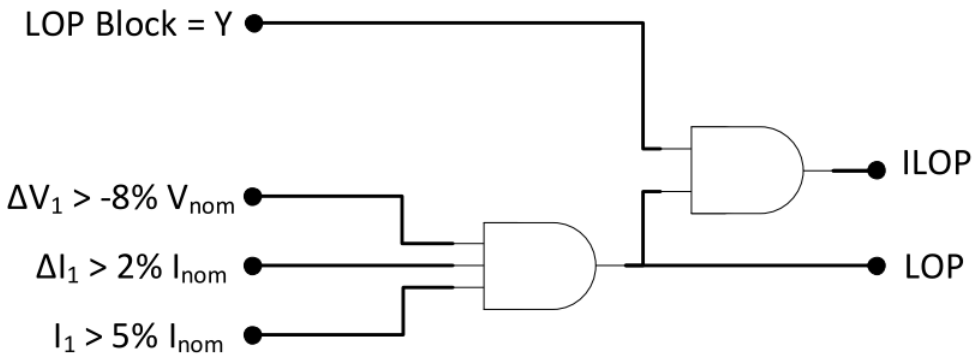

Figure 7.2: Generic Schematic - Loss of Potential

General idea of the 'loss of potential' scheme is also discussed in Section 4.6.7 of [17].

7.2 Protection Elements

In this section, we will discuss the primary protection elements of interest for the Thesis.

7.2.1 Mho Element - Distance Protection

Distance elements basically evaluate the distance of the fault from itself based on the effective impedance seen by the relay. The reach of this element is classified in Zones (usually 1-3).

- Zone 1: Instantaneous Trip
- Zone 2: Time delayed trip or permissive instantaneous trip
- Zone 3: Usually a reverse looking zone to prevent trips in Zone 1 and POTT Schemes in the US.

Ideally, for a radial system, $Z = V/I$ for bolted faults.

However, remote in-feed, fault resistance, series compensation and other phenomena severely affect the reliability of the above equation. Modern practice for Mho based distance elements is to use polarization and other compensation to reduce these effects. Today, many relays use the 'm' calculation, which is implemented differently by different manufacturers. Here, 'm' is the p.u. distance of the fault point from the relay. The base equation is given by:

$$m = \frac{V_{phase}.V^*_{pol}}{Z_L.(I_{phase} + k_0.3.I_0).V^*_{pol}} \tag{7.2}$$

Often, real or imaginary parts of the above equation may be used instead. Figure 7.3 shows the basic graphical implementation of a distance protection using Mho elements.

General idea of the distance protection scheme and specific details related to mho elements are also discussed in Section 4.5 of [17].

7.2.2 Differential Protection

The basic principle of line current differential protection is that the net current into the line will be nearly equal to the current leaving the line. If the difference in the

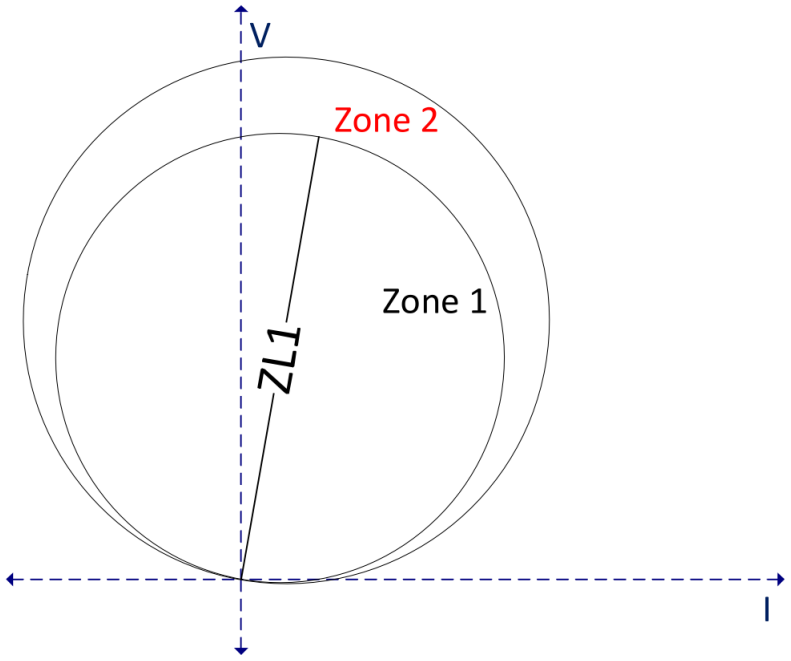

Figure 7.3: Mho Distance Element

current exceeds a threshold, the differential element operates.

However, there is always a natural unbalance in the systems. Also, line charging current and Current Transformer (CT) saturation during large fault currents will introduce more errors. Therefore, modern implementation of differential elements uses two quantities, namely, operating current, I_{op} and restraint current, I_{rst}. These are defined as:

$$I_{op} = |I_1 + I_2 + I_3 + \dots| \tag{7.3}$$

$$I_{rst} = |I_1| + |I_2| + |I_3| + \dots \tag{7.4}$$

Using (7.3) and (7.4),

$$r_{diff} = \frac{I_{op}}{I_{rst}} \tag{7.5}$$

The ratio, r_{diff} from (7.5) is used. Some relays use single, two or variable slope characteristics to determine the operating threshold. Basically, as both currents increase, the threshold will also increase.

Other relays (including the ones used for this report) use a more evolved scheme known as the *Alpha Plane*. Based on this algorithm, $Imag(r_{diff})$ is plotted against $Real(r_{diff})$ as shown in the Figure 7.4. As long as the plot is contained in the black marked region, the operation is considered safe. Outside the zone, the differential element will operate. This safe zone is defined using the settings of the relay. Figure 7.4 shows the same.

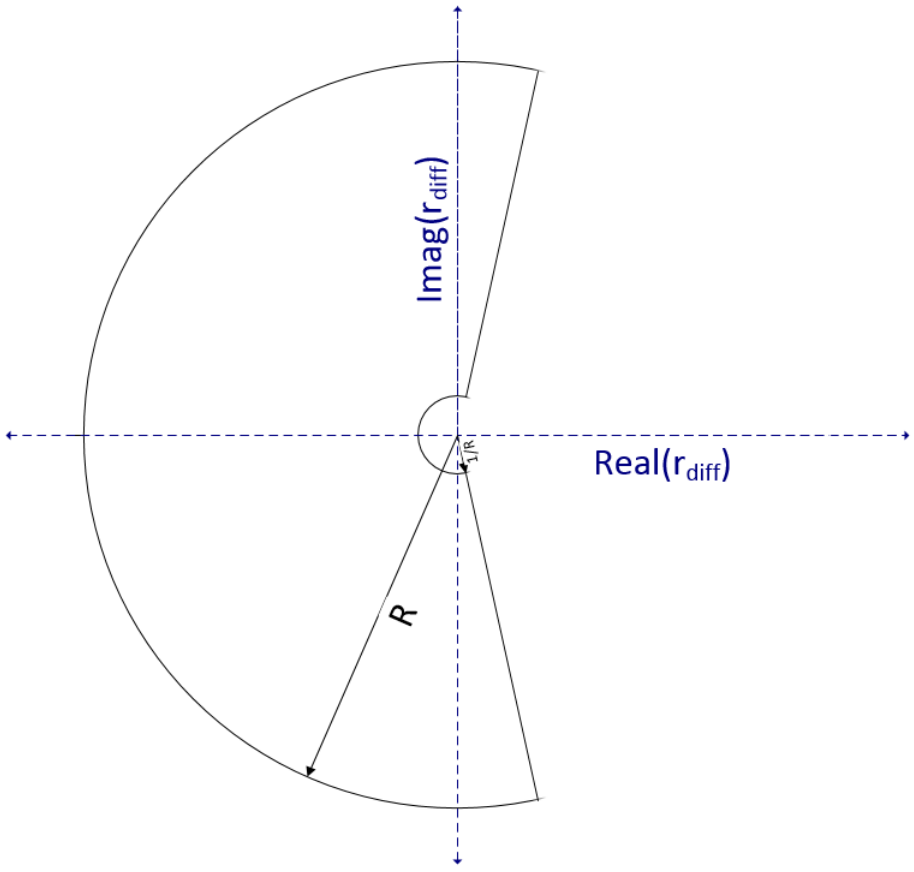

Figure 7.4: Differential Characteristics - Alpha Plane

General idea of the differential protection scheme and specific details related to Alpha plane are also discussed in Section 4.8 of [17].

7.3 POTT Scheme

POTT scheme uses a communication based approach to trip the relays faster. The basic idea is that if a fault occurs on a line, the relays on both ends will see in their Zone 1 or Zone 2. However, if both the relays see a fault in front of them, they send a permissive trip to the other relay. If a relay asserts the fault in zone 2 and receives a trip permission form the remote end, it trip immediately.

General idea of the 'POTT' scheme is also discussed in Section 4.7.1 of [17].

7.4 Fault Simulation and Analysis

Faults will be simulated on the 230kV Transmission line, as shown in Figure 5.5. Relay connected on the end with circuit breaker (Circuit Breaker (CB)) number 3 is referred to as the 'Type 3 Side Relay'. Relay connected on the other end (closer to CB number 4 is 'Grid Side Relay'.

Two scenarios will be discussed.

1. Mho Distance and Differential protection schemes are active.
2. Only Mho Distance elements are active and POTT Scheme is working. The communication channel for differential channel has failed.

Both the scenarios will be tested using four cases consisting of:

a. AG fault (Single Line to Ground)
b. ABG fault (Double Line to Ground)
c. AB fault (Line to Line)
d. ABCG Fault (3 phase to ground)

In each case, the fault is at 50% of the main transmission line. Please note that, the fault resistance has not been considered. In other words all the fault are bolted.

Expected behavior for conventional power systems:

1. The fault should be seen in Zone 1 by the relays at each end.
2. Directional supervisory elements should see the fault in front of them.
3. Zone 1 and Zone 2 Mho Elements should pick up.

    a. At least Ground elements for AG, ABG
    b. At least Phase elements for AB, ABCG

4. Faulted phases should be properly selected
5. No loss of potential indication
6. Both relay should send a permissive trip to the other relay.

7. Similar behavior for differential elements
8. Relay should trip nearly instantaneously with no significant delay

Note that the grid represents a conventional source. It is interesting to note that the protection schemes on grid side (a strong and more conventional source) had no problems. Both the distance and differential schemes, and the corresponding supervisory elements are seen to operate desirably. This also substantiates the claim towards expected fault behavior for conventional power systems. While presenting the fault events, the two events as seen from the Type 3 side and grid side relays, will be discussed in parallel. In addition, MATLAB® plots of sequence voltages, sequence currents, corresponding distance, directional and differential calculations using the event records will be presented. This provides a better insight to what the protection and supervisory elements see during the fault.

7.4.1 Event 1(a) - AG Fault (87COMM active)

Observations and Analysis for Event 1(a):

1. The current unbalance is not much for the Type 3 side relay (Figure 7.5). The voltage unbalance is prominent. This is because the controller for the Type 3 machine is current regulated and will quickly adjust modulation of its VSCs to remove the unbalance. In addition, the presence of the Y-Δ transformer with Δ on the Line side, makes the system an even weaker zero sequence source.

2. Grid side current is a strong source and conventional in nature (Figure 7.6). The current unbalance is clearly visible from the Sequence currents (Figure 7.7).

3. Distance elements of the grid side relay see the fault at 50% as it should be. Both Mho elements (Z1G - Zone 1 Distance Ground, Z2G - Zone 2 Distance Ground) assert. Z1G asserts shortly after Z2G and issues an instantaneous trip

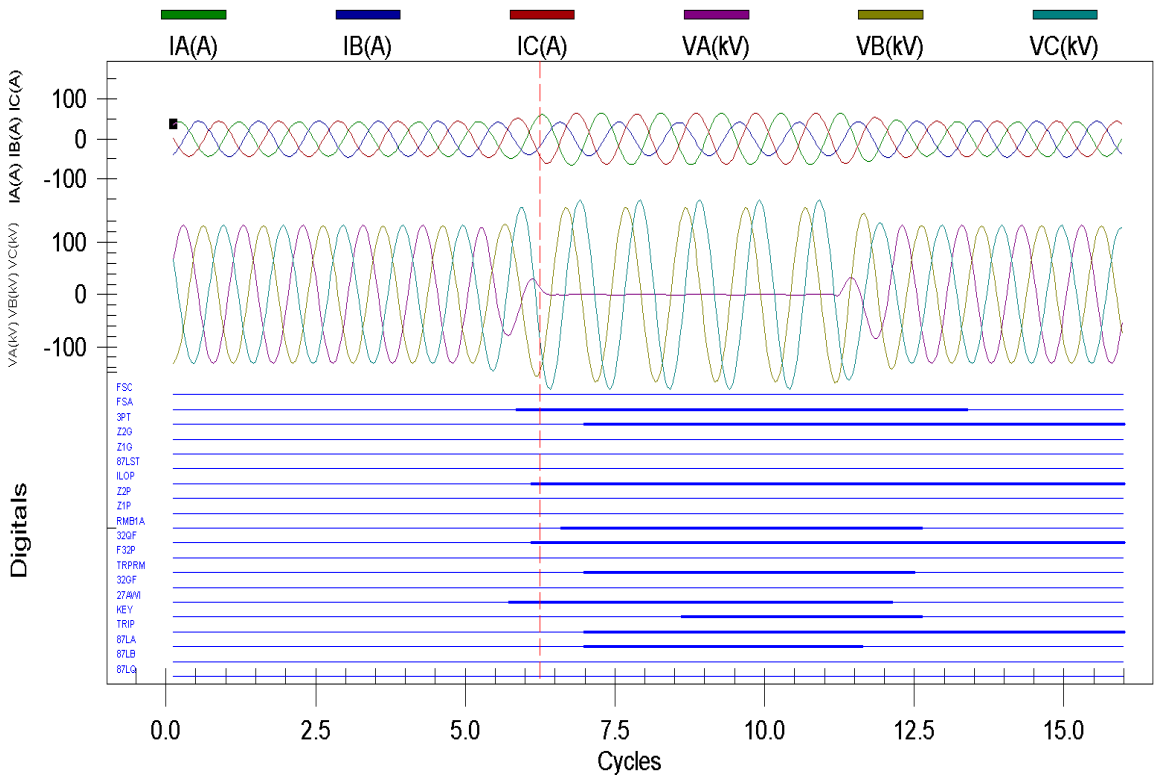

Figure 7.5: Event Report for Event 1(a) - Type 3 side Relay

for the Grid side. Trip permission under POTT is sent by grid side relay (KEY asserts) immediately after Z2G asserts.

However, Z1G or Z2G never pickup for Type 3 side relay. Note that fault selection, Relay Bit - Fault in Sector A (FSA) (Fault selection in Sector A - AG/Double Line to Ground fault - Phases B,C (BCG) fault), asserts. Therefore, the relay can see that the fault is either AG or BCG using the fault selection logic. None of the supervisory elements are blocking. Figure 7.9 shows that the fault appears beyond zone 4 (200%) to the Type 3 side relay. ***Analysis***: Since enough zero sequence current is not available, the fault appears farther than it should. Mathematically, it can be argued that I0 is not high enough to bring down the 'm' calculation close to 0.5.

4. For grid side relay, Directional elements see the fault in front of them (Figure 7.8). 32QF (Negative sequence based directional - Forward) and 32GF (Ground

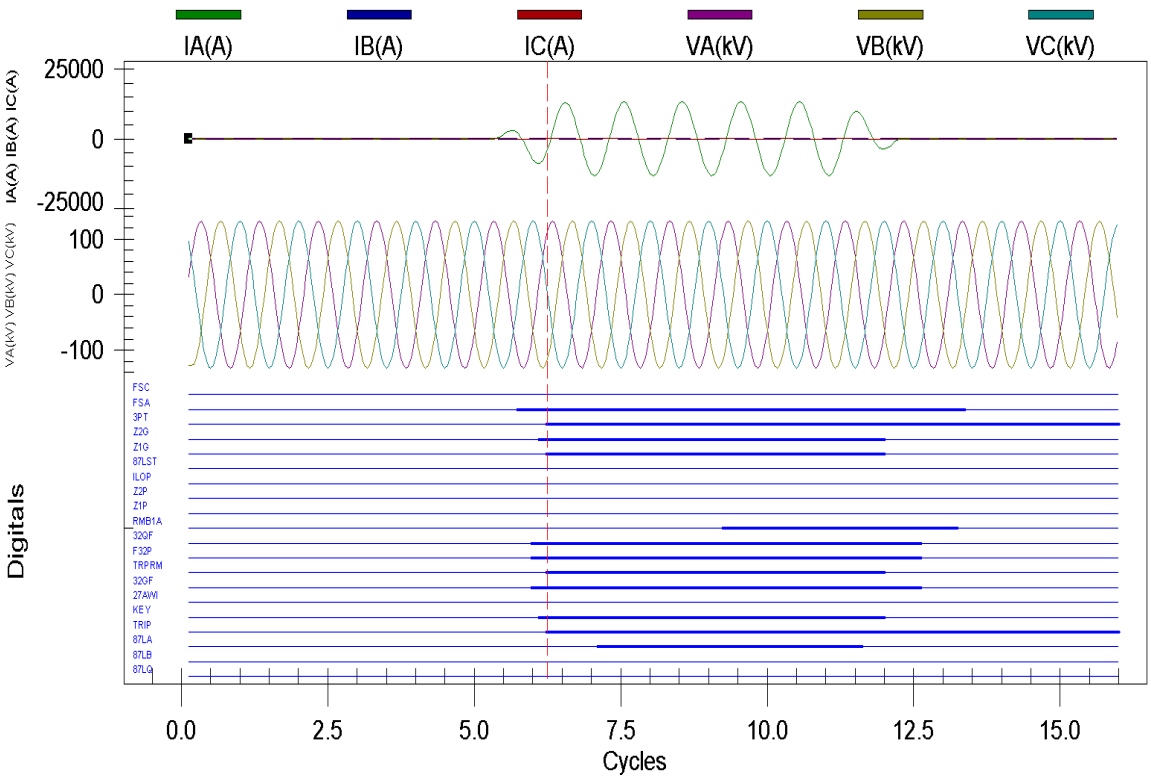

Figure 7.6: Event Report for Event 1(a) - Grid side Relay

current based directional - Forward) assert. Due to insufficient zero sequence current, only 32QF asserts for the Type 3 side relay.

5. Differential elements for Phase A, Negative and Zero sequence see the fault easily in their alpha planes (Figure 7.10) for both relays. However, differential elements pickup slower than mho elements.

   Type 3 side relay issues a trip after the phase differential element asserts (87LA - Line current differential in Phase A) picks up, even though it receives permission from grid side (RMB1A - Remote Mirror Bit for POTT scheme) o.5 cycles earlier. This is because its mho elements do not pickup.

   When the weak infeed logic is enabled, 27AWI (Undervoltage check on Phase A) asserts, and can be used for tripping the local relay using the permission from remote. This will be the case in event 2(a) when differential channel fails.

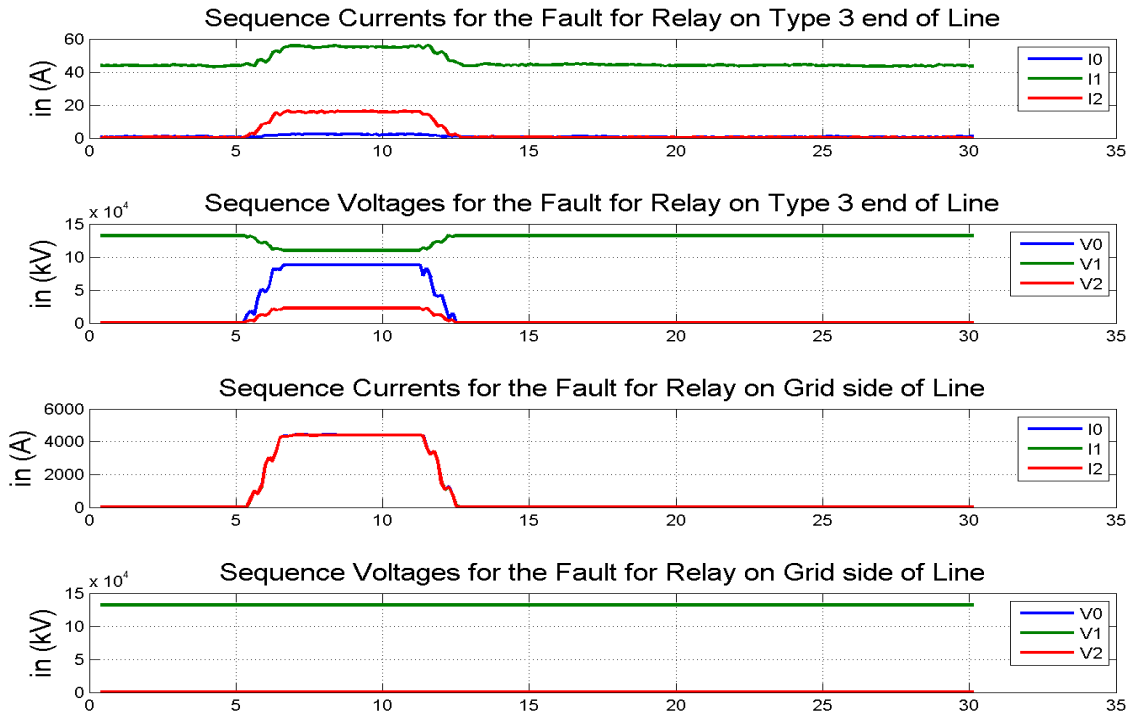

Figure 7.7: Sequence Current and Voltage Calculations using MATLAB® for Event 1(a)

7.4.2 Event 1(b) - ABG Fault (87COMM active)

Observations and Analysis for Event 1(b):

1. The current unbalance is relatively higher for the Type 3 side relay compared to event 1(a) (Figures 7.11 and 7.5). The voltage unbalance is also prominent. Unbalance is clearly visible in the current. (Figure 7.12). Sequence currents can be observed in Figure 7.13. There is not enough zero sequence current for the Type 3 side relay.

2. Directional elements see the fault in front of them (Figure 7.14). 32GF and 32QF assert on relays from both ends.

3. Fault selection logic should have asserted Relay Bit - Fault in Sector C (FSC), to indicate a sector C (Single Line to Ground fault - Phase C (CG)/ABG) fault. But it did not! Mho Ground elements for either relay do not pickup,

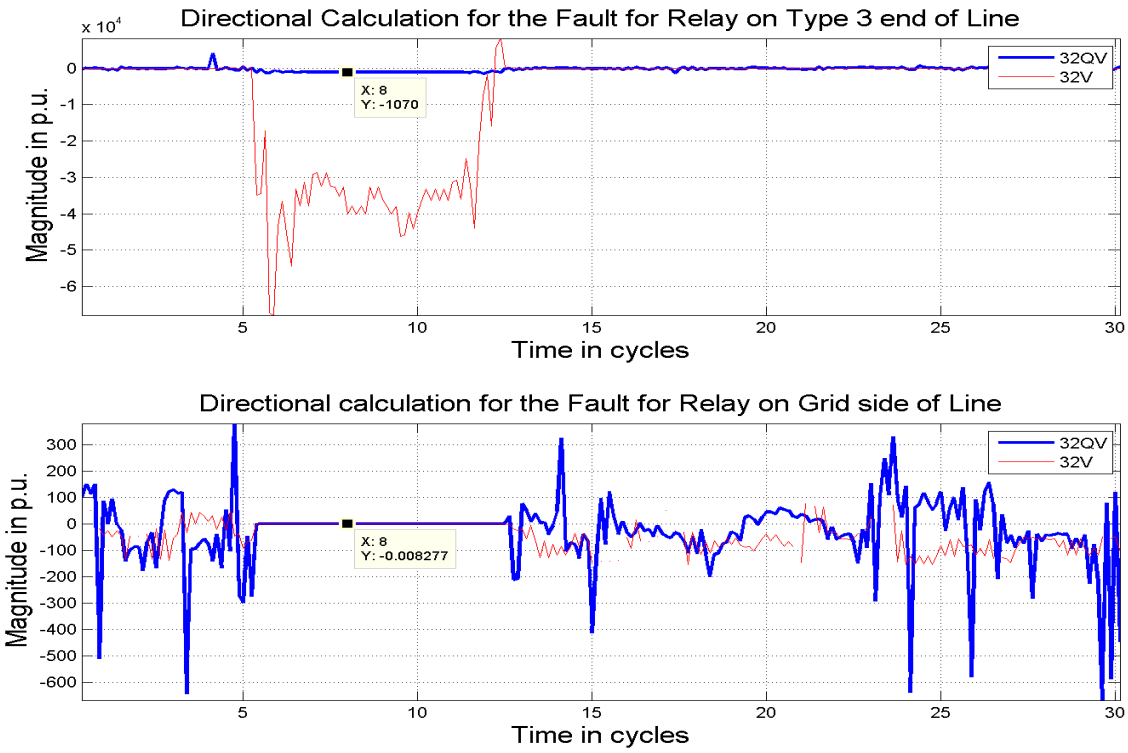

Figure 7.8: Directional Element Calculations using MATLAB® for Event 1(a)

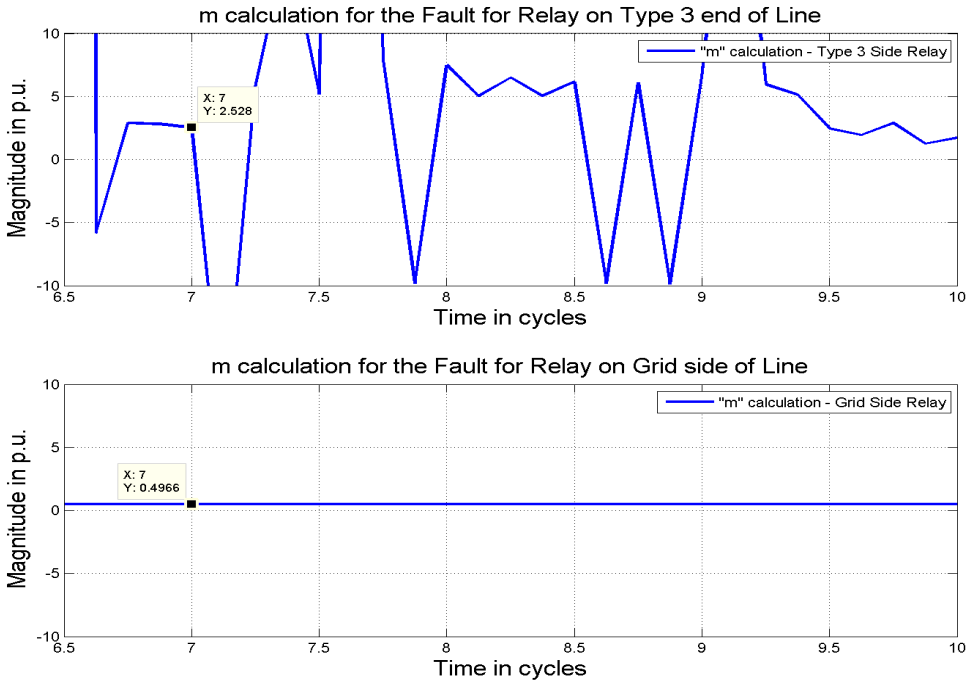

Figure 7.9: M Equation Calculations using MATLAB® for Event 1(a)

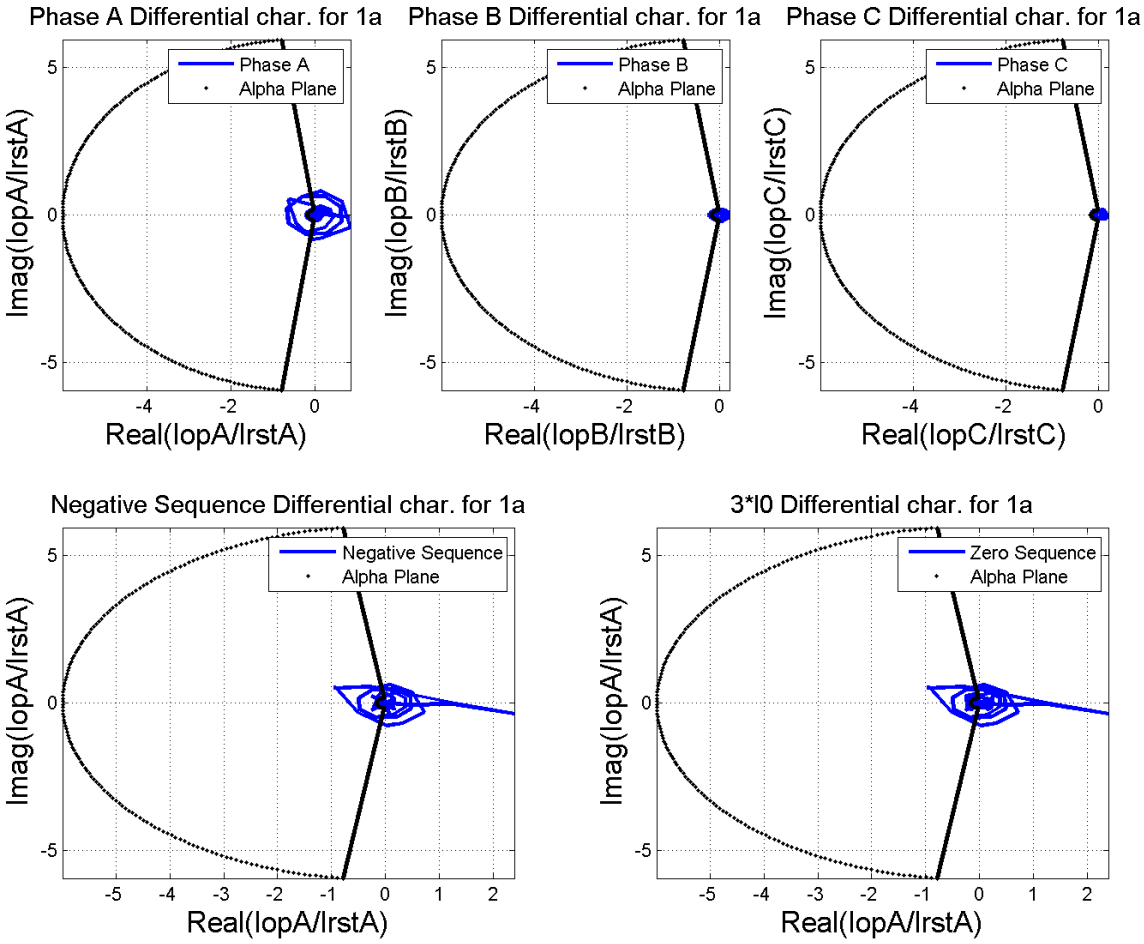

Figure 7.10: Differential Characteristic Plots using MATLAB® for Event 1(a)

even though the relays sees the fault at 50% of the line(Figure 7.15). This is because of the relay disregards the ground calculations if it notices a double line to ground fault. However, the Mho Phase elements (Z1P - Zone 1 Phase Distance, Z2P - Zone 2 Phase Distance) pickup and can trip the relay. However, they assert after differential elements in this case.

4. Differential elements for Phase A, B, C, Negative and Zero sequence see the fault easily in their alpha planes (Figure 7.16) for both relays. Grid side relay sees the fault first when the Phase Differential element in Phase A sees the fault (87LA assert) and issues an instantaneous trip. Negative sequence and Phase B differential elements (87LB) also follow soon. Type 3 side relay is sent the

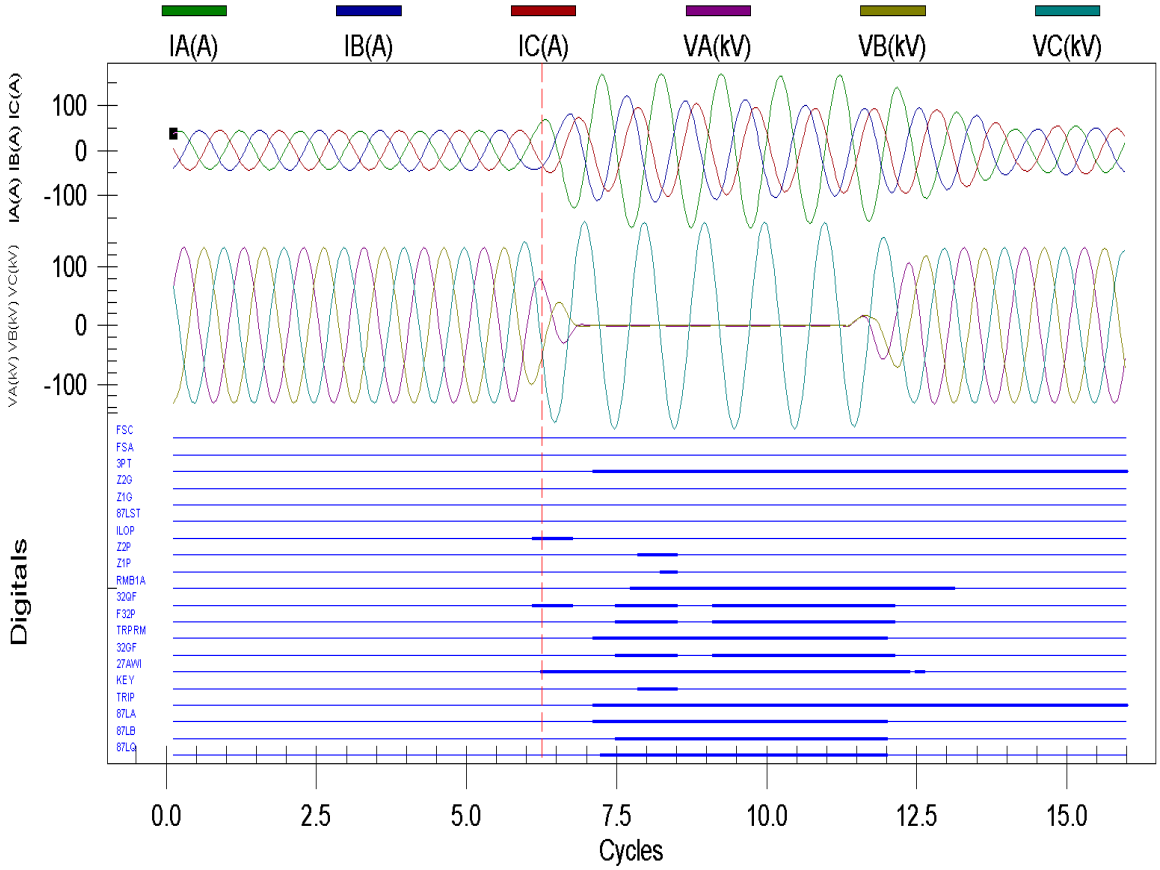

Figure 7.11: Event Report for Event 1(b) - Type 3 side Relay

permission to trip. Differential elements of the Type 3 side relay picked up at the same processing interval as when it received trip permission.

7.4.3 Event 1(c) - AB Fault (87COMM active)

Observations and Analysis for Event 1(c):

1. The voltages and currents seen by Type 3 side and grid side relays (Figures 7.17 and 7.18) is very similar to those in Event 1(b). Sequence currents can be observed in Figure 7.19. There is not enough zero sequence current for the Type 3 side relay.

2. Directional elements (32QF, 32GF) see the fault in front of them (Figure 7.20).

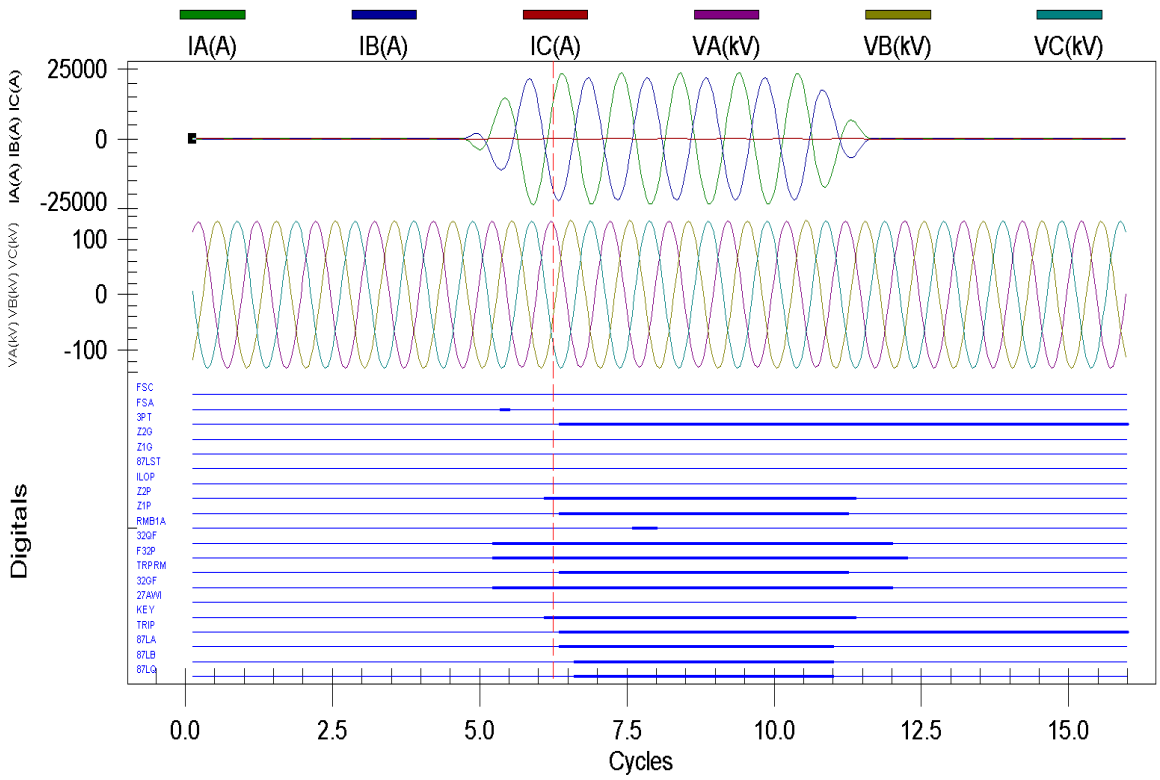

Figure 7.12: Event Report for Event 1(b) - Grid side Relay

However, for about half a cycle, forward directional elements do not assert for the Type 3 side relay.

3. Ground Mho Elements (Z1G, Z2G) for either relay do not pickup, even though the relays sees the fault at 50% of the line(Figure 7.21). This is expected for L-L faults. Phase mho elements (Z1P, Z2P) pick up for relays on both sides.

4. Differential elements for Phase A, B, Negative and Zero sequence see the fault easily in their alpha planes (Figure 7.22) for both relays. Phase A Differential element (87LA) of grid side relay sees the fault first and issues an instantaneous trip. Negative sequence and Phase B differential elements also follow soon. Type 3 side relay is sent the permission to trip. Type 3 side relay receives the trip permission and its Negative sequence differential (87LQ) also picks up at the same time.

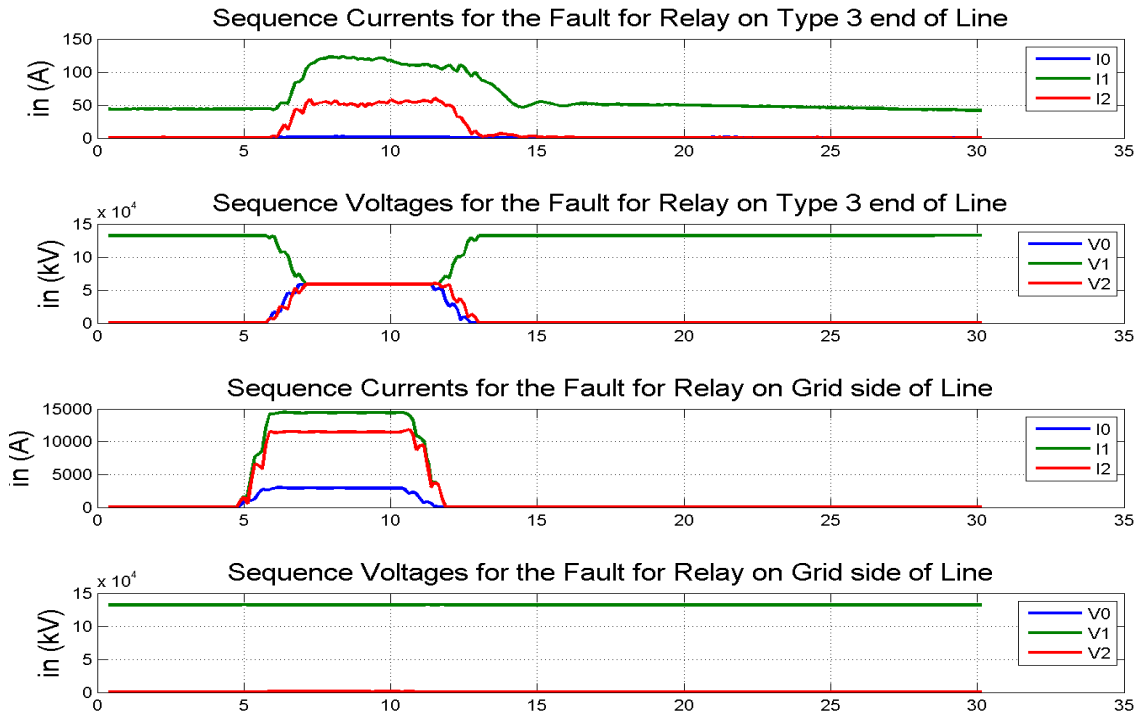

Figure 7.13: Sequence Current and Voltage Calculations using MATLAB® for Event 1(b)

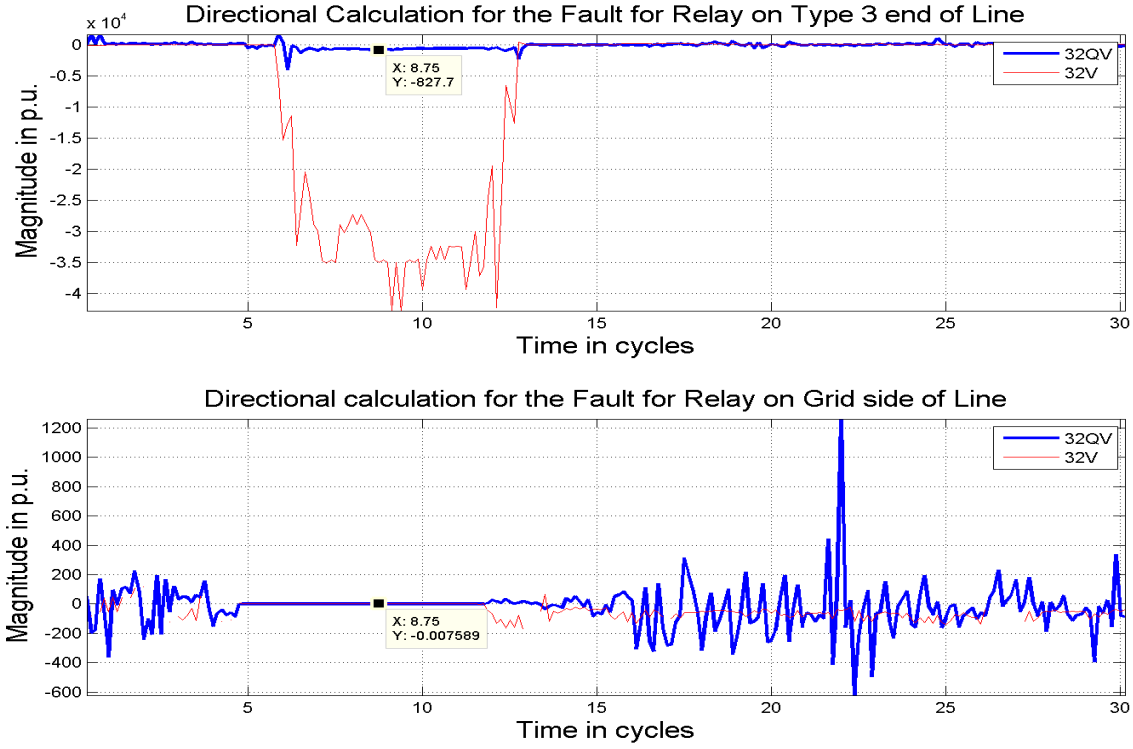

Figure 7.14: Directional Element Calculations using MATLAB® for Event 1(b)

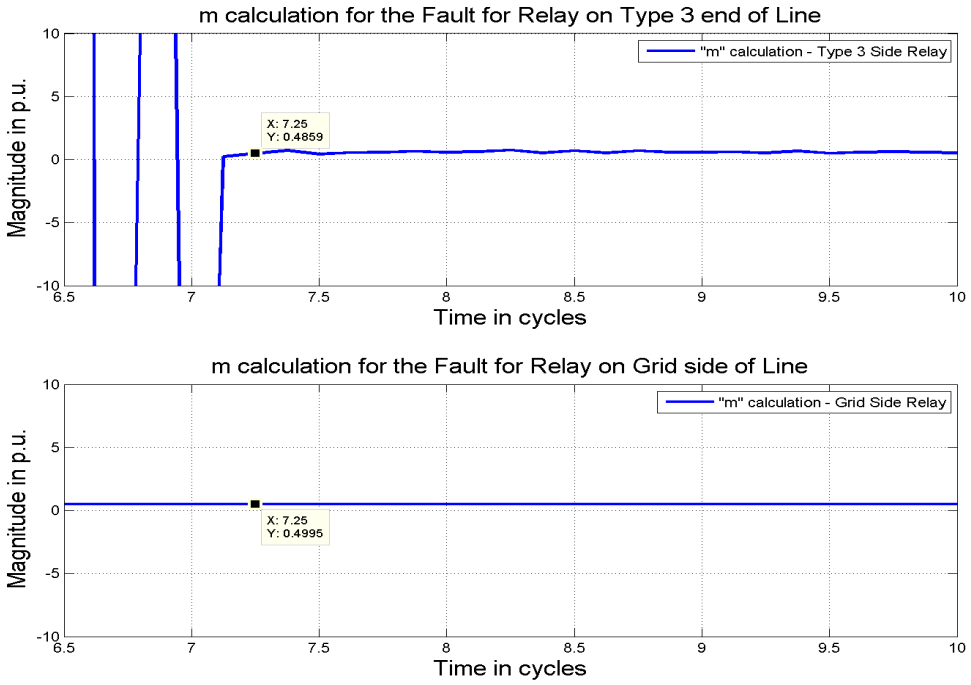

Figure 7.15: M Equation Calculations using MATLAB® for Event 1(b)

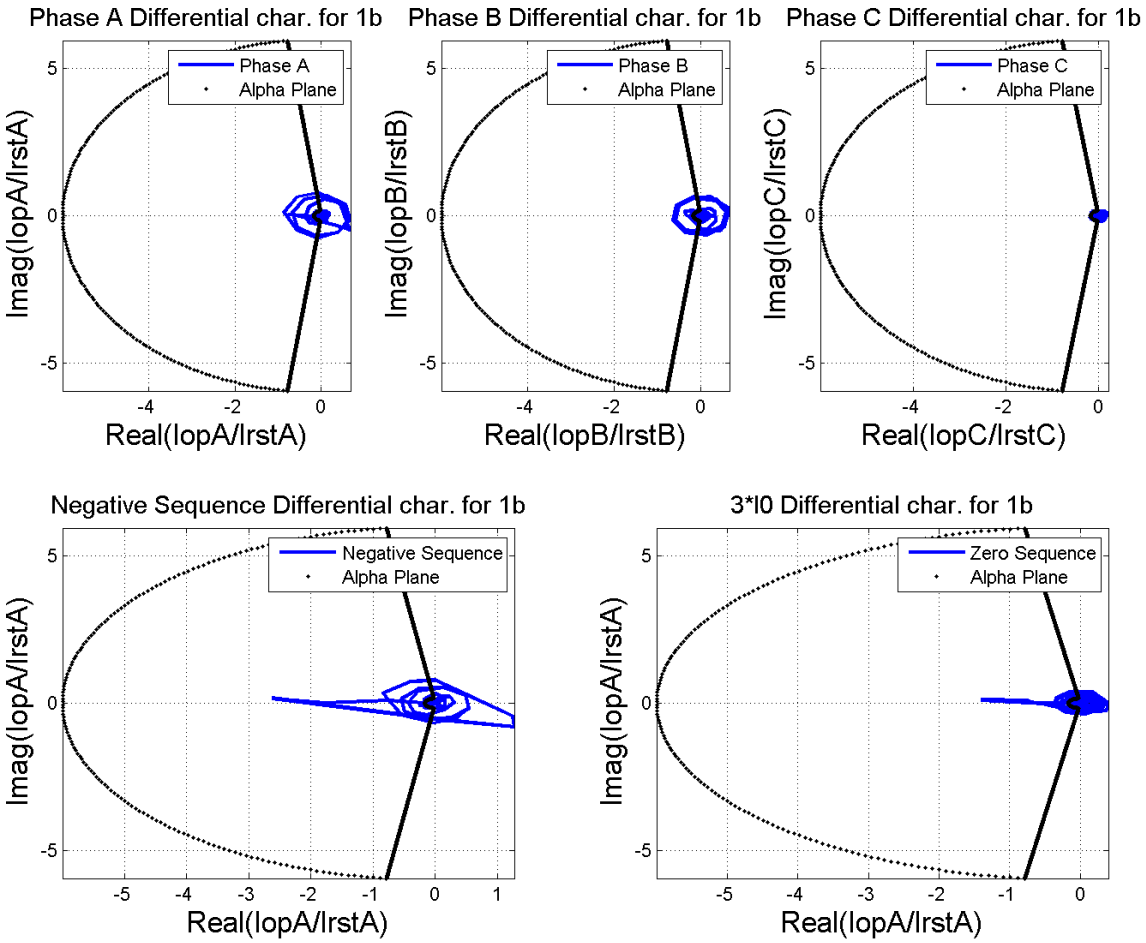

Figure 7.16: Differential Characteristic Plots using MATLAB® for Event 1(b)

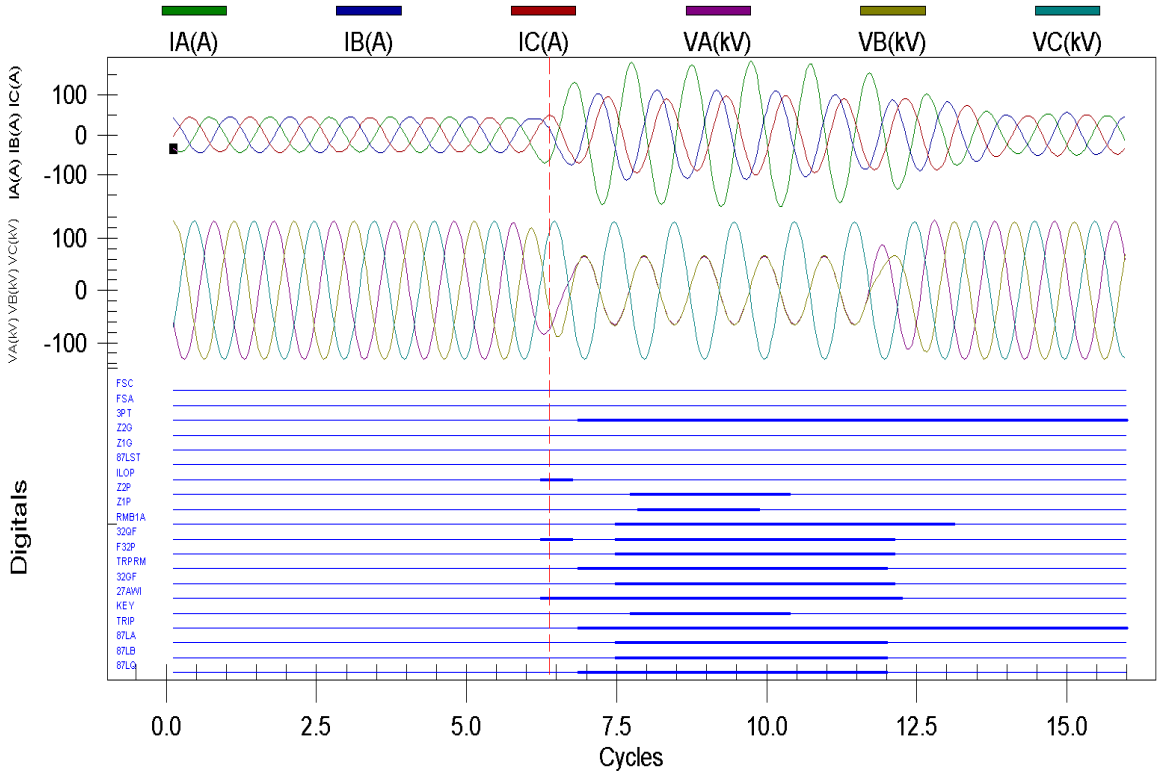

Figure 7.17: Event Report for Event 1(c) - Type 3 side Relay

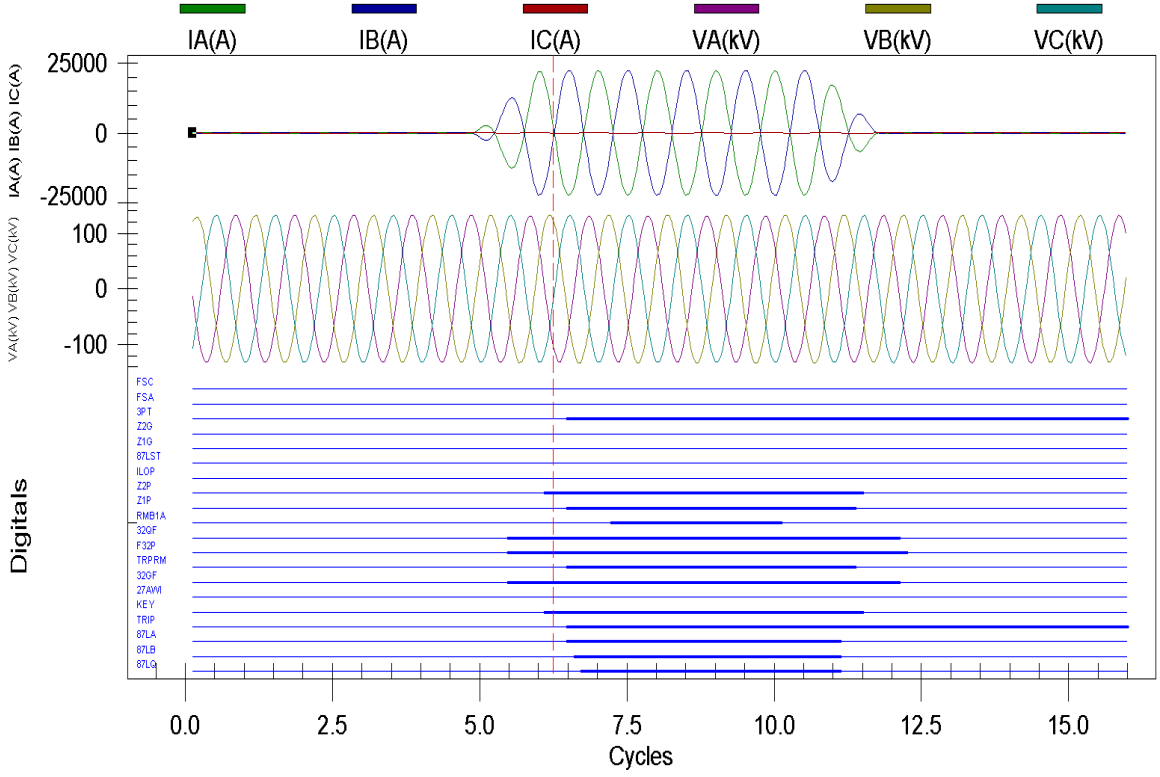

Figure 7.18: Event Report for Event 1(c) - Grid side Relay

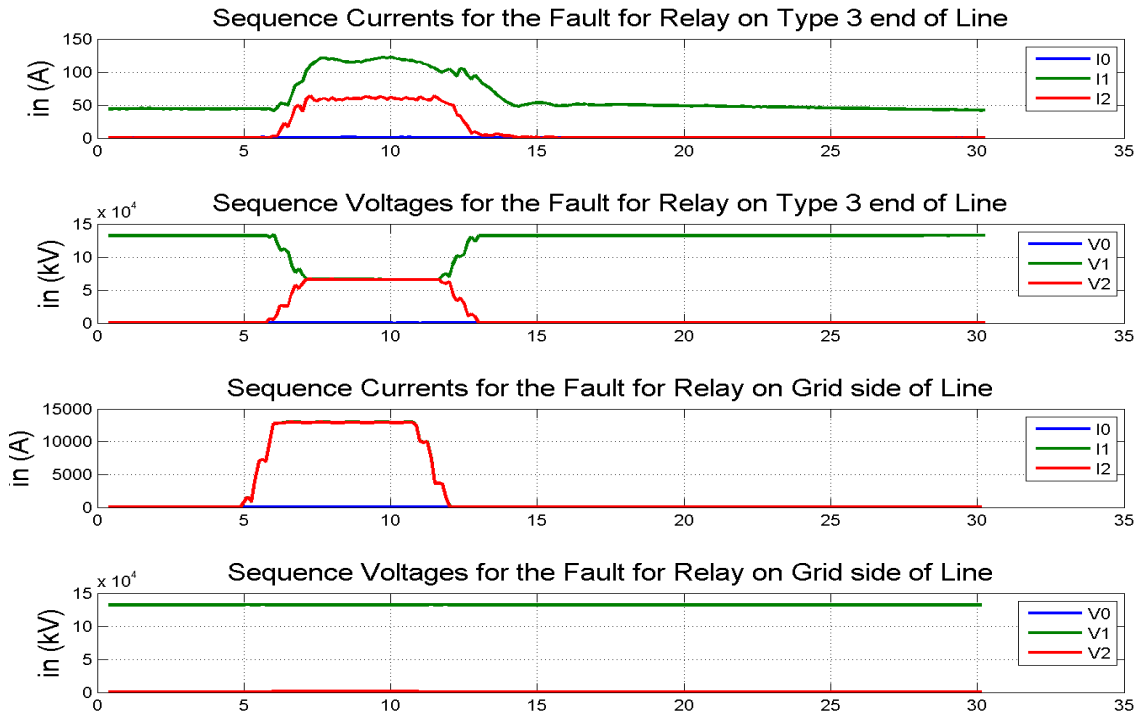

Figure 7.19: Sequence Current and Voltage Calculations using MATLAB® for Event 1(c)

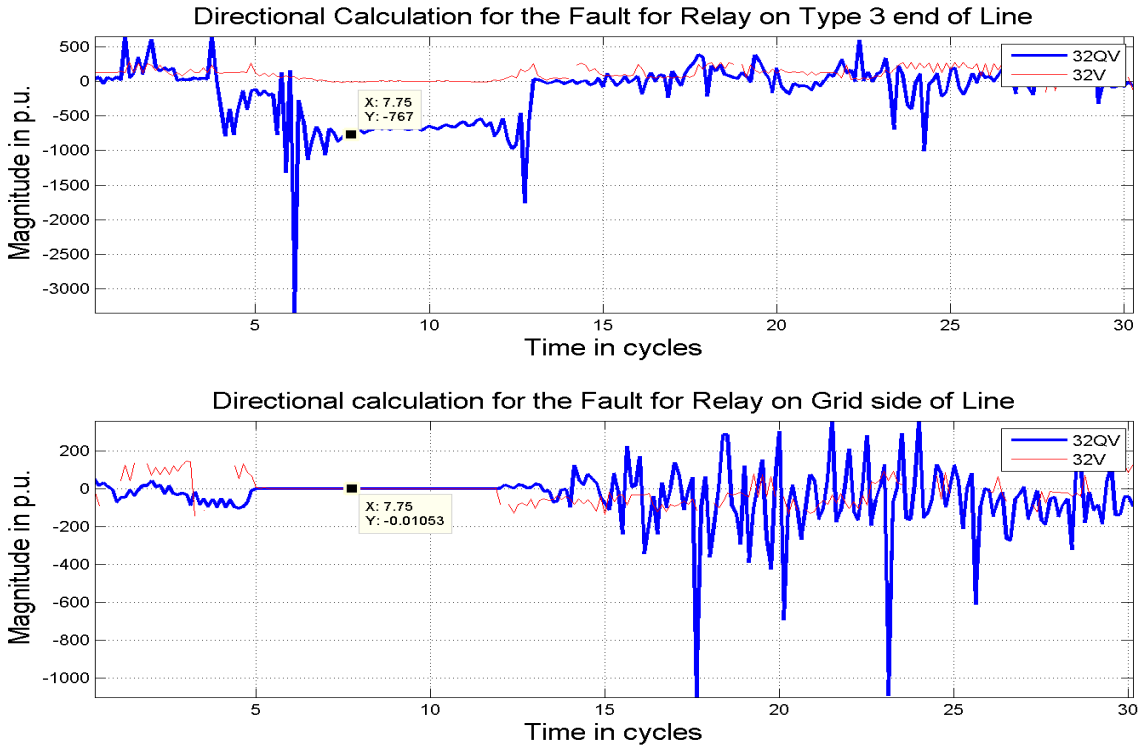

Figure 7.20: Directional Element Calculations using MATLAB® for Event 1(c)

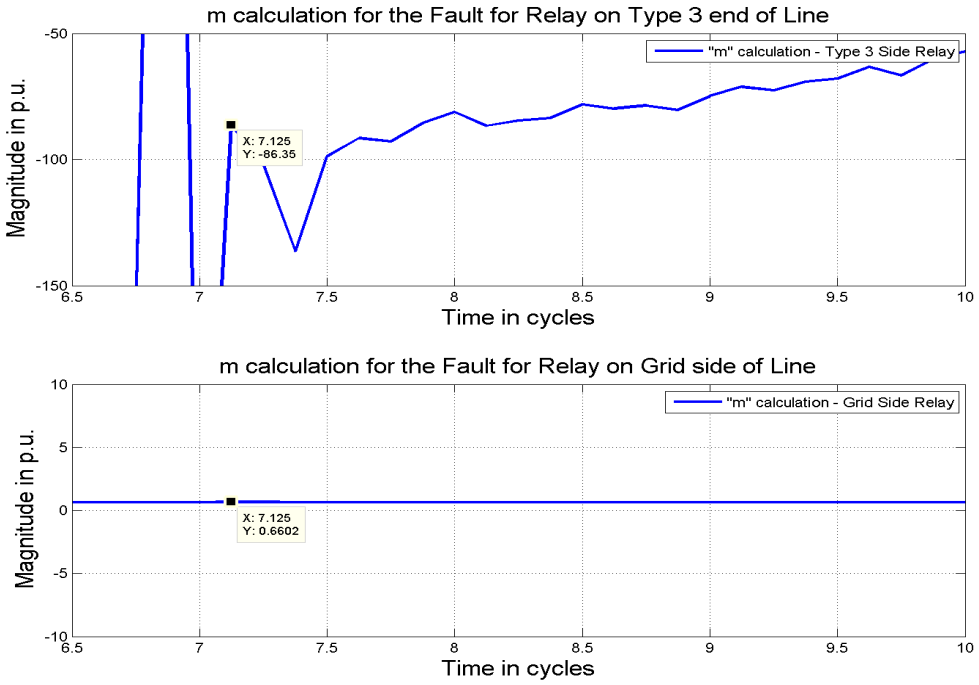

Figure 7.21: M Equation Calculations using MATLAB® for Event 1(c)

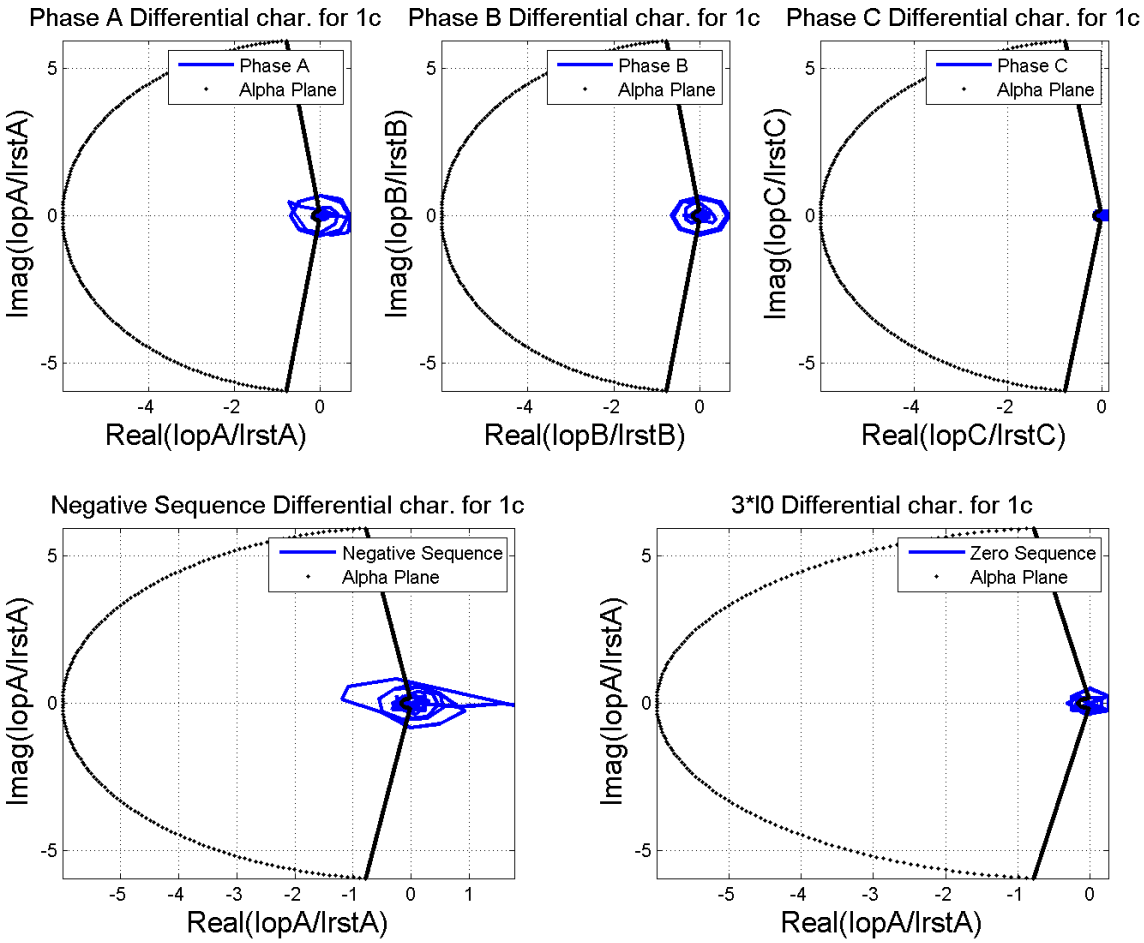

Figure 7.22: Differential Characteristic Plots using MATLAB® for Event 1(c)

7.4.4 Event 1(d) - ABCG Fault (87COMM active)

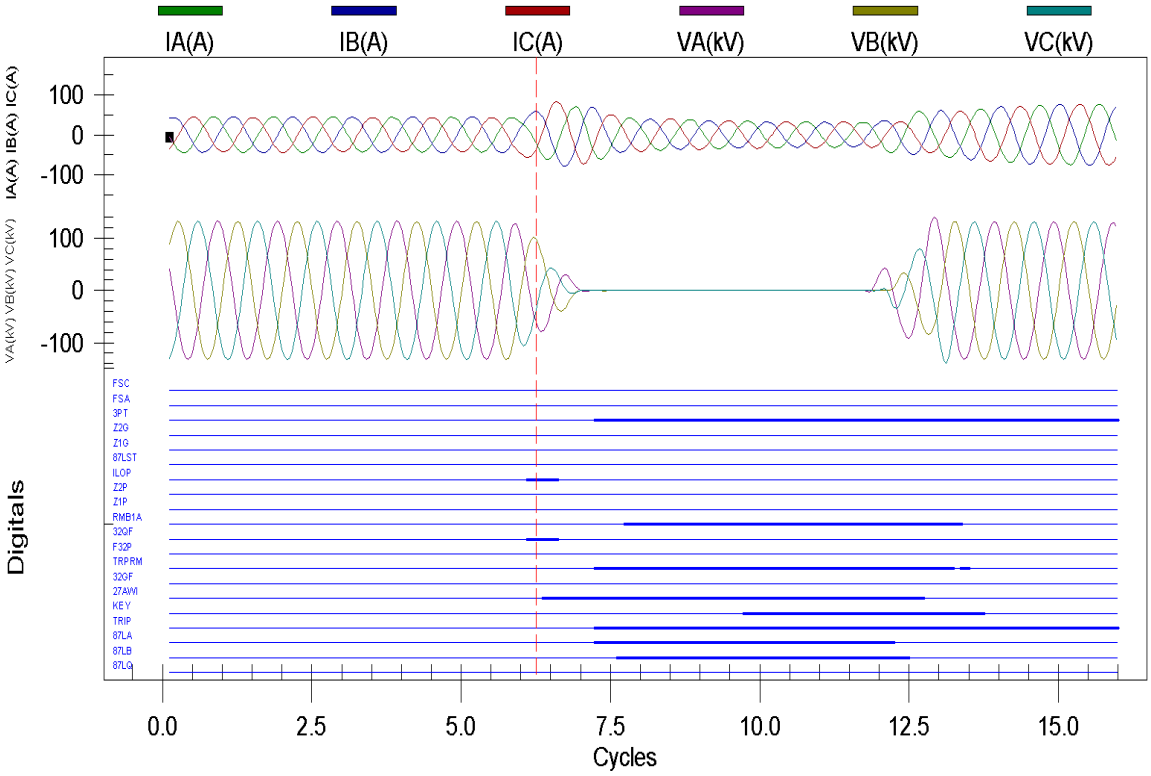

Figure 7.23: Event Report for Event 1(d) - Type 3 side Relay

Observations and Analysis for Event 1(d):

1. The current unbalance is not much for either relays (Figure 7.23 and 7.24). The interesting behavior of the sequence currents can be seen in Figure 7.25. This behavior can be attributed to the current regulation form the Type 3 aggregated wind farm.

2. Zero sequence current is virtually zero for both relays (Figure 7.24).

3. Directional elements see the fault in front of them (Figure 7.26).

4. Because of no zero sequence current, Mho ground elements (Z1G, Z2G) do not pickup again. Figure 7.27 shows that both the relays see the fault in their Zone 1.

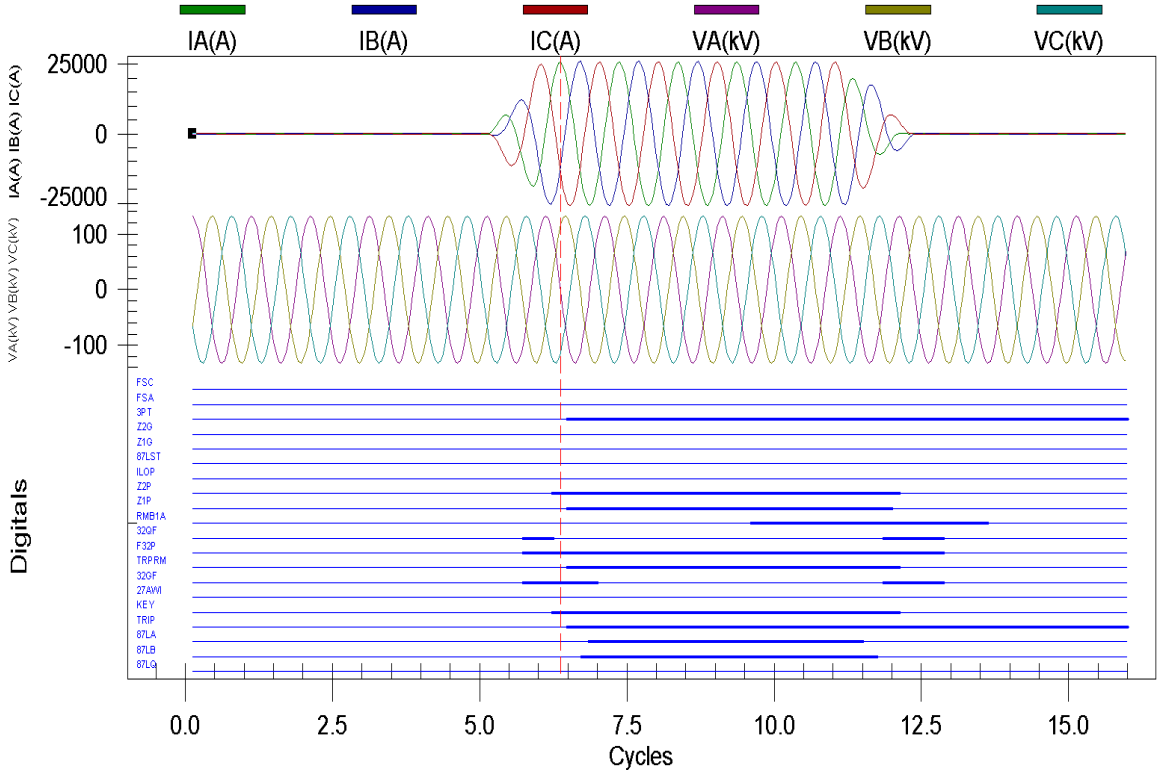

Figure 7.24: Event Report for Event 1(d) - Grid side Relay

5. Zone 1 phase element issues an instantaneous trip.

6. Differential elements for all phases, Negative and Zero sequence see the fault easily in their alpha planes (Figure 7.28).

Please note that, the differential communication channel is disrupted for all the cases 2(a)-(d). Therefore, the protection of the lines is dependent only on Mho Distance elements. This is done to study the protection of the line during communication failures, which is not very common, but can't be ruled out.

Similar faults were simulated, and no noticeable difference has been noted in terms of fault voltages and currents or the corresponding sequence currents. Only the differences will be highlighted.

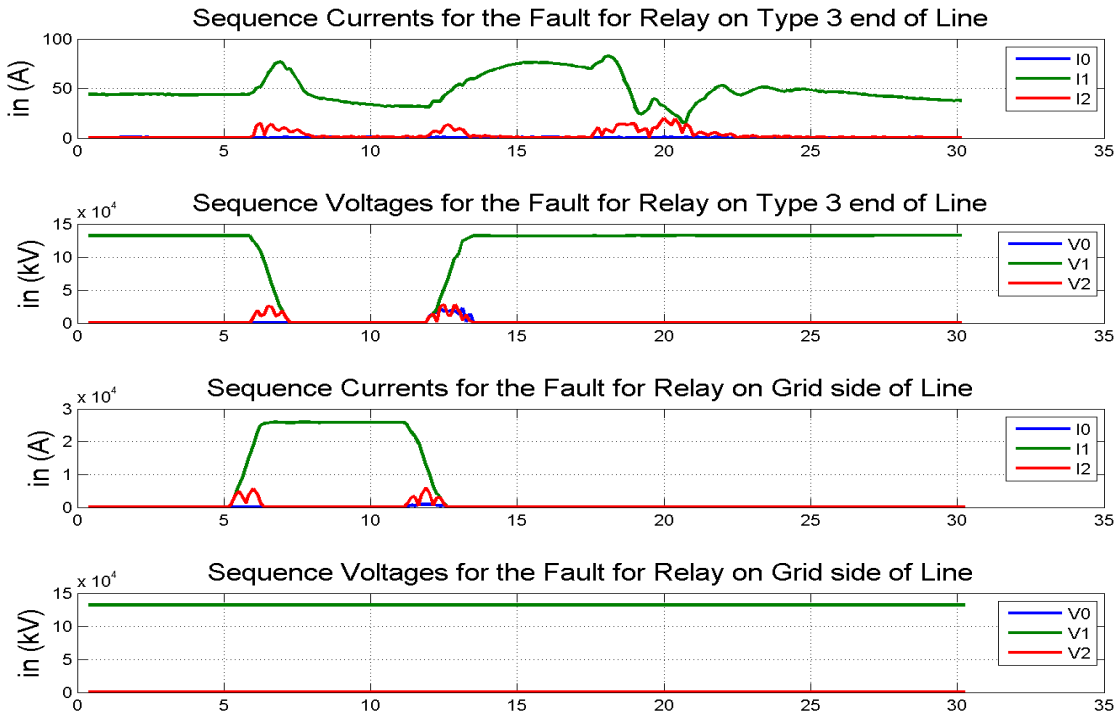

Figure 7.25: Sequence Current and Voltage Calculations using MATLAB® for Event 1(d)

7.4.5 Event 2(a) - AG Fault (87COMM failed)

Observations and Analysis for Event 2(a):

1. The Type 3 side relay isn't able to use its phase selection logic (FSA doesn't assert) due to insufficient line current (Figure 7.29). The change in sequence quantities is not much (Figure 7.31). Also, by the same logic as discussed in Section 7.1.3, Loss of potential is asserted.

2. Grid side relay sees the fault in zone 1(Figure 7.33) and issues an instantaneous trip (Z1G, Relay Bit - Trip Asserted (TRIP) assert) to its breakers(Figure 7.30). A trip permission (KEY asserts) is also issued for Type 3 side relay as soon as the fault was seen in Zone 1.

3. Directional elements see the fault in front of them (Figure 7.32).

4. Since the Type 3 side relay cannot see the fault in any zone (Z1G, Z2G do not

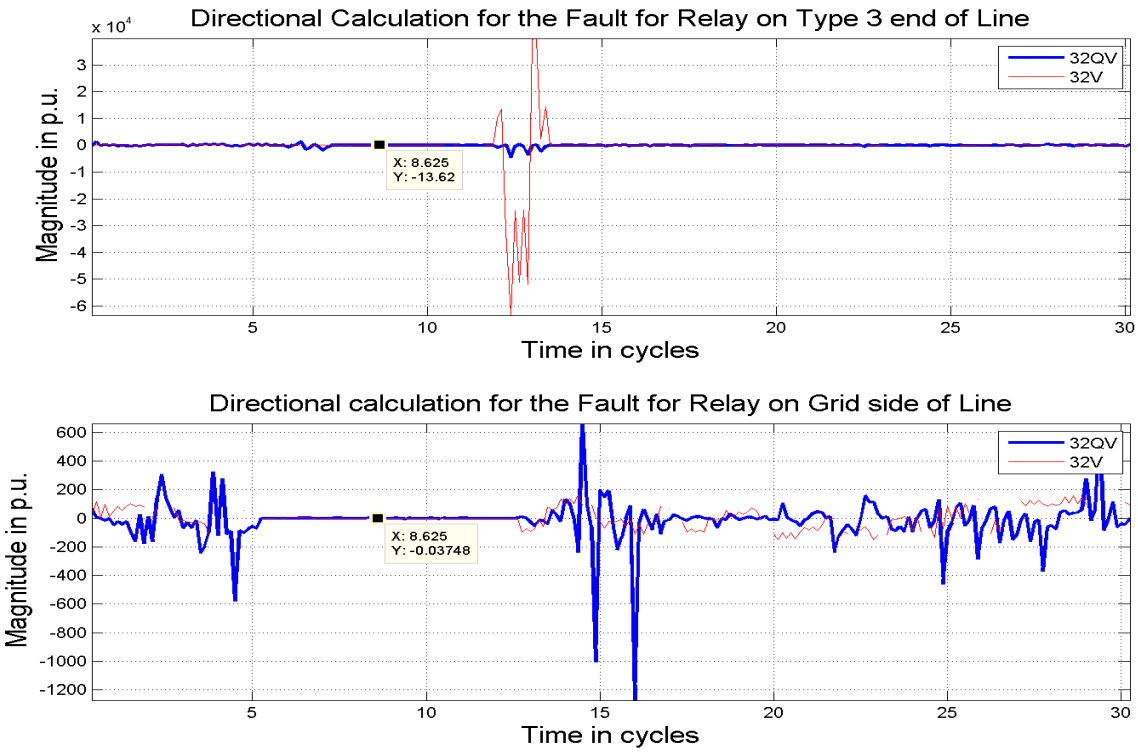

Figure 7.26: Directional Element Calculations using MATLAB® for Event 1(d)

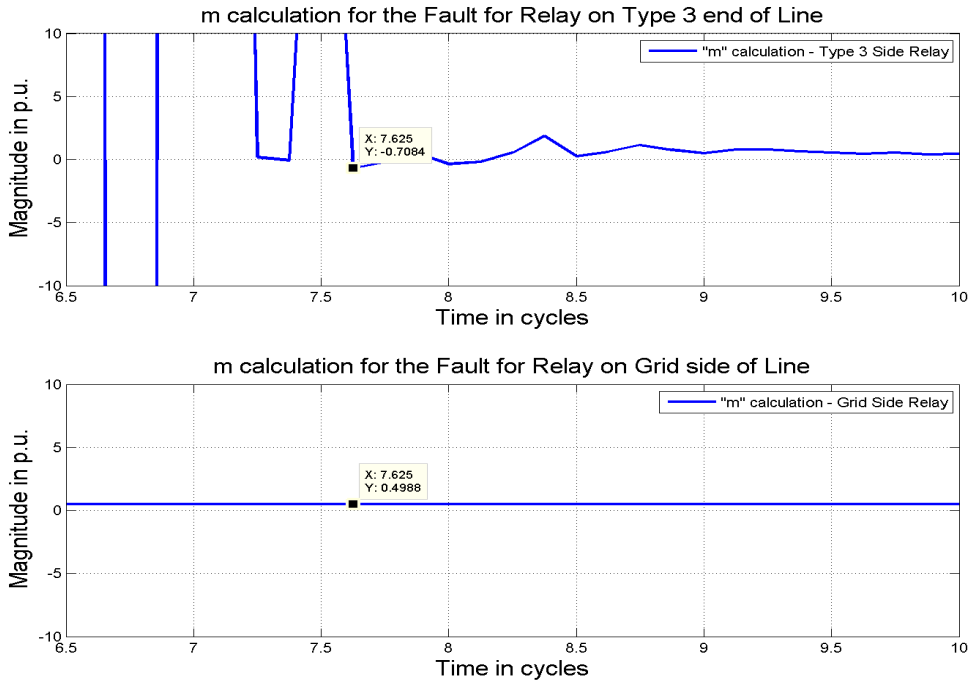

Figure 7.27: M Equation Calculations using MATLAB® for Event 1(d)

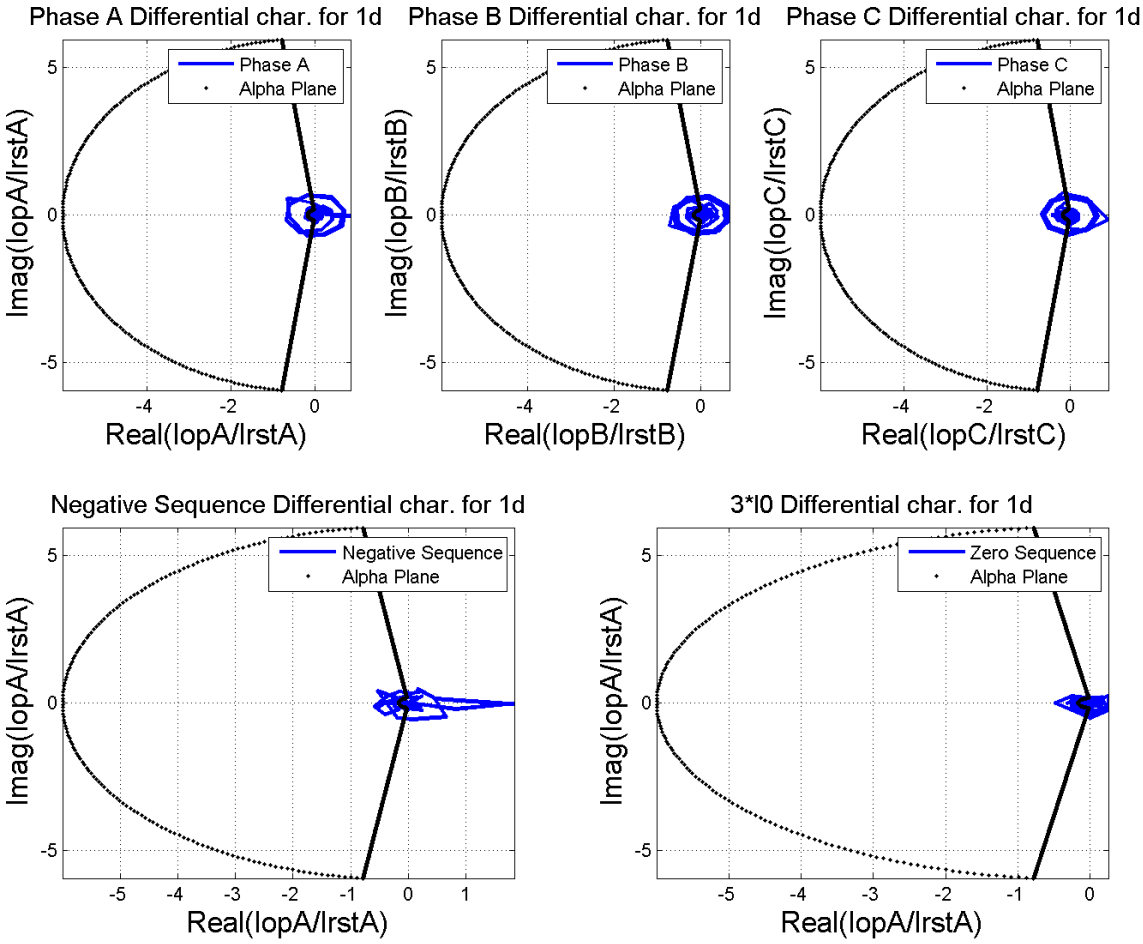

Figure 7.28: Differential Characteristic Plots using MATLAB® for Event 1(d)

assert), it trips after a delay based on the trip permission sent by grid side relay. Relay Bit - Permission to Trip asserted (TRPPRM) and TRIP assert 3 cycles (50ms) after 27AWI asserts. This trip is based on weak infeed logic.

7.4.6 Event 2(b) - ABG Fault (87COMM failed)

Observations and Analysis for Event 2(b):

1. Both the relays are not able to use its phase selection logic(Figures 7.34 and 7.35). FSC doesn't assert, as discussed for Event 1(b). The unbalance indicates that the change in current was sufficient (Figure 7.36) to not assert the loss of potential.

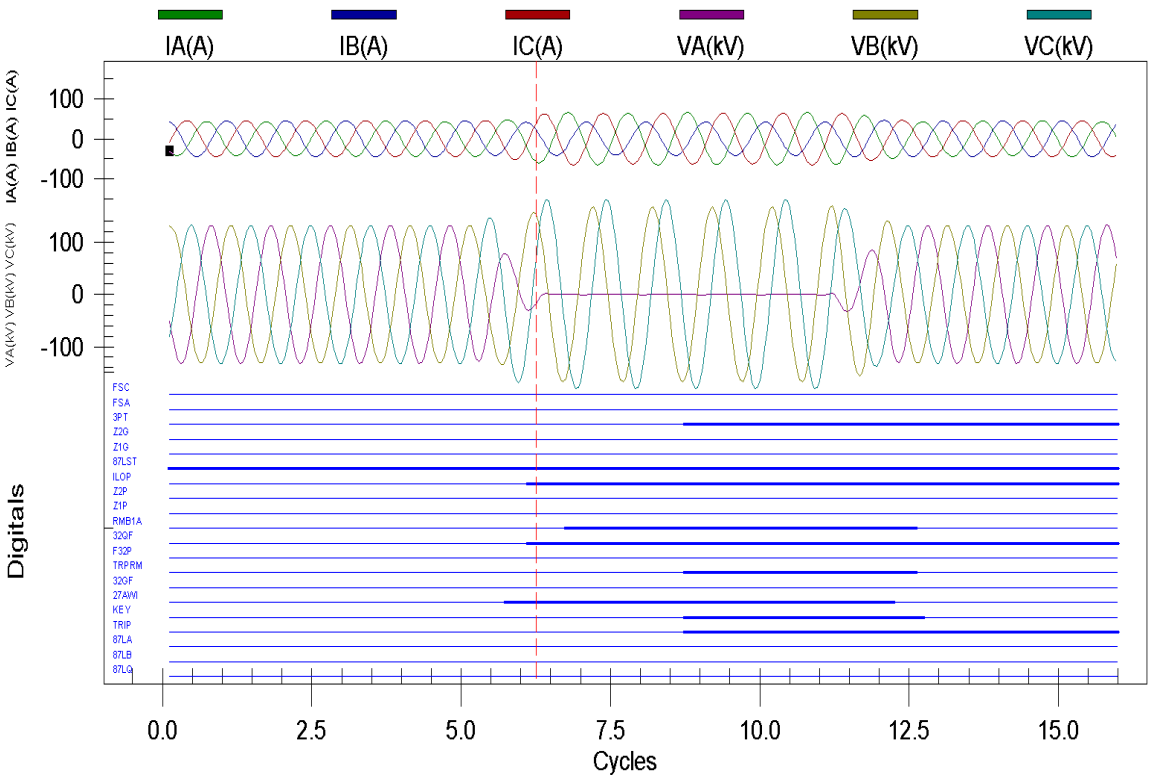

Figure 7.29: Event Report for Event 2(a) - Type 3 side Relay

2. Directional elements see the fault in front of them (Figure 7.37).

3. Similar to Event 2(a), grid side relay sees the fault in zone 1 using Mho phase elements (Figure 7.38) and issues an instantaneous trip to its breakers(Figure 7.35). A trip permission is also issued for Type 3 side relay as soon as the fault was seen in Zone 2.

4. The Type 3 side relay trips under POTT as soon as it sees the fault in its Zone 2. The permission to trip is already received from grid side relay.

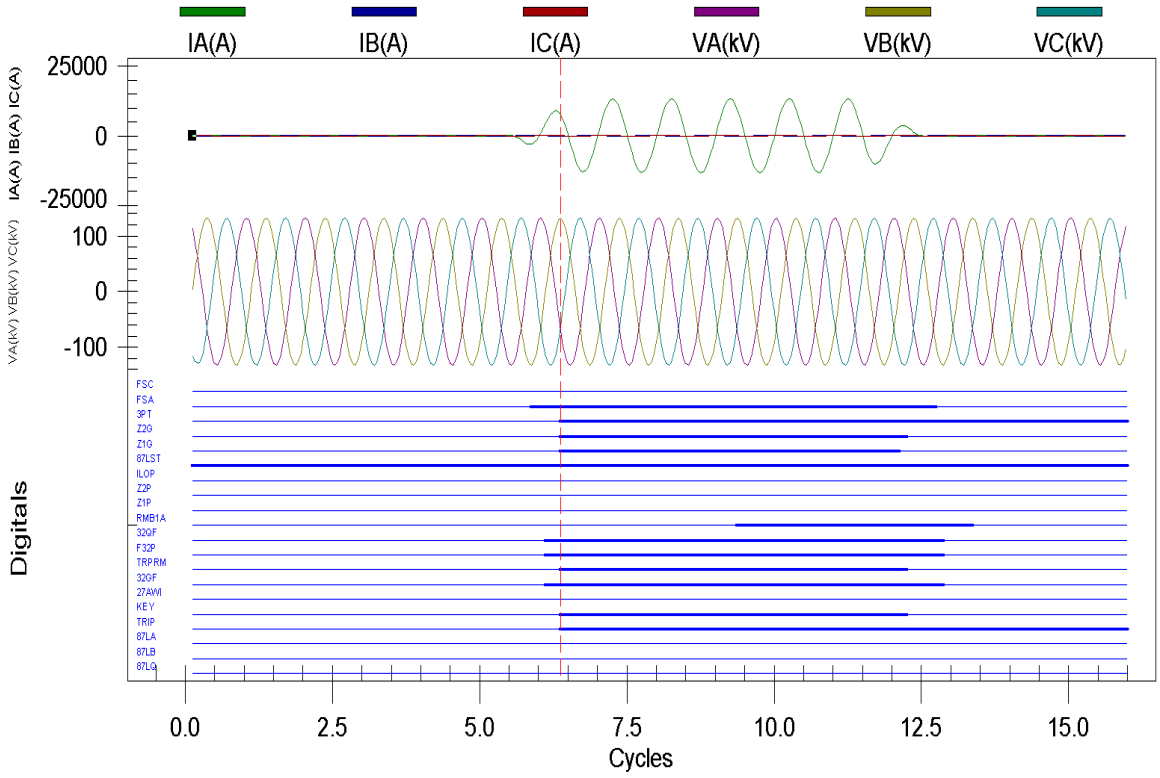

Figure 7.30: Event Report for Event 2(a) - Grid side Relay

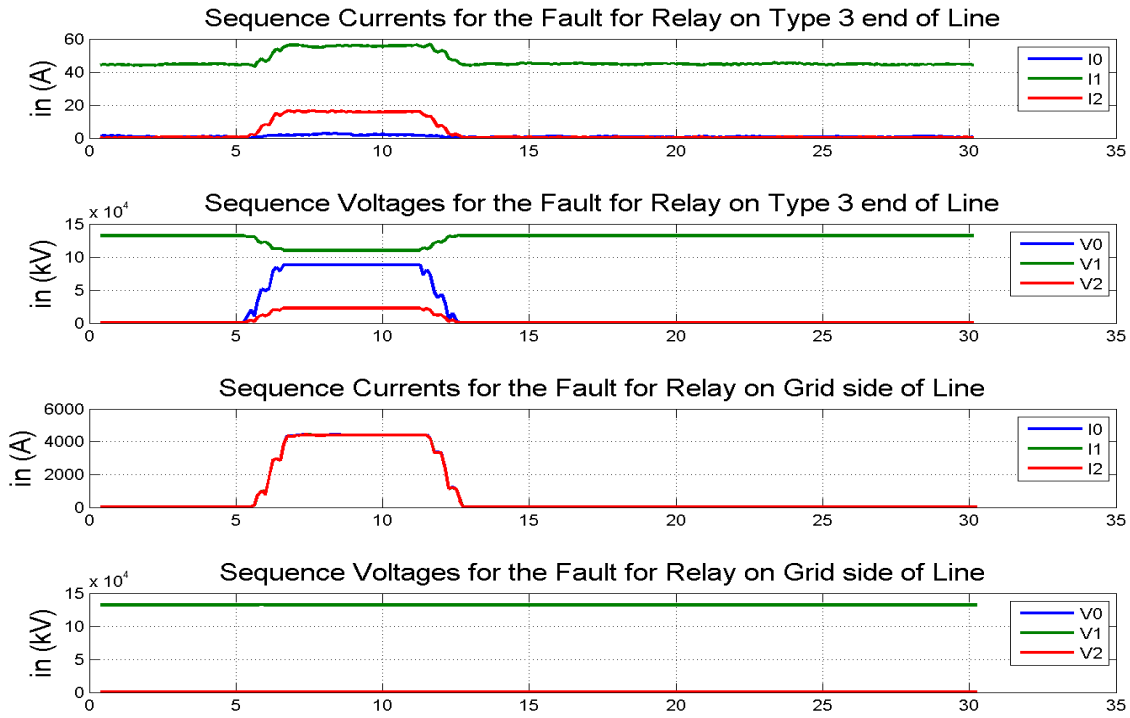

Figure 7.31: Sequence Current and Voltage Calculations using MATLAB® for Event 2(a)

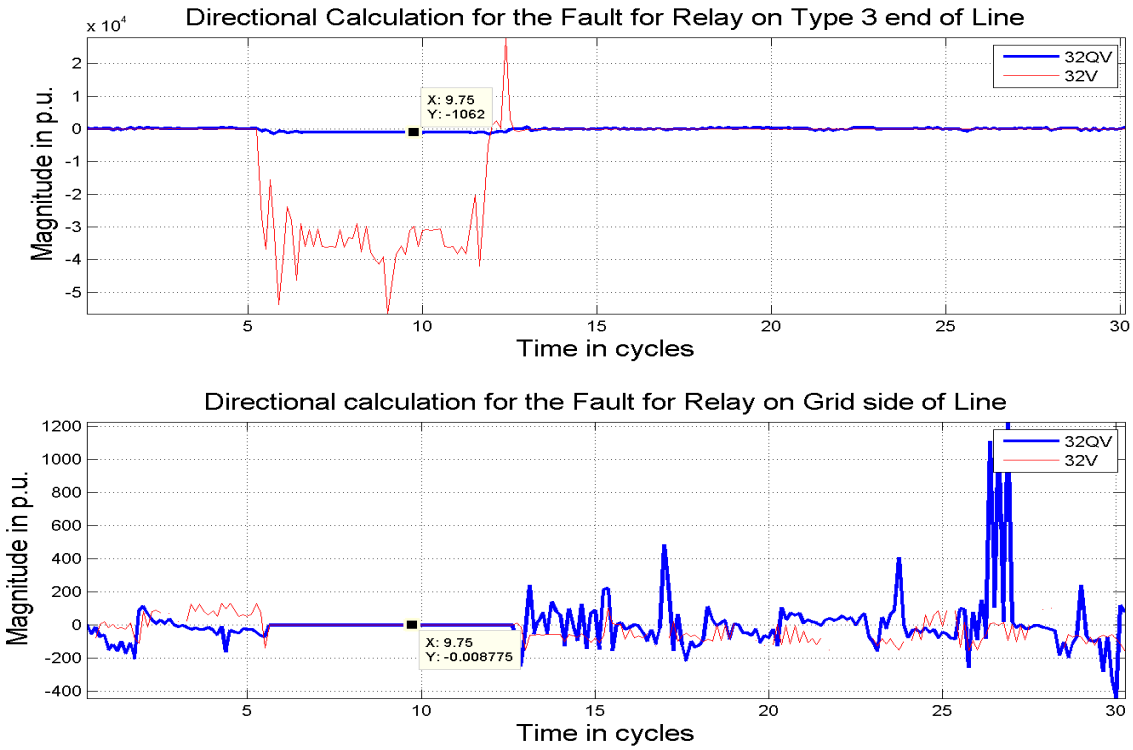

Figure 7.32: Directional Element Calculations using MATLAB® for Event 2(a)

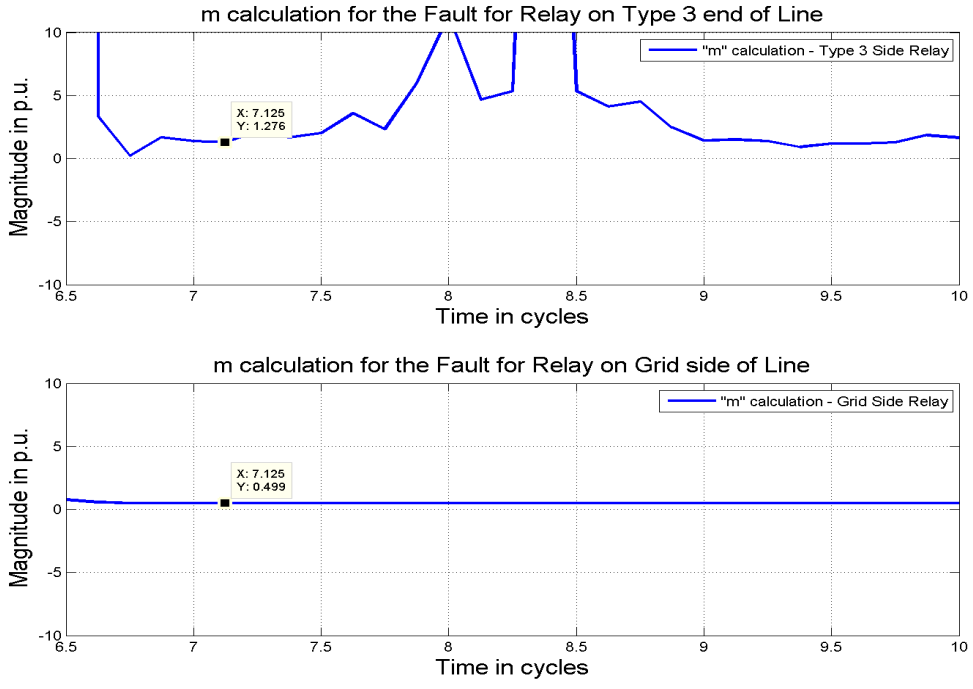

Figure 7.33: M Equation Calculations using MATLAB® for Event 2(a)

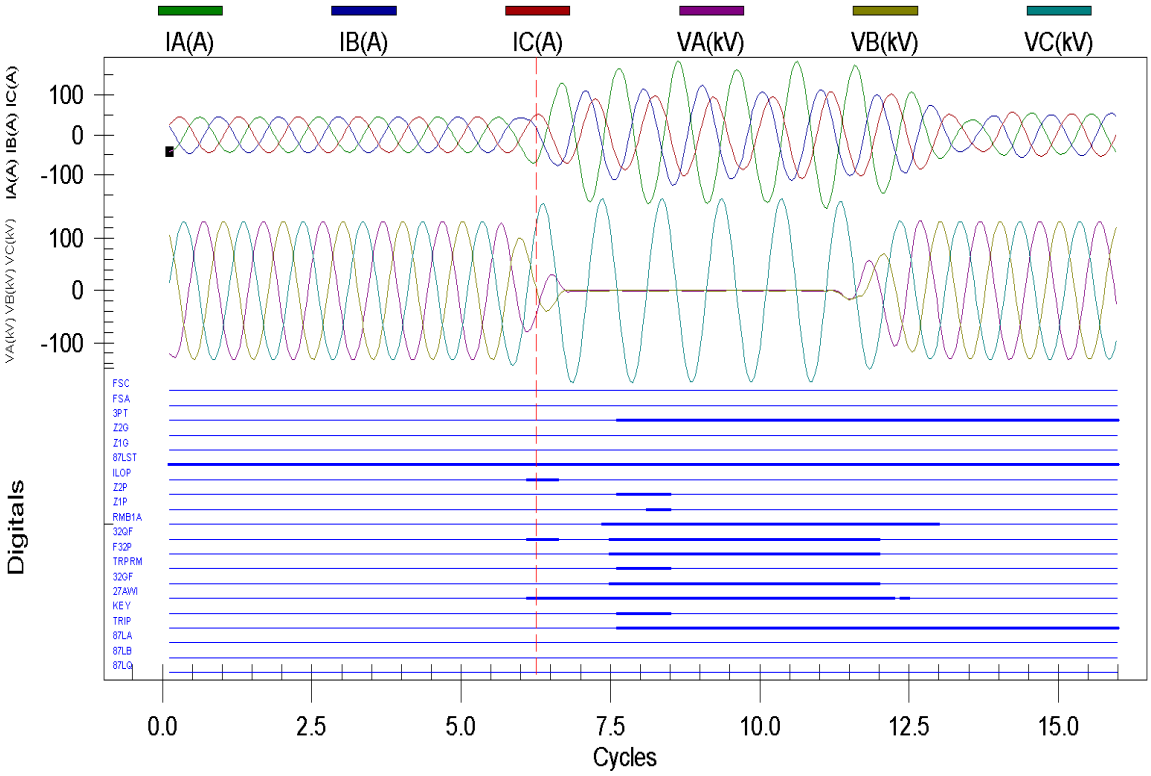

Figure 7.34: Event Report for Event 2(b) - Type 3 side Relay

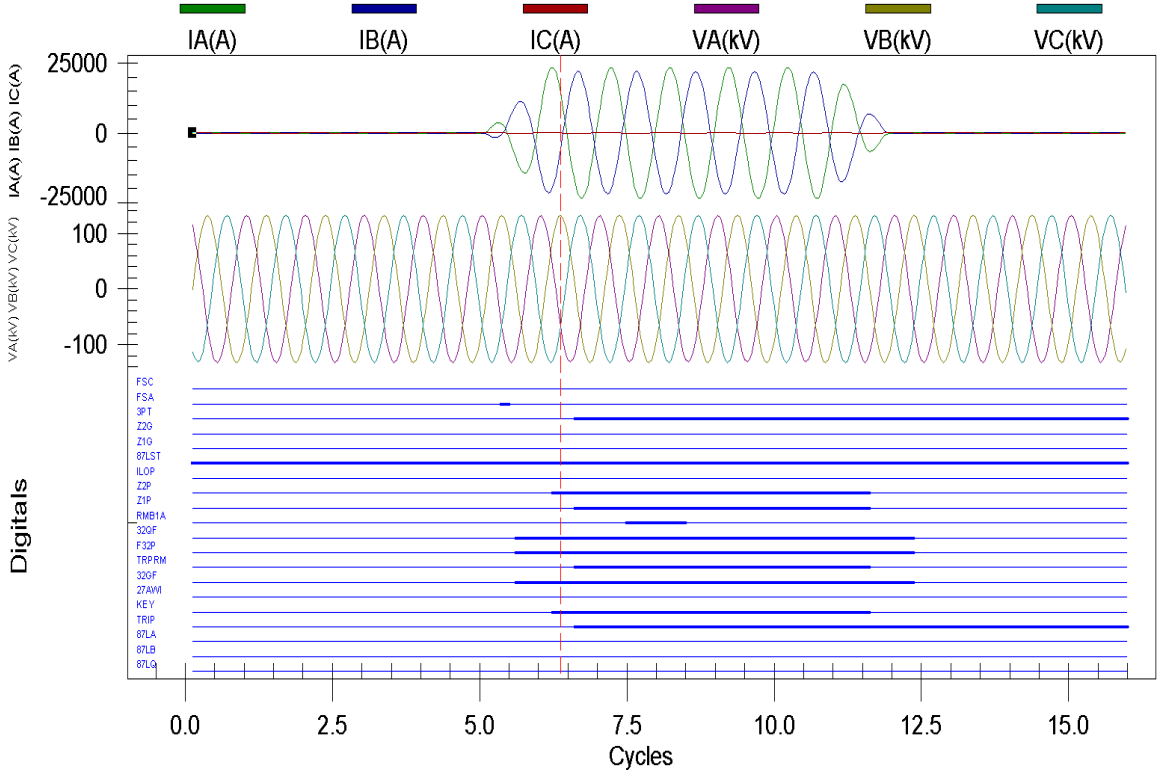

Figure 7.35: Event Report for Event 2(b) - Grid side Relay

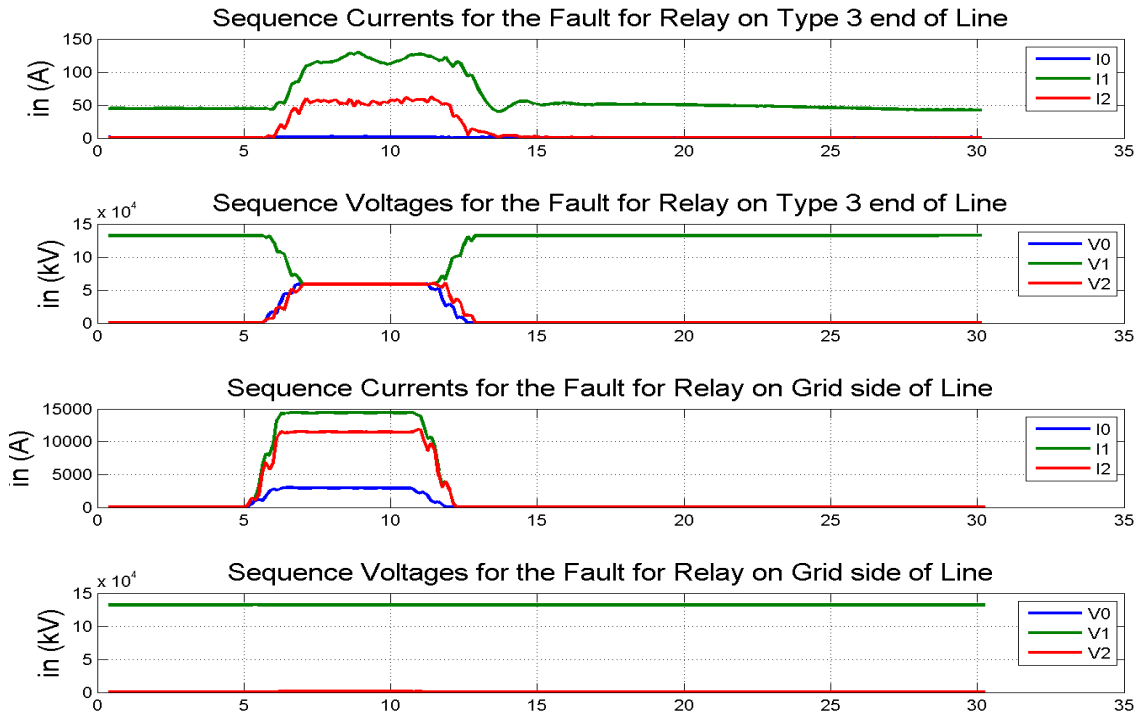

Figure 7.36: Sequence Current and Voltage Calculations using MATLAB® for Event 2(b)

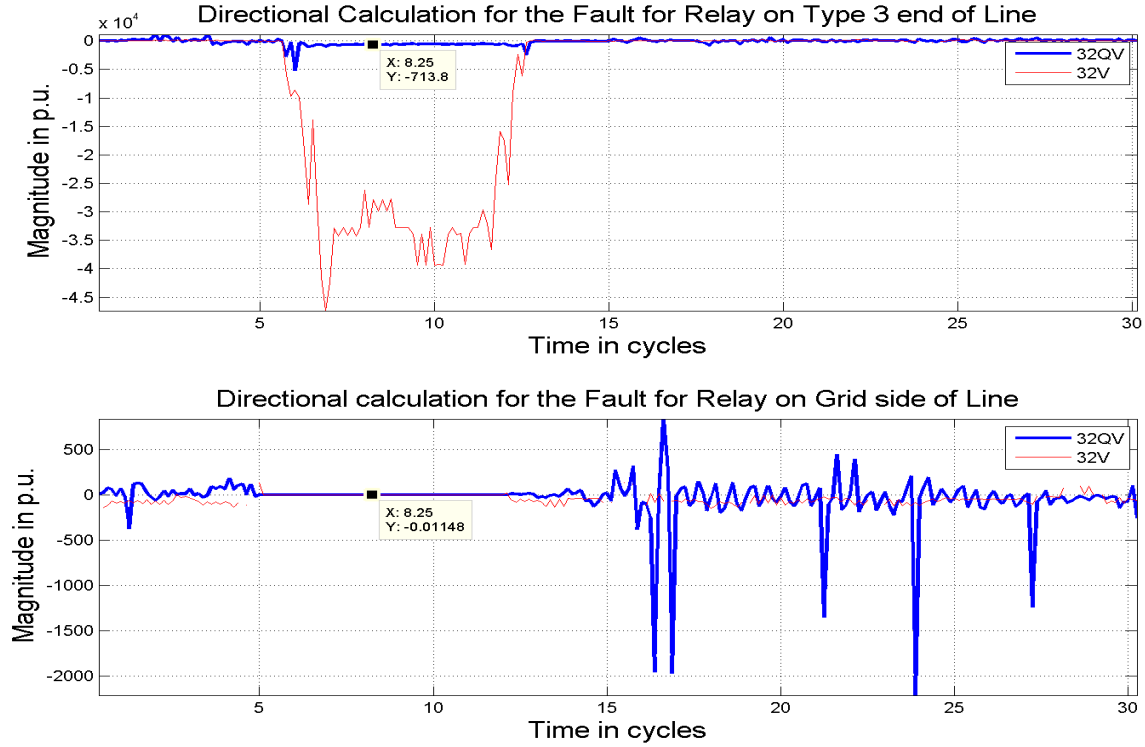

Figure 7.37: Directional Element Calculations using MATLAB® for Event 2(b)

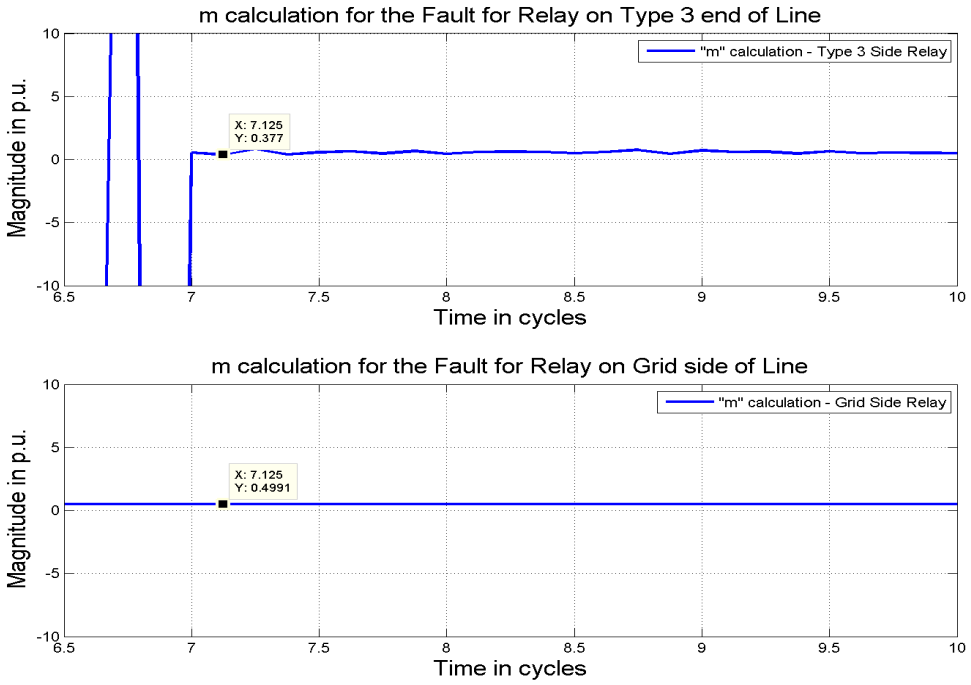

Figure 7.38: M Equation Calculations using MATLAB® for Event 2(b)

7.4.7 Event 2(c) - AB Fault (87COMM failed)

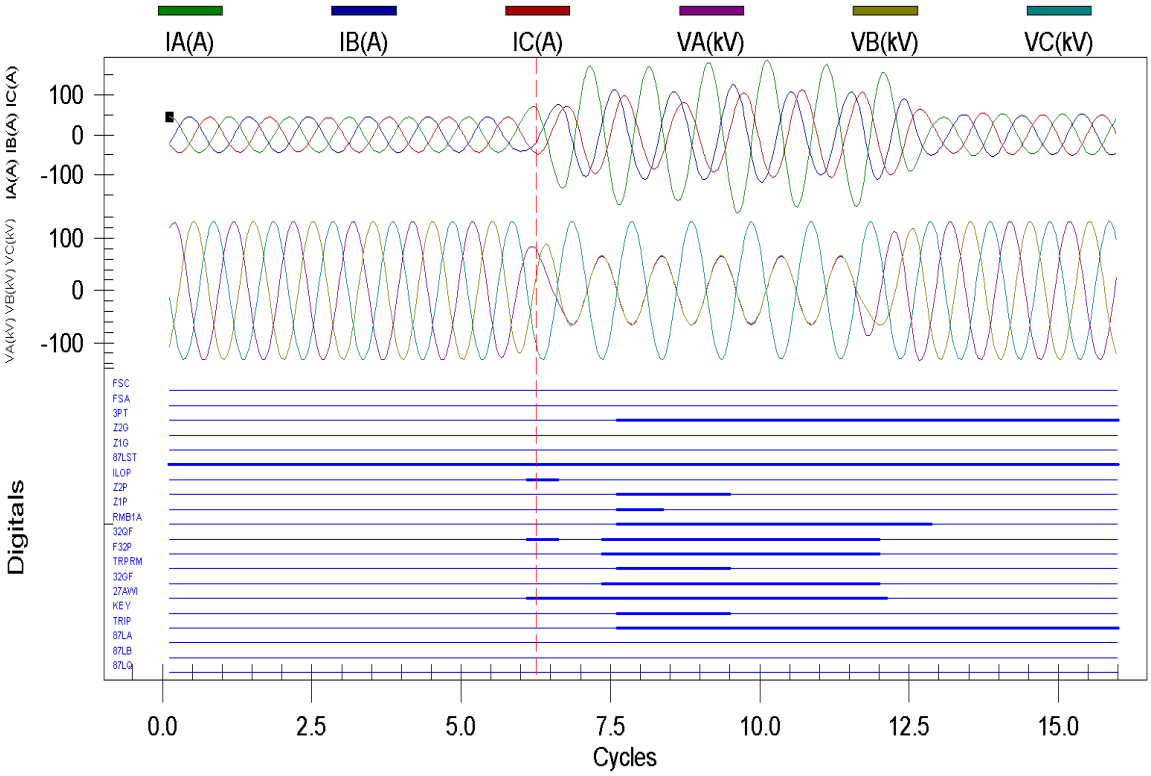

Figure 7.39: Event Report for Event 2(c) - Type 3 side Relay

Observations and Analysis for Event 2(c):

1. 7.39 and 7.40 present the voltages and currents for event 2(c). Zero sequence current is very negligible for both relays. However, the negative sequence current is again high (Figure 7.41).

2. Directional elements see the fault in front of them (Figure 7.42).

3. Similar to previous events, Mho phase elements (Z1P, Z2P) pick up. Grid side relay sees the fault in zone 1(Figure 7.43) and issues an instantaneous trip to its breakers (Figure 7.40). A trip permission (KEY) is also issued for Type 3 side relay as soon as the fault was seen in Zone 2.

4. The Type 3 side relay trips under POTT as soon as it sees the fault in its Zone

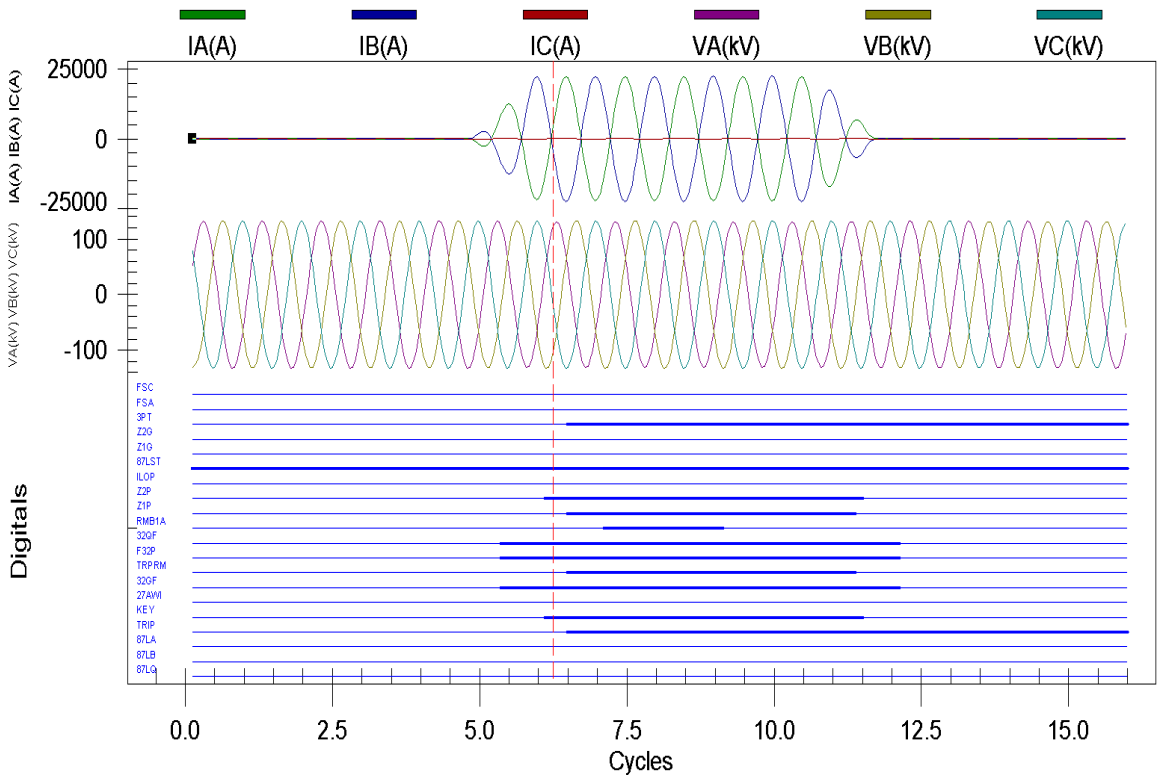

Figure 7.40: Event Report for Event 2(c) - Grid side Relay

2 (Z2P). The trip permission (TRPPRM) and Zone 1 Mho phase element (Z1P) are also asserted in the same processing interval.

7.4.8 Event 2(d) - ABCG Fault (87COMM failed)

Observations and Analysis for Event 2(d):

1. The response of the relays on both sides (Figures 7.44 and 7.45) is similar to Event 2(a). However, the unbalance currents have an interesting pattern, which reflects the action of Type 3 controllers (Figure 7.46). Similar behavior can be observed in the phase currents in the event report. There is an apparent oscillation like behavior.

2. The directional elements see the fault in front of them (Figure 7.47).

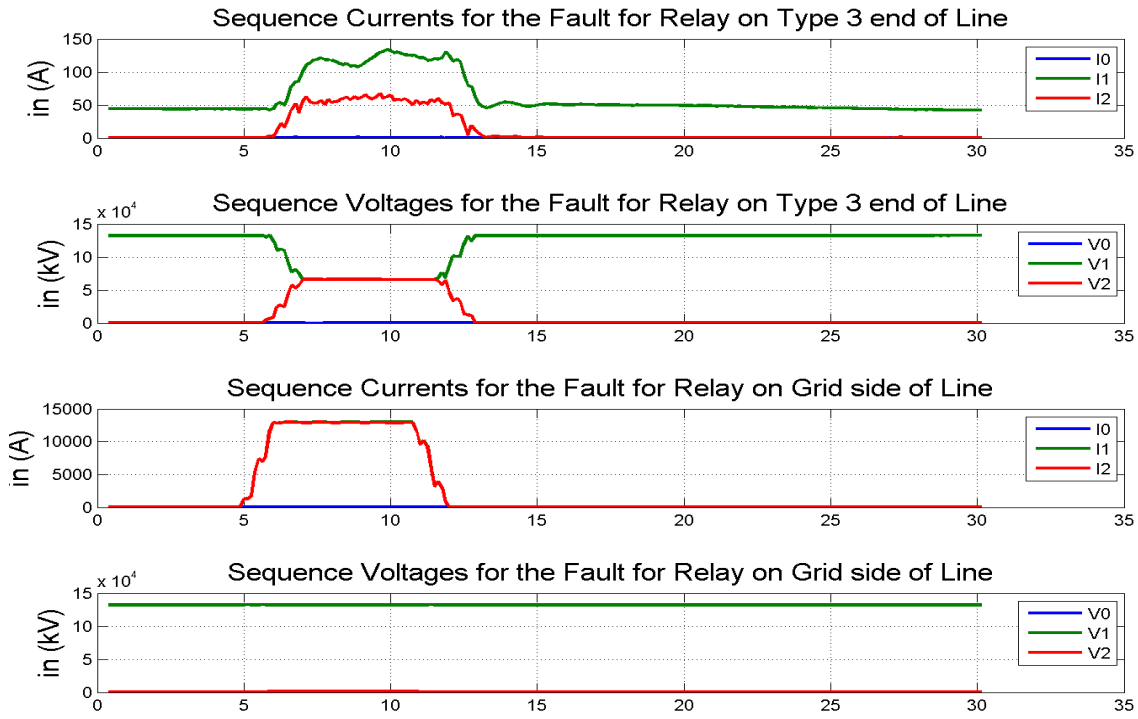

Figure 7.41: Sequence Current and Voltage Calculations using MATLAB® for Event 2(c)

3. Fault selection logic doesn't assert the fault in sector A, B or C (FSA, Relay Bit - Fault in Sector B (FSB), FSC) respectively, as expected.

4. Mho elements for the grid side relay pick up in both zones (Z2P followed by Z1P). 'M' calculations also show the same (Figure 7.48). The relay therefore, issues an instantaneous trip to its breakers (Figure 7.45). A trip permission (TRPPRM) is also issued for Type 3 side relay as soon as the fault was seen in Zone 2 (Z2P).

5. The Type 3 side relay never sees the fault in its reach (Z1P and Z2P don't assert). It issues the trip after a delay, based on the trip permission sent by grid side relay. As discussed before, this is because tweak infeed logic is enabled. Relay can convert a trip permission into TRIP after a delay.

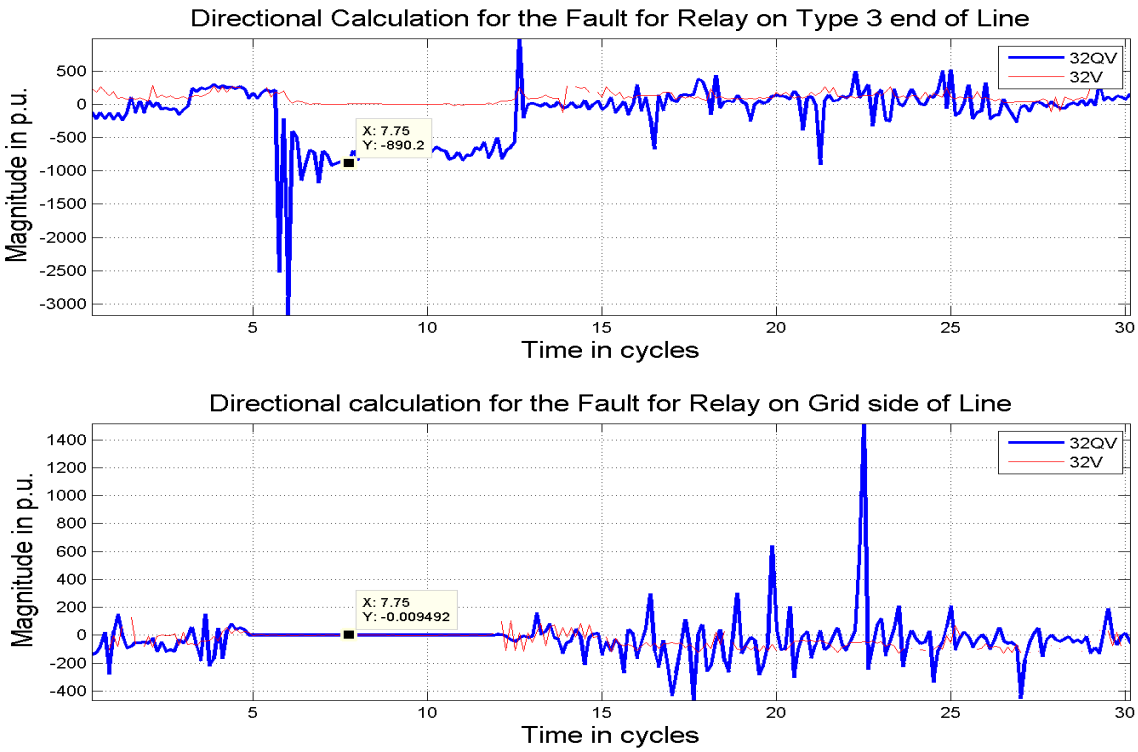

Figure 7.42: Directional Element Calculations using MATLAB® for Event 2(c)

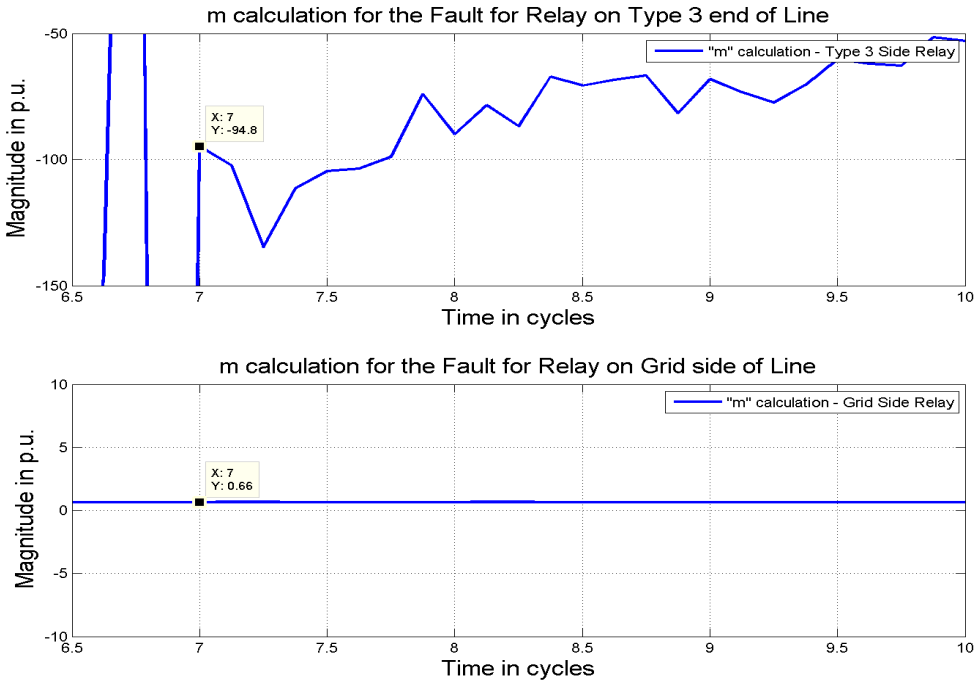

Figure 7.43: M Equation Calculations using MATLAB® for Event 2(c)

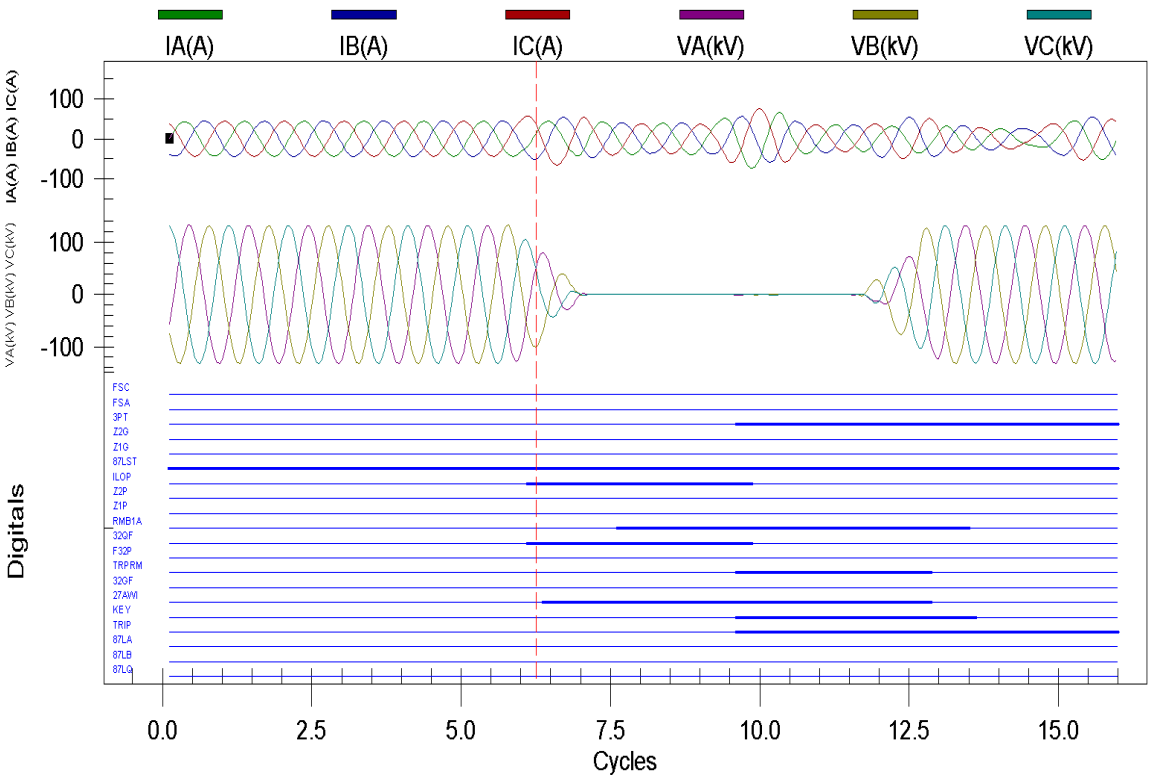

Figure 7.44: Event Report for Event 2(d) - Type 3 side Relay

7.5 Analysis of Results

1. ***Mho Distance Elements***

   The unusual behavior of power electronic converts makes it challenging for the relays with conventional relaying practices to respond to faults. We see the relays trip the breakers in all cases. However, the response is not same as for conventional systems.

   The Mho distance elements often saw the faults out of reach for a couple of cycles after the fault inception. In this cases, the grid side relay is tied to a conventional source, which behaves consistent to the expectations for modern relaying practices. The role of communication based schemes is very important. Without communication based relaying, the Type 3 side relay will not have tripped in more than 50% of the events.

2. ***Differential vs. Mho Distance protection***

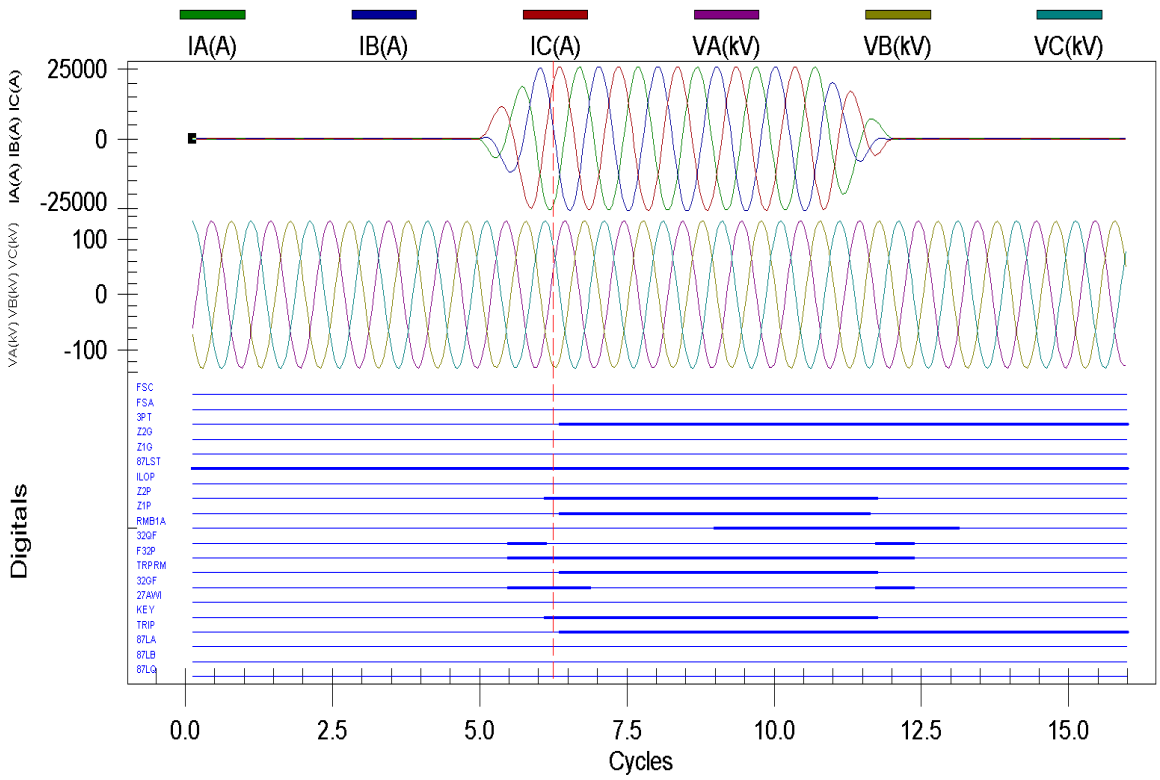

Figure 7.45: Event Report for Event 2(d) - Grid side Relay

Differential elements take a little more than cycle to pick up. The Mho distance elements are much faster (0.8-0.9 cycles) under regular conditions. However, the variable nature of VSC controllers makes fault detection using Mho elements very difficult. Differential elements utilize the advantage of one source being conventional and strong. Some differential schemes also have a minimum current threshold at each relay to qualify as a fault. Here, even with a weak Type 3 system on one end, the other end produced enough differential current for successful relay trips in all cases.

Some implementations of the differential schemes also have a minimum current check for each relay. These minimum thresholds have to be met before qualifying an event as a fault. With very small sequence current content, it is possible that even though the alpha plane asserts a fault, differential elements may be blocked by the lo

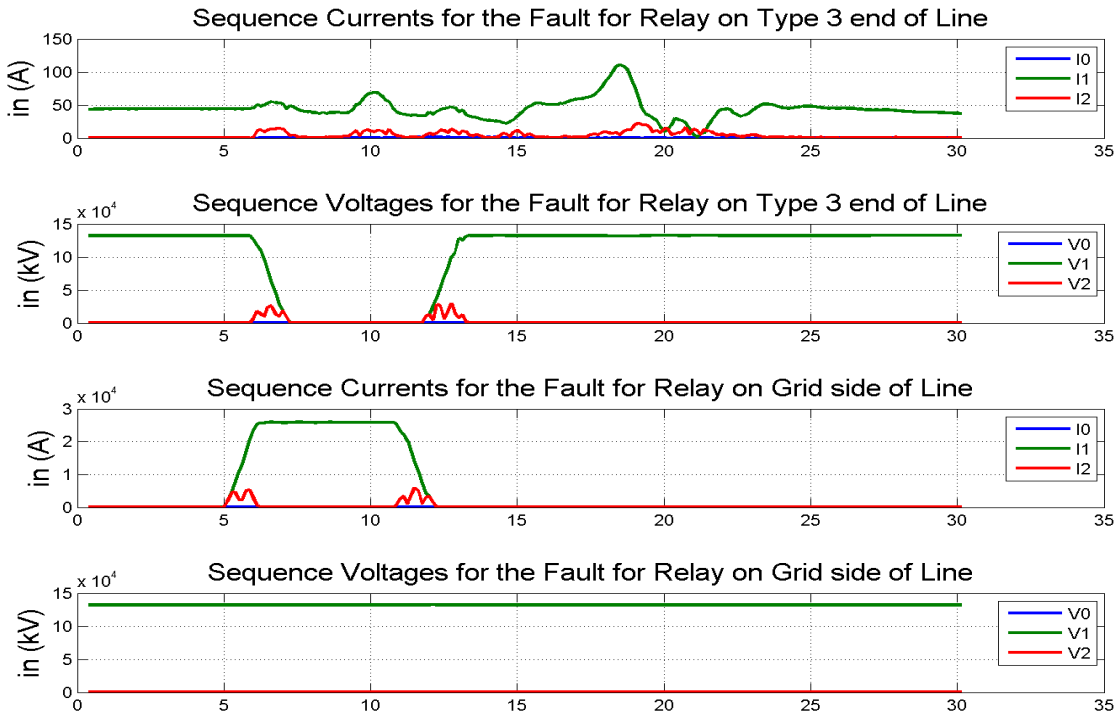

Figure 7.46: Sequence Current and Voltage Calculations using MATLAB® for Event 2(d)

The only critical element for all communication based schemes is the health of communication channels. Differential channels use fiber optic communication, which is relatively more prone to problems compared to serial communication cables used for POTT. Also, the elements may not perform so well for islanded systems or remote generation. This is because the sources on either ends may be weak, and not have enough fault current contribution.

3. ***Variable Nature of line currents during unfaulted conditions***

   Wind turbines and other variable sources like photovoltaics, do not produce constant power. Due to the variable nature of wind (air in general) geographically, wind turbines across the farm do not see the same quality and density of wind. Therefore, at the same point of time, some WTs may be generating in supersynchronous mode, while others are generating in subsynchronous model. It is highly possible, that some turbines may not be generating any power (are

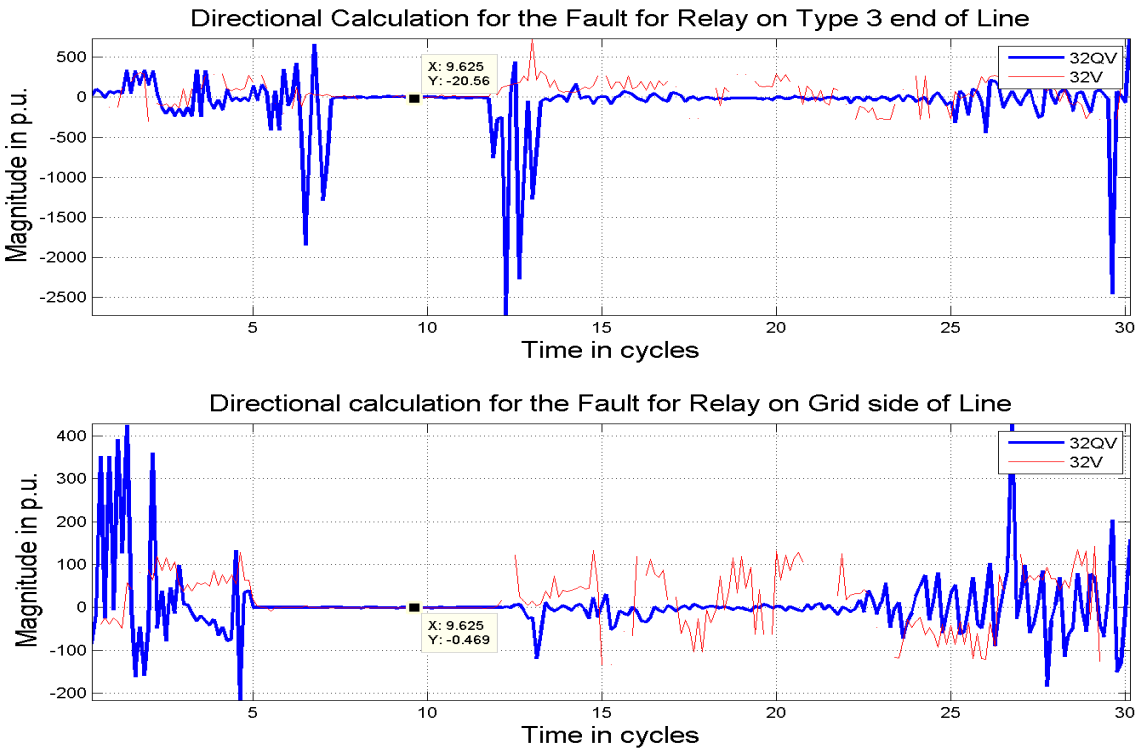

Figure 7.47: Directional Element Calculations using MATLAB® for Event 2(d)

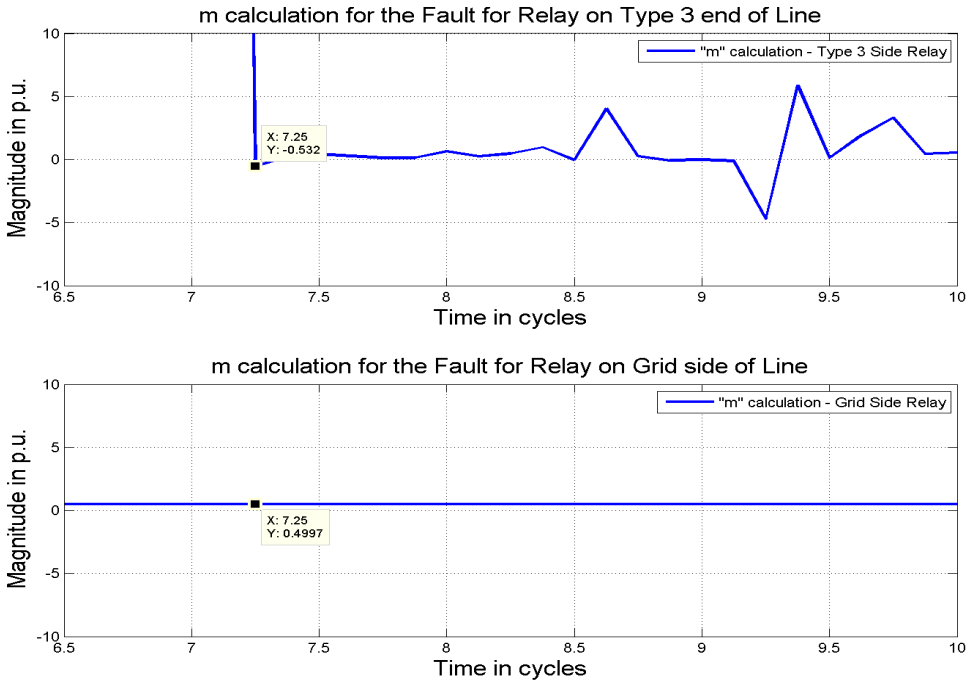

Figure 7.48: M Equation Calculations using MATLAB® for Event 2(d)

stalled). There will be situations where, a part of the wind farm is operating in supersynchronous mode, while other section is in subsynchronous mode. Some turbines may not be producing any power at all. Therefore, the line current will vary between 0-100% of the rated capacity. It is very difficult for the measuring CTs and the protection relays to maintain sensitivity and accuracy for the entire band easily.

4. ***Fault contribution due to different initial loads on the turbines***

   Influence of the controllers of a Type 3 WT on the net current output from the farm will depend on its respective generation too. Depending on the wind condition as described above, the fault behavior of the farm will vary for similar generation. This is because fault current contribution is also decided by the mode of operation of a DFIG. Best approach will be to test the performance for worst cases, and benchmark other scenarios accordingly.

5. ***Zero sequence dependent schemes***

   Type 3 WT systems are not very strong source for zero sequence currents. It is seen that even bolted faults can have very small contribution towards zero sequence currents. Therefore, schemes depending on these currents may not perform well under low wind conditions, when the line current is small. Schemes based on negative sequence quantities will be more dependable. In this case also, we observe discrepancies in fault selection and loss of potential detection. On one of the occasions, the directional elements also were indecisive for sometime about fault direction.

6. ***Minimum quantity checks***

   to provide additional security during relay operations, relays commonly use minimum quantity checks to supervise their supervisory and protection elements. These checks include phase and sequence voltage or currents, or the change in those quantities. As discussed, if the unfaulted power output from the farm is not much, some of these checks may not assert. This was observed in some cases

in analysis for this work too. Relays need to switch to more sensitive and/or secure mode, to maximize reliability in such periods of low generation.

7.6 Summary

In this chapter, the basic concepts of protection elements, associated supervisory elements, and communication based schemes are discussed. Then, the corresponding event reports for simulated faults on the Type 3 WT model are discussed. Finally, a comparative analysis of different relay bits is presented based on how they performed. Primary concerns are highlighted.

Chapter 8: Summary, Conclusions and Future Work

8.1 Summary

The results and analysis discussed in the Section 7.4 will be summarized in tables (8.1) and (8.1). Note that, the entries color coded as '**GREEN**' represent desired (and expected) behavior. '**RED**' color coded entries represent undesirable operations. The test cases with and without an active differential communication channels are separated as 'mode 1' and 'mode 2' respectively. When differential channel is not available, the corresponding entry is 'Not Applicable (NA)'.

Fault Type	Mode	Operated First	Operated??					TRIP issued by
			Z1G	Z2G	Z1P	Z2P	87	
AG	1	W: 87LA	N	N	N	N	Y	87LA
		G: Z2G	Y	Y	N	N	Y	Z1G
AG	2	W: 27AWI[1]	N	N	N	N	NA	27AWI*
		G: Z1G, Z2G	Y	Y	N	N	NA	Z1G
ABG	1	W: 87LA	N	N	Y	Y	Y	87LA
		G: Z2P	N	N	Y	Y	Y	87LA, Z1P
ABG	2	W: Z2P	N	N	Y	Y	NA	Z2P, RMB1A
		G: Z2P	N	N	Y	Y	NA	Z1P
AB	1	W: 87LQ	N	N	Y	Y	Y	87LQ
		G: Z2P	N	N	Y	Y	Y	87LA, Z1P
AB	2	W: Z1P, Z2P	N	N	Y	Y	NA	Z1P
		G: Z2P	N	N	Y	Y	NA	Z1P
ABCG	1	W: 87LA	N	N	N	N	Y	87LA
		G: Z2P	N	N	Y	Y	Y	87LA, Z1P
ABCG	2	W: 27AWI	N	N	N	N	NA	27AWI*
		G: Z2P	N	N	Y	Y	NA	Z1P

Table 8.1: Summary - Fault Wise Response of the Protection Element Bits

In this thesis, a single generator Type 3 WT averaged model is developed. The steady state behavior of the model is validated using standard speed torque characteristics and operational behavior of the Type 3 machines. Fault behavior is validated using field data. A 10-generator aggregated WT model is developed from the single turbine model and validated likewise. This aggregated model is connected to a test

Fault Type	Mode	Operated??			
		Fault Selection	Directional		Loss of Potential
			32GF	32QF	
AG	1	W: FSA	Y	Y	Y
		G: FSA	Y	Y	N
AG	2	W: None	Y	Y	Y
		G: FSA	Y	Y	N
ABG	1	W: None	Y	Y	N
		G: None	Y	Y	N
ABG	2	W: None	Y	Y	N
		G: None	Y	Y	N
AB	1	W: None	Y	Y	Y
		G: None	Y	Y	N
AB	2	W: None	Y	Y	N
		G: None	Y	Y	N
ABCG	1	W: None	N	Y	Y
		G: None	N	Y	N
ABCG	2	W: None	N	Y	Y
		G: None	Y	Y	N

Table 8.2: Summary - Fault Wise Response of the Supervisory Element Bits

network as shown in Figure 5.5. Faults are simulated was developed in the RTDS, with its controllers.

8.2 Conclusions

The fault simulations on the aggregated Type 3 model revealed some very important behavior. A few operational and sensitivity challenges for the supervisory elements and variable speed operation were also revealed. The conclusions are presented as under:

1. Type 3 WT controllers try to regulate the phase currents. During faults, this can reduce (and limit) the unbalance current leading to not so significant current contribution from the relays. As a result, the protection and supervision schemes depending on sequence quantities (usually currents) may face sensitivity issues.

2. Generation from the distributed sources have a large range of currents for normal operation. For periods of low generation, the relay sensitivity may not be sufficient to operate reliably.
3. Distance ground elements usually operate faster than differential elements.
4. Distance phase elements usually operate slower or at the same time as differential elements.
5. If there is not enough zero sequence current, the fault may appear farther to mho elements.
6. Weak infeed logic should be activated for the Type 3 WT relays. This allows the relay to trip even if local mho elements for WT aide do not see the fault based on trip permission from the grid side relay.
7. Differential elements assert all the faults properly. One of the reasons is identified to be the strong source on the grid end. If the other end is also a weak source, response of the differential elements may be a little different.
8. Fault selection didn't perform very well, when the zero sequence current was not sufficient.
9. Negative sequence directional elements saw the faults in all cases. Ground current based differential had troubles in some cases.
10. Negative sequence current based quantities performed better compared to zero sequence current based quantities.
11. Loss of potential check can have troubles if a fault occurs during periods of low generation.

8.3 Suggested Measures - Future Work

It may be argued that having a CT with a wider range of measurements and improved hardware in relays will resolve a part of sensitivity issue. However, the hardware limitations, cost, space and other hardware challenges may not allow these improvements to be implemented immediately.

Following are some suggested alternatives:

1. *Using more than one CTs*

   Modern relays have the ability to read currents on multiple channels. By connecting, two CTs with different ratios. One will have high accuracy range for 0 - 25% of the rated current and other with higher accuracy for unfaulted line currents being 25% and above.

   (a) The relay can be programmed to select between two channels based on the unfaulted RMS current measurements with a hysteresis band.

   (b) Relay will have different sets of settings based on the different CT ratios to ensure the coverage of its protection elements and healthy communication for communication based schemes.

2. Decrease the tripping time for Zone 2 distance elements of the relays on Wind farm side if communication failure is detected. This will lead to faster tripping if the Type 3 side relay sees no fault, while mho elements of the grid side relay see the fault in Zone 1 and sends the other end a trip permission.
3. *Communication between Collector and Line Side relays*

   Collector side relays will immediately see the change in generation from the wind turbines on their respective lines. Based on the system, these relays can be programmed to assert a communication bit if the primary current on their lines fall below a certain threshold. These bits can be communicated to the Line side relay using Generic Object Oriented Substation Events - A control model defined as per IEC 61850. (GOOSE) or other communication protocols.

   The Line side relay will switch to more secure settings when more than 'x' out of 'y' collector side relays report a drop in current below the predefined threshold.
4. *Communication between Relays and WT controllers*

   Abrupt changes in the line voltage currents maybe balanced out at the line

terminals. In order to do that, the converter will need to quickly react to the change in voltage/current and change its switching. In other words, controller sees the fault like behavior before any other part of the system. Therefore, if the relays and WT controllers can communicate their status in some way, this may be useful to identify fault conditions also.

References

[1] Thomas Ackermann. *Wind Power in Power Systems*. John Wiley & Sons, April 2012.

[2] Free Renewable Energy Resource Maps :: Wind Speed :: 3TIER. Internet: http://www.3tier.com/en/support/resource-maps/. [July 22, 2014].

[3] Global Wind Energy Council. GLOBAL WIND REPORT - ANNUAL MARKET UPDATE 2013. Annual, Global Wind Energy Council, 2014.

[4] RTDS technologies. Real time digital simulator controls library manual (RSCAD version). July 2013.

[5] Jeff Barsch, George Bartok, Gabriel BenmouyaI, Oscar Bolado, Brian Boysen, Sukumar Brahma, Stephan Brettschneider, Zeeky Bukhala, and Jeff Burnworth. Fault current contributions from wind plants. Technical report.

[6] Yaw Control. Internet: http://pclab.et.teiath.gr/hermes/yaw%20control_en.php. [July 22, 2014].

[7] Eduard Muljadi, Nader Samaan, Vahan Gevorgian, Jun Li, and Subbaiah Pasupulati. Short circuit current contribution for different wind turbine generator types. In *Power and Energy Society General Meeting, 2010 IEEE*, pages 1–8. IEEE, 2010.

[8] Sarah Probert. Generator fault ride through (FRT) investigation. Literature Review GEN FRT: S1, Transpower New Zealand Limited, February 2009.

[9] Donald W. Novotny and Thomas A. Lipo. *Vector control and dynamics of AC drives*, volume 2007. Clarendon press Oxford, 1996.

[10] Rishabh Jain, Brian K. Johnson, and Herbert L. Hess. Dfig based wind turbine system modeling in the real time digital simulator. In *North American Power Symposium, 2014 IEEE*, pages 1–6. IEEE, 2014.

[11] Amirnaser Yazdani and Reza Iravani. *Voltage-Sourced Converters in Power Systems*. Wiley, March 2010.

[12] William H. Kersting. *Distribution System Modeling and Analysis, Second Edition*. CRC Press, November 2006.

[13] Bin Wu, Yongqiang Lang, Navid Zargari, and Samir Kouro. *Power Conversion and Control of Wind Energy Systems*. John Wiley & Sons, September 2011.

[14] Yongbo Yang and Xiaoming Zha. Aggregating wind farm with DFIG in power system online analysis. In *Power Electronics and Motion Control Conference, 2009. IPEMC '09. IEEE 6th International*, pages 2233–2237, May 2009.

[15] M. Chaudhary, S.M. Brahma, and S.J. Ranade. Validated short circuit modeling of type 3 wind turbine generator with crowbar protection. In *North American Power Symposium (NAPS), 2013*, pages 1–6, September 2013.

[16] Francesco Sulla. *Fault Behavior of Wind Turbines*. PhD thesis, Lund University, 2012.

[17] Hector J. Altuve Ferrer and Edmund O. Schweitzer. *Modern Solutions for Protection, Control, and Monitoring of Electric Power Systems*. Schweitzer Engineering Laboratories, Incorporated, 2010.

[18] Manitoba Hydro. Bipole III transmission reliability project. Technical Report Chapter 3 - Project Description.

[19] SEL-411l relay - protection and automation system - instruction manual. Instruction manual, Schweitzer Engineering Laboratories, April 2014.

[20] Nasser Tleis. *Power Systems Modelling and Fault Analysis: Theory and Practice.* Newnes, November 2007.